DNA-Mediated Charge Transport for Long-Range Sensing and Protein Detection

Thesis by
Natalie Bloom Muren

In Partial Fulfillment of the Requirements for the Degree of Doctor of Philosophy

California Institute of Technology
Pasadena, California
2013
(Defended December 20, 2012)

Acknowledgements

I am forever grateful to the many people who supported me in this work and made possible this incredible opportunity to learn and grow. Above all, I must acknowledge my advisor Prof. Jackie Barton. Jackie, your vision, creativity, persistence, patience, guidance, and encouragement have been the fuel for this work and without you these pages would still be blank. To be surrounded by and contribute to this fascinating science for which you have such passion and enthusiasm has been an unbelievable privilege. Thank you for your confidence in me, which propelled me forward, and for your constant and unwavering dedication to my success at Caltech. I have learned so much from you and you have made me infinitely stronger—a stronger scientist, a stronger person. Thank you for these immeasurably precious gifts.

Thanks also to my thesis committee, Profs. Doug Rees, Dave Tirrell, and Harry Gray for supporting me on this journey. Your genuine interest in my work and well-being was clear from the beginning and helped me feel that I really could be successful here. Thank you for your thoughtful questions and suggestions during my exams and for all of your words of encouragement.

Experiments with single molecules make up an important piece of this work and would not have been possible without a close collaboration with Prof. Colin Nuckolls at Columbia University. Hanfei Wang, David Ordinario, and Alon Gorodetsky in the Nuckolls group worked hard to take these measurements and I am grateful that they persisted with these very challenging experiments.

I am thankful to every member of the Barton group who I've worked alongside and who create such a positive, supportive environment in which to learn and do

research. In particular I am grateful to the many Barton group members who collaborated on work with me or provided me with helpful guidance. I worked closely with Jason Slinker on several aspects of this work and he patiently taught me clean room technique and how to do successful photolithography. His dedication to getting the multiplexed chip platform up and running, especially in the frustrating beginning stages, and his willingness to let me be a part of this process were absolutely critical for my successful, continued application of this platform. Alon Gorodetsky was my first mentor and provided me with a solid foundation for conducting DNA CT chemistry. His attention to detail and insistence on proper technique from the beginning set the stage for me to ask more challenging questions. Marisa Buzzeo broke the concept of electrochemistry down into manageable pieces and helped me prepare for my candidacy exam. Along with her vast electrochemistry knowledge, Marisa's support and advice have been helpful throughout my time at Caltech. Amie Boal was also an incredible mentor who never seemed fazed by my persistent questions. I am grateful to Amie for her kindness and for giving me the security of always having someone just a few desks away who would know what to do.

In addition to these mentors I've relied on several Barton group members—Eric Olmon, Joey Genereux, Eddie Merino, and Russ Ernst, among others—who have always been available to discuss my questions or teach me how to perform a new technique or assay. I am also thankful for the hard work and input of other members of the electrochemistry subgroup, including Catrina Pheeney and Ariel Furst, who are always so willing to brainstorm and troubleshoot the obstacles that arise in electrochemistry experiments.

I must give special acknowledgement to Pam Sontz and Hang Song, two incredible people who, remarkably, joined Jackie's group at the same time as me. I ask myself constantly how we were lucky enough to become the Unstoppable Trio. Pam and Hang, thank you for your support, encouragement, and friendship; every step of this journey was easier because I had you two right by my side.

I am also deeply grateful to Mo Renta for her relentless dedication to making things work in the Barton group. Thank you, Mo, for your advice and for always being the person to go to when I needed direction on how to get something done.

I would also like to thank all of the staff in the chemistry department for their guidance through the various steps of this degree and for always going beyond their job descriptions to keep my research moving. Thanks for tracking down lost packages and fixing broken equipment and patiently responding to my questions with a helpful attitude.

I've had several important teachers who set me on this path and prepared me for success at Caltech. Steve Holman and Graham Dey sparked my first interest in scientific research and taught me the importance of conveying a story to which others can connect. The enthusiasm of my undergraduate advisor, Prof. Sarah Kirk, as well as that of other Willamette University chemistry professors Chuck Williamson and Karen Holman, helped to crystallize my interest in chemistry. Profs. Kirk, Williamson, and Holman guided me to excellent education and research opportunities and gave me the confidence to imagine that I could go to graduate school in chemistry.

Finally, I would like to thank my endlessly supportive family. Thank you to my Mom and Dad for raising me with a mind that is open and flexible enough to think about these things and for always making education such a priority. Thank you for being so

understanding and supportive during this process and for always believing so strongly in me. Thanks also to my amazing siblings, Dominic, Russell, and Kelly, for your creativity, for having thoughts, opinions, and interests, and for enriching my life just by being who you are. I feel very lucky to have the five of you and thank you for your encouragement along this path.

Abstract

The structural core of DNA, a continuous stack of aromatic heterocycles—the base pairs—that extends down the helical axis, gives rise to the fascinating electronic properties of this molecule that is so critical for life. This π-stacked structure facilitates a unique form of charge conduction, termed DNA-mediated charge transport (DNA CT). Experiments with diverse platforms, in solution, on surfaces, and with single molecules, collectively provide a broad and consistent perspective on the essential characteristics of this chemistry. Notably, DNA CT can proceed over long molecular distances, but is remarkably sensitive to perturbations in base pair stacking. These characteristics suggest that DNA CT may be used for long-range sensing both in nature and in nanoelectronic applications. Here, measurements of DNA CT with surface and single molecule platforms are used to (i) determine how ground state DNA CT varies over regimes of increasing distance and (ii) apply this chemistry to the electrical detection of DNA-binding proteins.

First, the design and fabrication of multiplexed, DNA-modified electrodes on silicon chips is reported. These lithographically patterned chips with 16 individually addressable gold electrodes allow for the measurement of DNA CT with four different types of DNA, side by side on the same surface, with four-fold redundancy. Discrimination of DNA with a single base mismatch and detection of sequence-specific restriction enzyme activity are both achieved with these chips. Scaling of these devices to microelectrode dimensions is also demonstrated. Importantly, these chips show greater reproducibility and consistency than commercially available rod electrodes. This

greater signal quality, combined with the capacity to examine different samples side by side, opens the door for more complex applications of this platform.

The fully developed, multiplexed chips are first used to compare DNA CT over short and long distance regimes. DNA is evaluated in this context because the efficacy of a long-range sensor, in either nature or nanoelectronics, is determined largely by its capacity to facilitate CT in a manner that is minimally affected by the CT distance. DNA CT over 34 nm in 100-mer monolayers is found to yield electrochemical signals that are comparable in size to shorter 17-mer DNA. Signal attenuation from a single base-pair mismatch in the 100-mer is also comparable to that for 17-mers, and confirms that CT in these 100-mer films is DNA-mediated. Efficient cleavage by a restriction enzyme indicates that the 100-mer DNA adopts a native, upright conformation. The alkanethiol linker used to anchor the DNA to the electrode is found to limit the electron-transfer rate for both DNA lengths. Thus the impact of increasing the CT distance on DNA CT is too small to be resolved by this platform, even over 34 nm. These measurements put DNA among the longest and most conductive molecular wires reported to date.

Next, DNA CT with multiplexed chips is extended to the electrochemical detection of methyltransferases, proteins that are attractive targets because of their prominent role in the initial stages of many types of cancer. Electrochemical detection of binding and activity by these proteins is achieved by two different methods. First, DNA-binding and base-flipping by these proteins disrupts the DNA π-stack and may be used for direct "signal OFF" detection. Using this method, the concentration- and cofactor-dependence of *Sss*I methyltransferase, the bacterial analog of human methyltransferases, are examined. Second, methylation-conferred protection of DNA against cutting by a

restriction enzyme may be used for "signal ON" detection of methyltransferase activity. With this approach, the use of both unmethylated and hemimethylated DNA substrates is demonstrated for the sensitive detection of both bacterial (*Sss*I) and human (Dnmt1) methyltransferase activity. Importantly, the electrochemical format of these assays requires minimal equipment, is low cost, and may be easily applied to high throughput studies, making it an accessible option for a variety of research and clinical settings.

Alongside work with this surface, electrochemical platform, a single molecule, carbon nanotube-DNA (CNT-DNA) platform is also used to evaluate DNA CT over increasing distances and to detect protein binding. CNT-DNA devices consist of a single molecule of DNA that is made to bridge a gap cut in a CNT covalently, such that current flow through the device is DNA-mediated. Upon introduction of DNA bridges of varying length (15-mer, 60-mer, and 100-mer), the device resistance is minimally affected, echoing the result of long distance electrochemistry experiments. These devices are also used to detect *Sss*I methyltransferase binding by the direct "signal OFF" method used with multiplexed chips; DNA-binding and base-flipping disrupts DNA CT and shuts off current flow through the device. CNT-DNA devices are used to electronically measure the sequence-specific, cofactor-dependent, and reversible binding of *Sss*I. DNA methylation catalyzed by *Sss*I is also detected based on its alteration of the protein-binding affinity of the device. This detection approach, which relies on DNA as both a recognition element and electrical transducer, represents a unique strategy for the specific, single molecule detection of protein binding and activity.

Table of Contents

List of Figures

Chapter 1

Chapter 2

Chapter 3

Chapter 4

Chapter 5

Chapter 6

List of Tables

Chapter 5

Chapter 6

Chapter 1

Platforms for the Study and Application of DNA Charge Transport

Adapted from Muren, N. B., Olmon, E. O., and Barton, J. K. (2012) *Phys. Chem. Chem. Phys. 14*, 1375-13771, and Sontz, P. A., Muren, N. B., and Barton, J. K. (2012) *Acc. Chem. Res. 45*, 1792-1800.

Introduction

The structure of double helical DNA, with two dynamic strands of complementary bases that encode a meaningful sequence, has long been conceptualized as an elegant construct for the storage, expression, and transmission of the genetic instructions of life. Beyond the capacity to manage information, though, this structure also imparts DNA with the capacity to conduct charge; the continuous π-stacked array of heterocyclic aromatic base pairs that extends down the helical axis forms an efficient path for long-range charge transport (1, 2). The importance of DNA-mediated charge transport (DNA CT) in directing biological processes is just now being illuminated, and this property shows great promise for use in nanoelectronics and biosensing applications.

Since the initial postulate of DNA conductivity by D. Eley and D. Spivey in 1962 (3), numerous studies, using multiple techniques, have confirmed and expanded our understanding of DNA CT. Data from experiments in solution, on surfaces, and with single molecules, collectively provide a broad and consistent perspective on the essential characteristics of this chemistry (1, 2). For systems in which donors and acceptors are electronically well coupled to the π-stack, DNA CT can proceed over long molecular distances. However, this process is remarkably sensitive to perturbations in base pair stacking.

This thesis encompasses work on both fundamental measurements of DNA CT over long distances and the use of this sensitive chemistry for protein biosensing. These exciting branches of study are only possible because of the strong foundation from which they extend. Our thorough understanding of the defining attributes of DNA CT, built with experimental data from diverse platforms, is outlined in this first chapter. Specific

focus is given to ground state electronic platforms, including DNA-modified electrodes and carbon nanotube-DNA (CNT-DNA) devices, as research for this thesis was performed with these platforms. Subsequent chapters describe work that builds up and out from this strong foundation, toward a broader understanding and practical applications of DNA CT.

Diverse Platforms Reveal the Characteristics of DNA CT

Just like the characteristics of gene expression and inheritance, the characteristics of DNA CT originate from the unique structure of DNA. At the most basic level, *DNA CT is mediated by the overlapping π orbitals of the stacked nucleotide bases*. In fact, the first proposal that DNA might conduct charge was based mainly on structural observations. Eley and Spivey noted that the aromatic bases of DNA, the very bases that encode genetic information, stack next to each other with an interplanar spacing similar to graphite and thus, like sheets of graphite, can form a conductive path of overlapping π orbitals that extends down the helical axis (3) (Figure 1.1). A critical feature that distinguishes the DNA duplex from solid π-stacked materials, though, is that DNA is a macromolecular array in solution, with dynamical changes in π-stacking that occur on the picosecond to millisecond time scales (4).

Several solution, surface, and single molecule platforms that have been developed to probe DNA CT are illustrated in Figure 1.2. DNA CT has been investigated with photophysical methods, appending donors and acceptors to either end of the DNA duplex. Long-range oxidative damage by DNA CT has been examined using DNA-binding photooxidants to promote oxidation of guanines in the duplex from a distance.

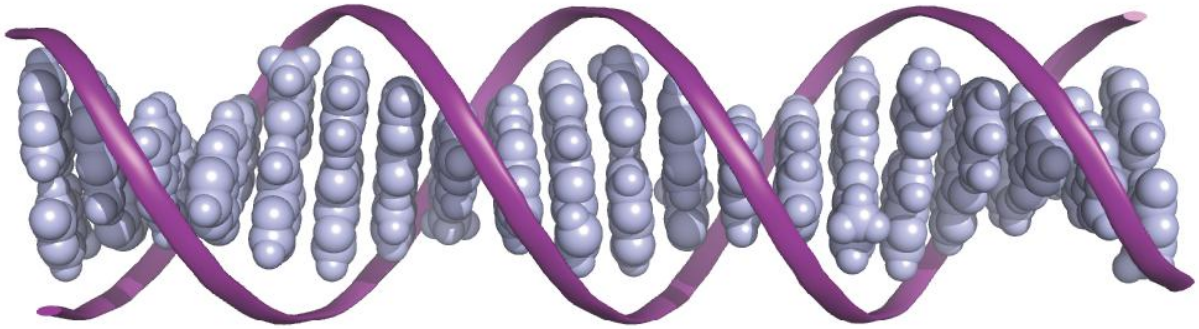

Figure 1.1 The structure of DNA facilitates charge transport. The aromatic bases (grey) of DNA stack with each other like a pile of coins and are wrapped by a sugar phosphate backbone (purple ribbon). The overlapping π orbitals of these stacked bases form a conductive core down the helical axis that mediates the flow of charge. This structure resembles that of stacked graphite sheets and, indeed, undamaged, well stacked DNA is found to have the same conductivity as that measured perpendicular to graphite. Importantly, the conformation of this structure is not static; dynamic motions within this macromolecular array contribute to the mechanistic complexity of DNA CT.

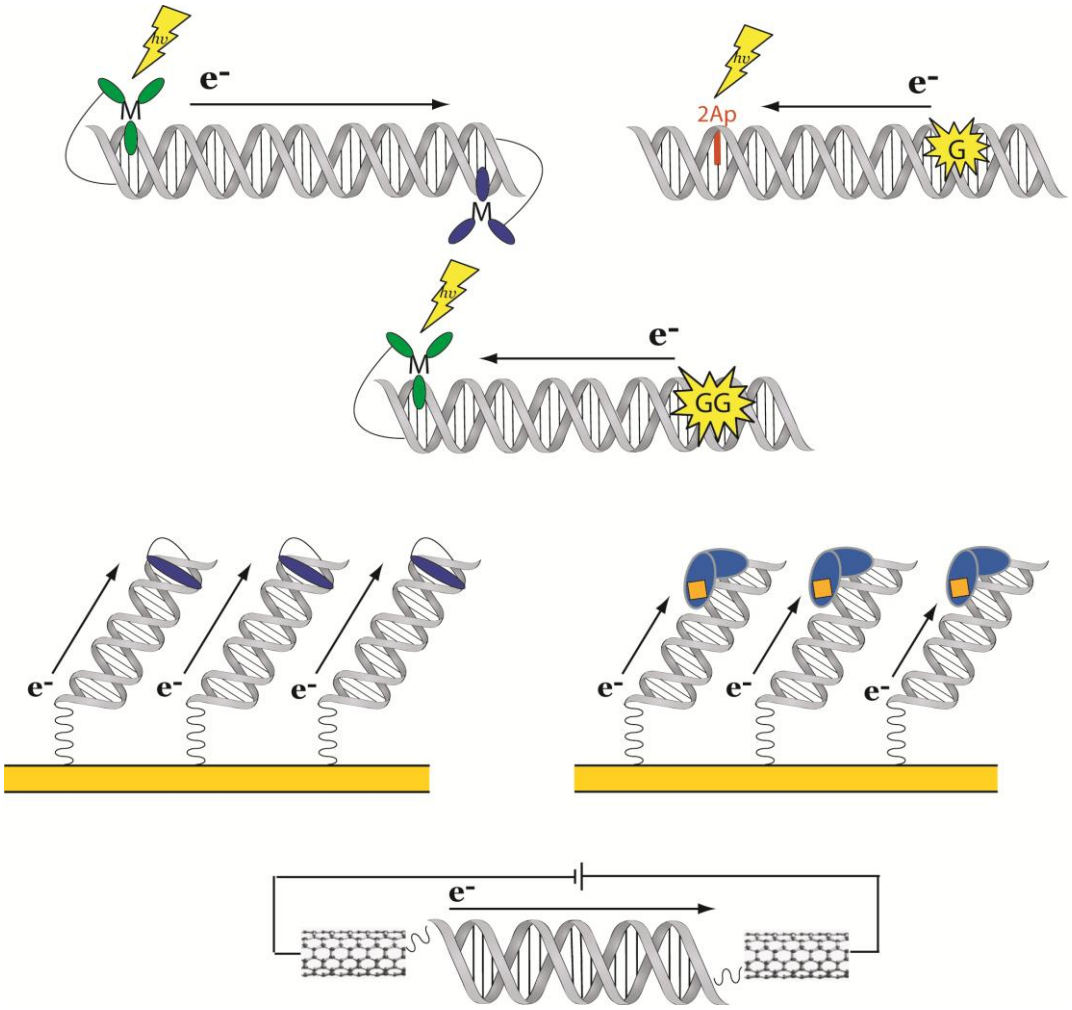

Figure 1.2 Platforms for the study of DNA CT. Top row, spectroscopic solution platforms: (left) photoactivated luminescence and quenching between covalent metallointercalators and (right) photoactivated fluorescence of base analog 2-aminopurine and quenching by guanine. Second row, biochemical solution platform: photoactivated oxidation of guanine doublets by a covalent metallointercalator. Third row, electrochemical surface platforms: DNA-modified electrodes with (left) a covalent redox probe and (right) a bound protein with a redox-active cofactor. Fourth row, single molecule platform: DNA covalently bridges the gap in a carbon nanotube device.

Additionally, DNA CT in the ground state has been probed both in electrochemical studies and in single molecule nanoscale devices.

Remarkably, despite the diversity of techniques employed, a conserved set of characteristics for this process are observed: a) efficient DNA CT is heavily dependent on the proper electronic coupling of the donor and acceptor to the π-stack and between the bases of the DNA bridge, b) DNA CT is highly sensitive to the structural integrity of the stacked path of bases between the donor and acceptor, c) the distance dependence of DNA CT is very shallow, and this parameter is often limited by the platform used to make measurements rather than by the length of the DNA itself, and d) DNA CT is conformationally gated by the dynamic motions of the donor/bridge/acceptor system as they move in and out of CT-active configurations and form domains over which charge can delocalize.

Coupling to the DNA π-Stack

A first, critical feature of DNA CT was identified during initial work to build functional solution platforms to probe this process: *DNA CT requires effective electronic coupling of the donor and acceptor to the base pair π-stack.* A variety of small molecule donors and acceptors that have been used for the study of DNA CT in both solution and surface platforms are illustrated in Figure 1.3. The first platform to measure DNA CT utilized metallointercalators that were covalently attached to 15-mer DNA duplexes in solution (5). The donor and acceptor, $Ru(phen)_2dppz^{2+}$ and $Rh(phi)_2phen^{3+}$ respectively, both have aromatic ligands that allow them to intercalate and interact directly with the DNA π-stack. When the donor is photoexcited, complete quenching occurs due to rapid

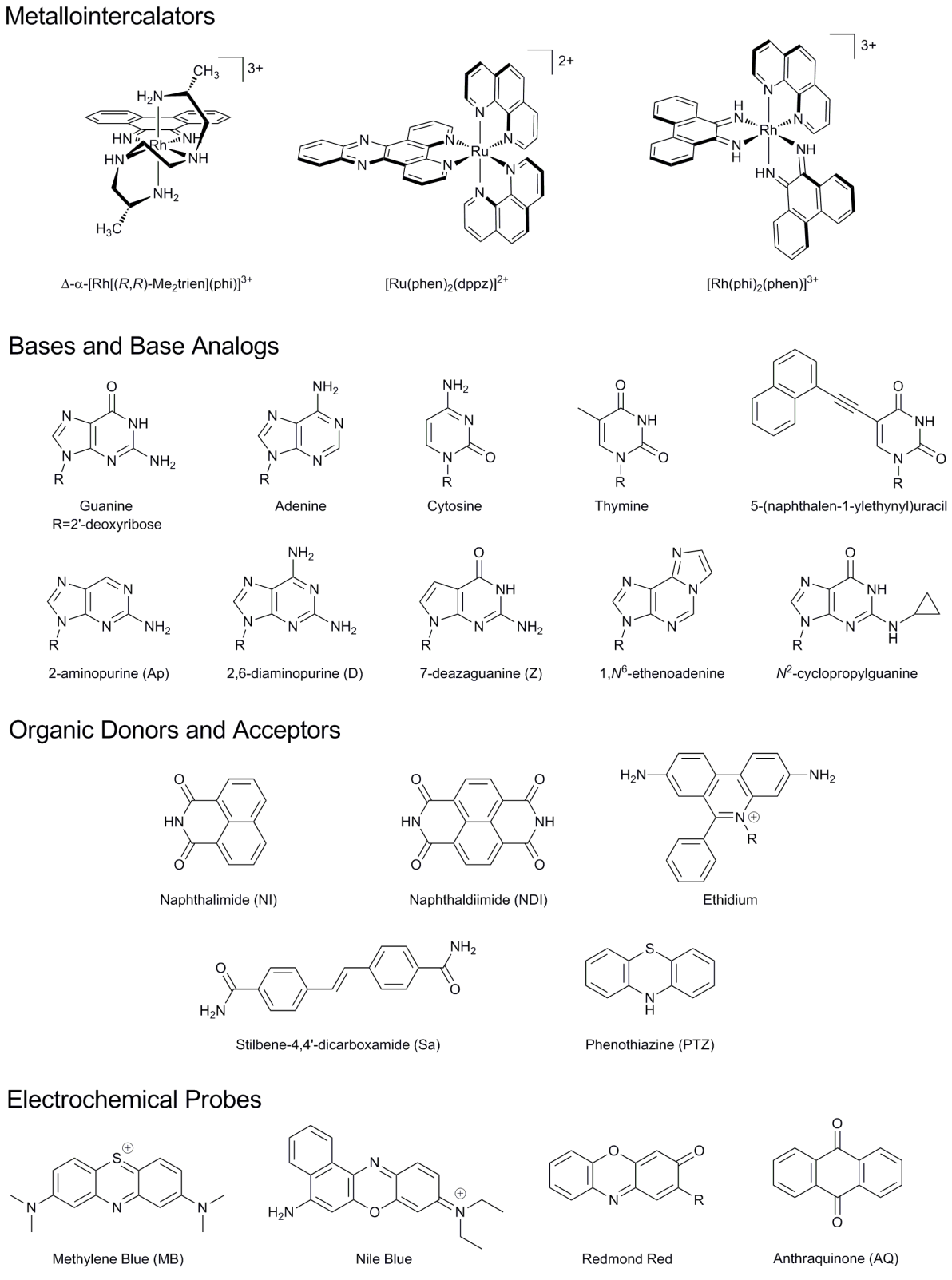

Figure 1.3 Small molecule probes used for the study of DNA CT.

CT to the acceptor. This quenching occurs only when the donor and acceptor are bound to the same duplex and does not occur when $Ru(phen)_2(phen')^{2+}$, a poor intercalator, is substituted for the donor. This result illustrates that DNA CT is necessarily an intraduplex process, which donors and acceptors must access through effective electronic coupling into the base pair π-stack.

In a later variation on this platform, the pendant donors and acceptors were completely eliminated by using modified bases to examine photoinduced DNA CT in the duplex (6). The base analogs 2-aminopurine (2-Ap) or $1,N^6$-ethenoadenine (A_ε) were incorporated into 12-mer DNA duplexes in solution, and used to promote photooxidation of guanine. In these experiments, quenching of 2-Ap occurred far more rapidly and with a far more shallow distance dependence, than did quenching of A_ε. This result is consistent with the different structures of these analogs that allow for well integrated stacking of 2-Ap into the DNA helix and poor stacking of A_ε. Clearly, for effective DNA CT, coupling with the π-stack is key.

Sensitivity to Perturbations of the DNA π-stack

Studies with solution-based platforms also revealed a second important characteristic: *DNA CT is highly sensitive to the integrity of the π-stack of the bases between the donor and the acceptor*. The sensitivity of DNA CT to single base mismatches was first demonstrated in studies of photoinduced quenching of ethidium tethered to DNA by a rhodium complex intercalatively bound and tethered at the other terminus (7). In addition to the loss of quenching by this pair that is observed when the

double helix is melted apart, the introduction of a single base mismatch between the donor and acceptor severely decreases the quenching yield (7).

This exquisite sensitivity to such a subtle structural perturbation as a single base mismatch has been observed across experimental platforms, including surface (8-10) and single molecule (11) platforms which are described in greater detail later in this chapter. These ground state platforms have allowed for the identification of a variety of other distortions to the structure of the DNA π-stack that attenuate DNA CT (Figure 1.4) including a variety of base lesions (12) and protein binding events (13-15). Importantly, it is specifically perturbations to the stacked bases that inhibit the flow of charge; the addition of methyl groups to the DNA bases (15) or the introduction of breaks (nicks) in the sugar phosphate backbone (16) do not affect DNA CT as these modifications do not alter the structure of the π-stack. This sensitivity to perturbations in stacking forms the basis of DNA CT-based electrical biosensors.

Shallow Distance Dependence

As the limits of these experimental platforms were pushed to try to understand the limits of DNA CT itself, another critical characteristic of this chemistry emerged: *the distance dependence of DNA CT is very shallow*. To probe the distance dependence of DNA CT, experiments were performed in solution to measure long-range guanine oxidation from a distal, covalent metallointercalator photooxidant; after irradiation, the location of DNA-mediated photooxidation in the duplex is determined by biochemical sequencing (17, 18). Irrespective of the DNA-bound photooxidant, significant oxidative damage is observed at the 5′-guanine of guanine doublets, the site of lowest oxidation

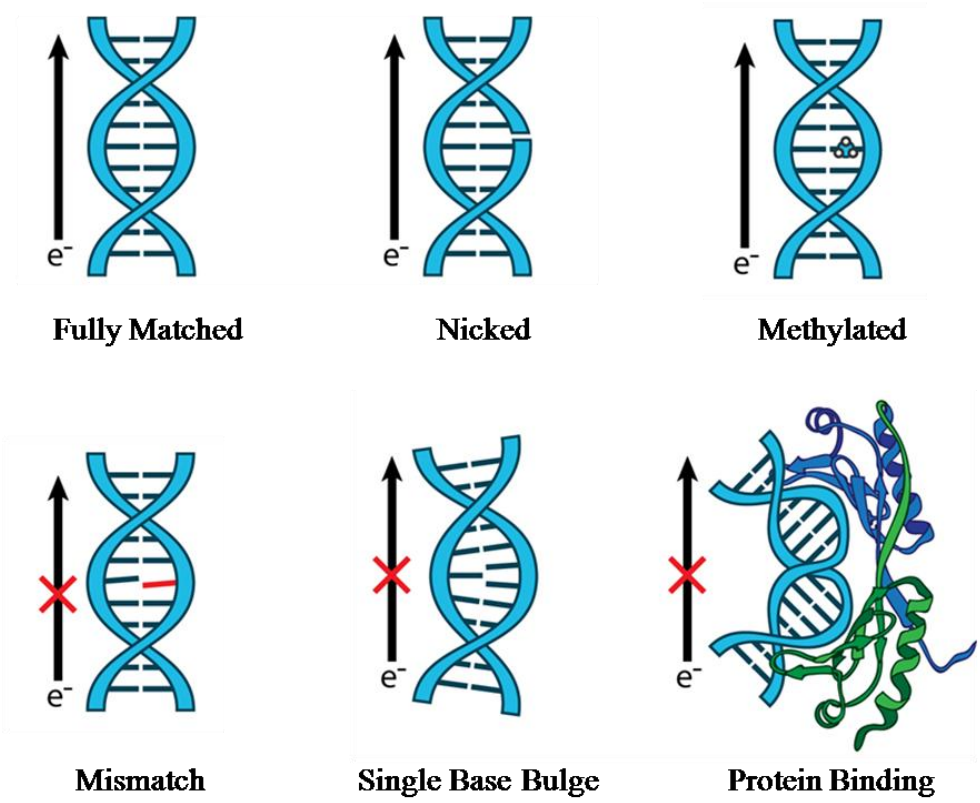

Figure 1.4 Structural perturbations to the base pair π-stack inhibit DNA CT. For efficient DNA CT, bases in the duplex must be well stacked with each other to achieve proper π-orbital overlap and electronic coupling. This occurs naturally in the case of fully matched DNA (top row, left). Nicks in the sugar phosphate backbone (top row, center) and and methylation of the DNA bases (top row, right) do not interfere with the π-stack and thus do not inhibit DNA CT. However, attenuation of DNA CT is observed for perturbations that disrupt the π-stack including single base mismatches (bottom row, left), single base bulges (bottom row, center), and bound proteins that severely kink the DNA (bottom row, right). The attenuation in DNA CT caused by these structural perturbations, and others, has been measured with solution, surface, and single molecule platforms.

potential in the DNA. Indeed, in an oligonucleotide duplex with a Rh intercalator tethered to one end, oxidation is observed not only at the 5′-guanine of the guanine doublet in the center of the duplex, but also at the 5′-guanine of the guanine doublet located near the distal end of the duplex. With this platform, photooxidation that is insensitive to the separation distance up to the longest distance measured, 20 nm (60 bp), was observed (18). Moreover, the integrity of the intervening stack of DNA is critical for the generation of oxidative damage to DNA from a distance, independent of the DNA-bound photooxidant employed.

More recently, the distance dependence of ground state DNA CT was examined electrochemically on a multiplexed electrode surface, as detailed in chapter 3 (10). Using this platform DNA CT was measured to a distal redox probe over 34 nm (100 bp). Remarkably, the redox signal size and the degree of signal attenuation from the incorporation of a mismatched base is the same as that observed for much smaller (17 bp) duplexes (10). Also, like the shorter duplexes (19), the rate of DNA CT through the 100-mer is still limited by the tunneling rate through the alkane-thiol linker. Even with this limit, these measurements indicate that DNA is competitive with the longest and most conductive molecular wires reported to date. Clearly, as indicated by both of these solution and surface experiments, DNA CT occurs at rates and over distances that stretch beyond the physical limits of the platforms that have been designed thus far to make such measurements. Indeed a fundamental shift is necessary to imagine the scale on which DNA can rapidly and sensitively transport charge and understand the implications of this vast capacity for biology.

Conformational Gating and Charge Delocalization

In work to understand a mechanism for DNA CT, evidence for a fourth key feature of this chemistry was observed: *DNA CT is conformationally gated by the alignment of CT-active domains over which charge can delocalize*. The important role of structural dynamics in mediating DNA CT became clear in early observations on the effect of sequence-dependent flexibilities on DNA CT, and from this work it was proposed that long distance CT might occur through hopping between delocalized domains (20). The extent of delocalization, and the resulting physical definition of a domain, would clearly depend heavily on the dynamic motions that allow segments of the assembly to achieve CT-active conformations. Femtosecond spectroscopy experiments in solution provided strong support that dynamic motions within the DNA structure actually gate DNA CT; the CT rate is determined not by individual bases but by the simultaneous alignment of multiple components of the assembly, including the bases, the donor, and the acceptor, into CT-active conformations (21).

The formation of discrete domains of delocalized charge was illustrated in greater detail by solution fluorescence studies in which a periodic length dependence was observed for the quenching yield of photoexcited 2-Ap by guanine across adenine tracts (22). That CT through the DNA duplex essentially encounters a gate at each sequential length of 3–4 base pairs indicates that this length is ideal for the formation of a CT-active, delocalized domain (22). A similar periodic length dependence was measured for CT between photoexcited $[Rh(phi)_2(bpy')]^{3+}$ and N^2-cyclopropyldeoxyguanine (^{CP}G) (23). Recently, it was observed that the mechanism of DNA CT is actually dictated by the capacity of different lengths of DNA to form delocalized domains (24). For this

work, ^{CP}G oxidation by photoexcited 2-Ap across adenine-tracts was measured. For DNA CT over a full turn of the DNA helix, a coherent CT mechanism is favored. For segments that are not integer multiples of the 3–4 base pair length that is ideal for the formation of a delocalized domain, the ^{CP}G oxidation yield decreases, indicating that CT must switch from a coherent to incoherent mechanism (24).

Consideration of conformational gating and charge delocalization is critical for a viable mechanistic description of DNA CT. However, the two most prominent models used to describe DNA CT, superexchange and localized hopping, do not account for the impact of these structural dynamics. Not surprisingly, significant inconsistencies exist between the experimentally observed characteristics of DNA CT and these models (25). In the superexchange model, the orbitals of the DNA bridge are higher in energy than the donor and acceptor such that charge must tunnel through and only virtually occupy the DNA bridge (26). Thus, the probability of tunneling and virtual occupation of the bridge becomes less and less favorable with increasing distance between the donor and acceptor, and an exponential distance dependence is expected (26). The shallow distance dependence observed for DNA CT over long distances is wholly incompatible with superexchange in DNA (10, 25).

In localized hopping, the orbitals of the DNA bridge are close in energy to the donor and acceptor and thus short hops between low-potential guanine sites in DNA that actually occupy the bridge are predicted to result in a much more shallow distance dependence (26-28). However, this mechanism is not sufficient to explain DNA CT through adenine tracts (29). Also, in experiments involving guanine oxidation over various lengths of T, A, and mixed A/T bridges, it is the flexibility of the intervening

sequence, not the length of the tract, that is the dominant factor in determining the oxidation yield; the introduction of a GC segment within TA tracts actually decreases the yield of DNA CT (20). The exquisite sensitivity of DNA CT to single base mismatches that has been observed for all platforms is also poorly explained by a hopping mechanism. The suggestion that guanine-containing mismatches interrupt DNA CT by proton abstraction (30) is inconsistent with experimental observations in which the degree of CT attenuation correlates with the thermodynamic destabilization of the mismatch (8).

Another inconsistency with the localized hopping mechanism is routinely observed in electrochemistry experiments where the potentials that are applied for reduction of the small molecule redox probe are far below the reduction potentials of the bases (up to 1 V difference) (31). Given this discrepancy, charge injection to an isolated base for localized hopping would be extraordinarily slow, at least 4–5 orders of magnitude slower (25) than the linker-limited rate of 30 s^{-1} that is measured through our DNA-modified electrodes (10, 32, 33). Thus, to account for the observed DNA CT on electrochemical platforms, the CT mechanism must necessarily involve a decrease in the energy gap between the Fermi level of the electrode surface and the oxidation potential of the individual bases; this cannot be explained within the bounds of the localized hopping mechanism.

The inclusion of conformational gating and charge delocalization in a mechanistic description of DNA CT helps to reconcile these inconsistencies. While allowing the shallow distance dependence that comes with hopping between discrete domains, these phenomena provide reason for the impact of base dynamics and sequence flexibility.

Conformational gating and charge delocalization also help to explain why such severe attenuation of DNA CT is observed when the structure of the DNA π-stack is distorted. Structural perturbations to the π-stack cause the affected bases to preferentially adopt un-stacked conformations. When it comes to the formation of delocalized domains that facilitate CT, a primarily un-stacked base functions like a rotating disc in a multi-disk combination lock that is stuck on the wrong number. Although the other disks might turn fluidly to the correct combination the disk that is stuck in the wrong orientation will still prevent the lock from opening. Likewise, the bases surrounding a lesion, mismatch, or bound protein may be free to move into CT-active conformations, but the un-stacked base disrupts the formation of a domain over which charge could delocalize, dramatically shutting off DNA CT. Charge delocalization additionally accounts for the fast CT rates that are measured electrochemically: states in which the charge is delocalized over large domains would necessarily be lower in energy than a state in which the charge is localized on an individual base, thus enabling charge injection at the applied potentials used in electrochemistry experiments.

Ground State Platforms for DNA CT

In contrast to solution-based strategies for the study of electron transfer, surface and single molecule platforms provide a solid handle to anchor study molecules into defined conformations (34). In the case of DNA-modified electrodes, this handle is the electrode surface which replaces the donor and allows for the controlled application of a potential (31, 35, 36) In the case of carbon nanotube-DNA (CNT-DNA) devices, this handle is the carbon nanotube, which isolates a single DNA molecule within a defined

electrical circuit (11, 15). While solution studies necessarily involve excited-state measurements, DNA-modified electrodes and CNT-DNA devices allow for the study of ground-state electron transfer processes. Importantly, these platforms are highly compatible with the aqueous, buffered environments that biomolecules require to maintain their native, biologically relevant structure. The isolation of a DNA-mediated path as the only route for CT in these platforms has allowed for the study of fundamental characteristics of DNA CT as well the application of this sensitive chemistry for electrical biosensing. Significantly, the characteristics of DNA CT, identified first in solution studies and outlined in previous sections, are consistently observed for these ground state platforms.

DNA-Modified Electrodes

To form DNA-modified electrodes, DNA duplexes are modified with a linker on one end that allows for their self-assembly into monolayers on an electrode surface. Most commonly, alkanethiol linkers (37) are used for the attachment to gold electrodes, but for experiments that require a wider potential window pyrene linkers (38) allow for attachment to graphite electrodes. The Barton laboratory has thoroughly characterized the structure of these assemblies with a variety of techniques including radioactive labeling (13, 37, 38), atomic force microscopy (13, 38–40), and scanning tunneling microscopy (41). These studies have confirmed that film density can be controlled by Mg^{2+}, which promotes dense packing (13, 37, 38). Additionally, the duplexes adopt an upright orientation with an angle relative to the surface that can be modulated by the applied potential; in the absence of a potential, duplexes are oriented at a ~45° angle to

the surface and with the application of positive or negative potentials, the anchored duplexes are attracted to or repelled by the surface, respectively, from this set point (38, 39). Thus, the DNA duplexes function as highly sensitive extensions of the electrode surface into solution.

In order to study CT that is mediated by these DNA extensions, a redox-active probe moiety is incorporated at or near the end of the DNA that is distal from the surface. For this purpose, noncovalent (8, 12, 37, 38, 42-45) and covalent (9, 10, 13, 14, 16, 19, 32, 33, 46, 47) redox probes have been employed as well as DNA-binding proteins that are redox-active (48-53). After assembly of the DNA monolayer, the modified electrode is treated with a backfilling agent, such as mercaptohexanol, to passivate the surface against direct reduction of the redox probe and to remove nonspecifically adsorbed DNA. In the completed DNA-modified electrode, CT is mediated from the electrode surface to the redox probe via the intervening path of well stacked DNA bases. Importantly, experiments with this platform are all performed in aqueous, buffered solution such that the DNA maintains a native, CT-active conformation.

Noncovalent Redox Probes

In the development of this platform, noncovalent, redox-active small molecules were initially used as probes for DNA CT. For these experiments, electrodes with densely packed DNA films are required in order to prevent access of the freely diffusing probe molecules to the surface. In these dense films, the probe is restricted to binding at the top of the duplex, thereby allowing for the interrogation of DNA CT in duplexes containing a single base mismatch (37, 42). The mismatch sensitivity of a variety of

small molecule redox probes was investigated including the DNA groove binder $[Ru(NH_3)_6]^{3+}$ and the DNA intercalators methylene blue (MB), $[Ir(bpy)(phen)(phi)]^{3+}$, and daunomycin (42). As in solution studies, it was observed that a close interaction between the probe and the DNA π-stack is essential for reduction that is sensitive to a mismatch and thus DNA-mediated; reduction of the DNA intercalators was significantly inhibited by the presence of a mismatch while reduction of the DNA groove binder $[Ru(NH_3)_6]^{3+}$ was unaffected (42).

A more in-depth look at the behavior of $[Ru(NH_3)_6]^{3+}$ as compared to MB in this platform clearly illustrates how the DNA functions as an extension of the electrode surface for molecules that can properly access the DNA CT pathway of the π-stacked bases (43). For both $[Ru(NH_3)_6]^{3+}$ and MB, high salt conditions decrease the number of molecules that are reduced, reflecting the inhibition of electrostatic and intercalative DNA binding modes, respectively. This result indicates that the reduction of both probes is dependent on their tight binding to DNA. However, polymerization of 2-naphthol to completely passivate the electrode surface against direct probe interaction reveals fundamental differences in the pathways by which these probes are reduced. While reduction of MB is minimally affected by this total passivation (~3% signal reduction), reduction of $[Ru(NH_3)_6]^{3+}$ is decreased significantly (~70% signal reduction) (43). Thus, while $[Ru(NH_3)_6]^{3+}$ is reduced directly at the electrode surface and the DNA functions simply as a charged guiderail that helps to facilitate its diffusion toward the surface, MB does not require access to the surface for its reduction. Instead, the ability of MB to intercalate into the DNA duplex and interact directly with the π-stacked bases allows it to access a DNA-mediated pathway for reduction that extends through the DNA, above the

passivated surface; here the DNA functions as an electrical conduit through which charge is conducted from the surface directly to the distally bound probe.

Additional work with this platform showed that not only must the redox probe be well coupled into the DNA π-stack, but the proper stacking of the bases themselves is also critical for DNA CT to occur. Further work with the MB probe showed that its DNA-mediated signal may be amplified in an electrocatalytic cycle with ferricyanide (42) and used to sensitively detect all base mismatches (8) and a variety of DNA lesions (12) by an attenuation of DNA CT to the MB redox probe. Electrochemical measurements of DNA CT through A-form DNA (DNA/RNA hybrid duplexes) showed that, like B-form DNA, this conformation can efficiently mediate charge through stacked bases, and mismatches within its sequence are readily detected (44). In contrast, Z-form DNA, which is more rigid and has significantly less intrastrand base stacking than B- and A-form, shows significantly attenuated DNA CT (44). Incorporation of a 3′-endo-locked nucleotide into B-form DNA, which is known to disrupt base stacking, causes signal attenuation similar to that caused by the incorporation of a mismatch (45). However, incorporation of this modified nucleotide into A-form DNA, which can better accommodate its structure into the base stack, does not show attenuation in DNA CT.

Covalent Redox Probes

The development of covalent redox probes for the DNA-modified electrode platform opened the door for more precise characterization of DNA CT, as the location of the probe in the duplex could be defined. Initial work made it clear that, like noncovalent probes, electronic coupling to the π-stack is absolutely required for the DNA-mediated

reduction of covalent probes. For MB that is covalently attached by a flexible alkane linkage to the distal end of the DNA, a redox signal is observed for low ionic strength conditions that permit intercalation of the tethered MB into the duplex (43). However, in a high salt environment that discourages intercalation, no redox signal for MB is observed despite its attachment to the DNA (43). This result mirrors the ionic dependence of the DNA-mediated reduction of freely diffusing MB and again highlights the importance of the direct electronic connection between the redox probe and the π-orbitals of the stacked DNA bases for DNA CT to occur; intercalation is still required for reduction of the covalent MB probe as the σ-bonds of the alkane linkage alone do not provide this electronic connection.

Intercalation is not the only mechanism by which to establish this electronic coupling to the π-stack. In a study that investigated different linkages to covalently attach the redox probes anthraquinone (AQ) or 2,2,6,6-tetramethylpiperidine 1-oxyl (TEMPO) directly to a modified uridine base, rigid acetylene linkages allowed for the DNA-mediated reduction of both probes that was sensitive to the incorporation of mismatches (32). In contrast, alkane linkages for both probes resulted in significantly weaker redox signals that were not influenced by mismatches. In these cases, although the acetylene holds the probe rigidly away from the DNA and prevents interaction directly with the base stack, this conjugated linkage still provides a connective path that electronically couples the probe to the base stack. The alkane linkages do not create this electronic conjugation and, in contrast to the previous example with MB, do not structurally allow for direct interaction between the redox probe and DNA π-stack. These examples illustrate an added level of complexity to the use of noncovalent probes in

measuring DNA CT processes: the covalent linkage now functions as the critical gatekeeper that can either promote or prevent the redox probe from achieving a CT-active conformation. In addition to MB, AQ, and TEMPO, the linkages and conditions necessary for the DNA-mediated reduction of a variety of other covalent redox-active moieties have been described including daunomycin (13, 16, 19, 33), disulfide bonds (46), Redmond Red (47), and Nile Blue (9, 10, 14) (Scheme 1.1).

Covalent tethering of the redox probe makes it possible to use this platform for more detailed, fundamental characterization studies of DNA CT. The directionality of the mismatch effect on DNA CT was clearly established; incorporation of a C·A mismatch in the DNA between the gold surface and a covalent daunomycin probe causes significant signal attenuation, while the reverse case, in which the mismatch is located above the daunomycin relative to the surface, shows no signal attenuation (33). The incorporation of nicks in the sugar-phosphate backbone of the duplexes that make up the DNA-modified electrodes causes no signal attenuation of a covalent daunomycin probe (16). In contrast, the incorporation of a single base mismatch causes significant signal attenuation for both intact and nick-containing DNA, again illustrating that DNA CT propagates through the stacked base pairs, not the sugar-phosphate backbone (16).

Additionally, covalent tethering opens the door for ground state distance dependence studies of DNA CT that are not possible in solution platforms or with noncovalent electrochemistry. Initial experiments in this area demonstrated that the covalent placement of daunomycin at different positions along a 15-mer duplex (50 Å) does not influence the signal intensity or splitting of the cathodic and anodic peaks as measured by cyclic voltammetry (33). For DNA CT over similar DNA distances, the

contribution of the alkanethiol tether that attaches the DNA to the gold electrode on the rate of DNA CT was investigated and it was determined that the number of methylene units in the tether absolutely dominates the observed CT rate (19). These results echoed the shallow distance dependence that had been observed in solution experiments. Extension of DNA-modified electrodes from single electrodes to multiplexed chips (chapter 2) allowed for the more complex experiments and precise side-by-side controls that are needed for reliable measurements of DNA CT over very long distances (9). Using this multiplexed platform, a shallow distance dependence for DNA CT over 100 base pairs (340 Å) to a covalent Nile Blue redox probe was measured (chapter 3) (10).

The use of covalent probes eliminates concern about direct surface reduction of freely diffusing probes, making it possible to use low density DNA films and expand this platform to biosensing applications, such as the detection of nucleic acid hybridization and protein binding, which require spatial access to the surface-tethered DNA duplexes. In developing this technology for the electrochemical detection of DNA-binding proteins and their activity, proteins that perturb the DNA π-stack upon binding were found to cause a dramatic attenuation in the DNA-mediated signal of the distally attached redox probe (13, 14). This effect was sensitively measured for the DNA methyltransferase *Hha*I and uracil-DNA glycosylase (UDG), which both flip a base out of the DNA base stack upon binding, as well as the TATA-binding protein (TBP), which kinks the DNA by 90°. Proteins that do not bind DNA, such as BSA, or proteins that bind but do not distort the DNA, such as the *Pvu*II restriction enzyme bound to its methyl-protected restriction site, do not cause this signal attenuation.

As an important and informative control, the effect of binding by wild-type *Hha*I and the mutant Q237W of *Hha*I was compared (13). Wild-type *Hha*I inserts glutamine 237 into the DNA base stack to flip out the target base, and this disruption of the DNA CT path results in significant signal attenuation of the redox probe. However, binding by the Q237W mutant of *Hha*I results in only minimal attenuation of the redox signal. In this case, the Q237W mutant inserts tryptophan into the base stack instead of glutamine, and this aromatic, heterocyclic amino acid fills the place of the flipped base in the π-stack, restoring the DNA-mediated flow of charge to the probe (13). This control underscores the central role of the stacked DNA bases in forming a conduit for DNA CT. Building on these initial studies, work toward the multiplexed, electrochemical detection of human methyltransferases has been performed (chapters 5 and 6). This work is aimed at the development of clinical assays for methyltransferase activity that may be used for cancer screening and drug development.

Proteins as Redox Probes

Small molecules are not the only redox-active players that can participate in DNA CT. The DNA-bound potentials of numerous proteins with redox-active cofactors, such as [Fe-S] clusters, may be measured with the DNA-modified electrode platform. For these experiments, electrodes are assembled with DNA that is modified only with a thiol tether; upon protein binding, redox-active cofactors within the protein that are well coupled to the DNA π-stack serve to report a DNA-mediated CT signal (48). Like small molecule redox probes, the integrity of the DNA π-stack is critical for strong electrochemical signals from these proteins; the incorporation of intervening abasic sites,

lesions, or mismatches in the DNA-modified electrode significantly attenuate the redox signal (48-50).

Such biologically integrated redox probes can be used to monitor protein activity that involves the coupling of the redox cofactor to the π-stack. For example, the flavin cofactor of the light-activated DNA repair enzyme photolyase can be used to electrochemically monitor this protein as it binds and repairs pyrimidine dimer lesions (49). Upon initial binding of photolyase to thymine dimer-containing DNA, a weak signal from the flavin cofactor is observed due to the destacked lesion that disrupts DNA CT and inhibits proper coupling of the flavin cofactor to the π-stack. Upon photoactivation, the redox signal gradually increases as photolyase repairs the thymine dimer and restores efficient DNA CT to the flavin cofactor. Following this, the redox signal gradually disappears as the protein dissociates from the now repaired DNA.

The profound ramifications of strong coupling to the DNA π-stack are perhaps best illustrated by extensive work with the [4Fe-4S] cluster-containing base excision repair enzymes MutY, EndoIII, and AfUDG (48, 50-53). In electrochemical studies of these proteins, DNA-modified electrodes are essential for measuring relevant DNA-bound potentials (51). Electrochemical studies of EndoIII on bare graphite electrodes and DNA-modified graphite electrodes reveal that DNA binding shifts the redox potential of the $[4Fe\text{-}4S]^{2+/3+}$ couple by >200 mV and stabilizes the $[4Fe\text{-}4S]^{3+}$ state, thereby converting the cluster into a form that is redox-active under physiologically relevant conditions (51). Importantly, the redox state of the cluster influences the binding affinity of EndoIII for DNA, and in this way, long-distance, DNA-mediated redox of the cluster can influence protein binding and localization (52).

Multiple experiments following this observation support a model in which this coupling and DNA-mediated redox activity is essential for the search process that these proteins undertake to efficiently locate and repair damage in the genome (52). Proteins that are well coupled to the DNA π-stack and thus can access DNA CT have the capacity to participate in long distance, DNA-mediated signaling to coordinate search efforts and promote the localization of repair proteins around sites of DNA damage. An electrochemical study of EndoIII variants with mutations around the [4Fe-4S] cluster clearly illustrates this model (53). Mutants that exhibit large electrochemical signals and are thus well coupled to the DNA are also proficient at localizing near DNA damage, as observed by atomic force microscopy. On the other hand, EndoIII mutants that exhibit small electrochemical signals, and thus poor coupling to the DNA, do not localize near mismatches. Thus, the degree of coupling of the [4Fe-4S] cluster to the π-stack relates directly to the ability of the protein to utilize DNA CT for long-distance signaling to locate and respond to DNA damage. These exciting experiments are just the beginning of work that suggests a critically important role for DNA CT as a signaling mechanism to coordinate complex biological processes.

Carbon Nanotube-DNA Devices

Conductivity measurements of single molecules allow for an understanding of the fundamental electronic properties of these molecules that cannot be achieved through bulk platforms (54). However, the study of single molecule, ground state, DNA conductivity presents a significant challenge that is clearly foreshadowed by observations from bulk solution and electrochemical experiments; the nature of the electrical

connection to the DNA and the integrity of the π-stacked duplex structure are critical to make meaningful conductivity measurements. Most initial experiments of single or few molecules of DNA by others utilized platforms with inconsistent or poorly defined electrical connections, and the DNA was not maintained in an aqueous, undamaged state. Not surprisingly, these experiments measured a full range of electrical behavior for DNA from insulating to semiconducting to conducting (55-58).

Experiments using AFM (59) and STM (41, 60, 61) of DNA films provided more consistent measurements as these methods involve better defined electrical connections for the DNA duplexes and allow measurements to be taken under aqueous conditions. Measurements from these experiments included low resistances for well matched DNA and increased resistance with a single base mismatch. However, since at least dozens of molecules can make contact with the probing tip in these experiments, these platforms did not allow for truly single molecule measurements of DNA conductivity.

Carbon nanotube (CNT)-based devices provide a platform that has well defined electrical contacts and has previously been used to measure the electrical properties of a variety of small molecule molecular bridges (54, 62). To fabricate CNT-DNA devices, CNTs are grown on silicon wafers and metal source and drain electrodes are patterned over them to incorporate them into electrical circuits. Ultra high resolution electron beam lithography is then used to cut gaps of defined width in the CNTs. This method of cutting results in carboxylic acid functionalization at each terminus of the CNT gap, such that amine-modified DNA can be reacted to bridge the gap covalently. The width of the gap can be tuned to fit different lengths of DNA precisely. Importantly, these devices are compatible with an aqueous environment for DNA, and the similar diameter of the CNT

and DNA duplex restricts covalent attachment to a single duplex within the gap. The source-drain current of these DNA-bridged devices can then be measured as a function of gating voltage to characterize the conductivity of the DNA relative to the un-cut device.

Single Molecule Measurements of DNA Conductivity

Using these DNA-CNT devices, the resistance of DNA duplexes 6 nm in length was measured as 0.1–5 MΩ (11). Importantly, this range encompasses the resistance value (~ 1 MΩ) that would be expected through layered sheets of graphite of similar dimensions (11). Thus, this platform makes it possible to validate the initial postulate of DNA conductivity by Eley and Spivey, that the π-stacked bases of DNA might conduct charge in the same way as the structurally similar stacked π orbitals of graphite sheets (3).

The covalent attachment of both 5′ and 3′ ends of one strand of the duplex within the CNT gap yields a robust device to which different, noncovalent, complementary strands may be hybridized. In this way it is possible to cycle between resistance measurements of matched and mismatched duplexes on the same device (Figure 1.5). Such experiments show that charge flow through these devices is exquisitely sensitive to the introduction of a variety of single base mismatches, with resistances increasing ~300-fold upon hybridization of a mismatched strand (11). These devices are also readily recognized and cut by a restriction enzyme, which also shuts off the conductivity of the device. This sensitivity to mismatches and restriction activity, which mirror results seen with solution and electrochemical platforms, shows that resistance measurements are indeed from DNA CT through single duplexes that adopt biologically relevant conformations.

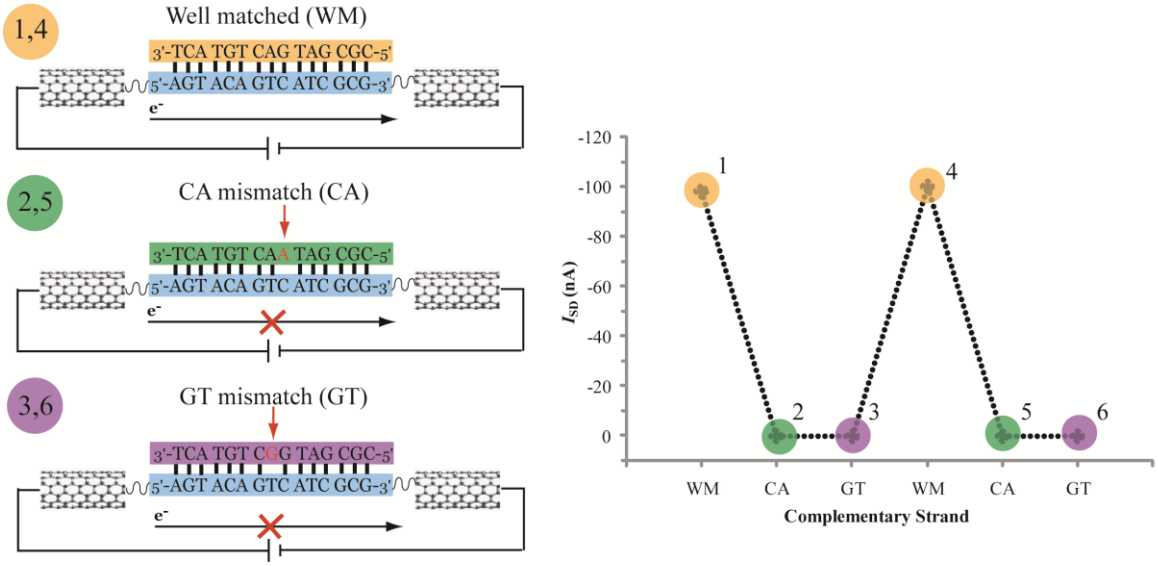

Figure 1.5 Single molecule experiments illustrate the sensitivity of DNA CT to mismatches. Left illustration: DNA CT is measured in a single DNA duplex that covalently bridges a gap in a carbon nanotube device. One strand (blue) is covalently attached by its 3′ and 5′ ends while the other strand can be freely exchanged between well matched complements (orange) and strands that introduce a single base mismatch (green, purple). Right plot: the source-drain current (I_{SD}) measured at the gating voltage V_G = -3 V is shown for the series of well matched and mismatched strands in the device. The colors and numbers of the points in the series correspond to the different strands in the left illustration. Clearly, current through the device is cut off in duplexes that contain a single base mismatch and restored when the bridging DNA strand is re-hybridized with its well matched complement.

Building on these studies, this single molecule platform has now been used to measure the distance dependence of DNA CT as well as detect the binding and activity of *Sss*I methyltransferase (chapter 4) (15). Initial resistance measurements of single DNA molecules of varying length suggest agreement with the shallow distance dependence measured in solution and on electrochemical surface platforms. Experiments with *Sss*I methyltransferase also mirror results from electrochemical surface platforms: the binding and base-flipping action of *Sss*I shuts off current flow through the device in a manner that is sequence-specific, cofactor-dependent, and reversible (15).

Summary

Studies of DNA CT with photooxidation, spectroscopy, and electrochemistry, in solution, on surfaces, and with single molecule techniques, and using a variety of donors and acceptors have established a solid, experimentally-based foundation to understand this chemistry. These complementary vantage points are collectively valuable as they serve to validate shared characteristics and cast light on pieces of the DNA CT puzzle that are only visible from a particular experimental platform. Despite the diversity of platforms employed, a common set of characteristics for CT processes that are mediated by DNA have been consistently observed. Namely, the electronic coupling of the donor and acceptor to the π-stack of DNA is required to access DNA CT. The CT itself is highly sensitive to the structural integrity of the stack of bases between the donor and acceptor pair. For donors and acceptors that are well coupled to structurally undisturbed, undamaged DNA duplexes, the DNA can mediate CT that is rapid and has an extremely shallow distance dependence which allows this process to efficiently occur over very long distances. Additionally, this rapid rate is gated by the dynamic motions of the bases, donor, and acceptor as they move in and out of CT-active conformations.

Despite these consistent observables, a mechanism for DNA CT is still not well defined. DNA CT clearly does not fit within the bounds of either superexchange or hopping models. Experiments suggest that transient delocalization of charge across multi-base domains must necessarily play an important role. Given the dynamic and structural complexity of the DNA molecule and the variability introduced by different sequences, donors, and acceptors, it is likely overly restrictive to confine this process to a single mechanistic description. Instead, as we continue to shed light on DNA CT from

diverse experimental viewpoints it will be important to validate known characteristics and integrate new observations into a mechanistic understanding that is consistent with the complexity of this process.

The thesis work described here utilizes DNA CT chemistry and builds upon the strong foundation that has been established by these solution, surface, and single molecule platforms. Chapter 2 describes the extension of the DNA-modified electrode platform to a multiplexed format that opens the door for more complex experiments with side-by-side controls. This multiplexed platform is put to use in Chapter 3 for the ground state measurement of DNA CT over 34 nm (100 base pairs). Chapter 4 describes single molecule work with CNT-DNA devices to also evaluate DNA CT over increasing distances, as well as detect *Sss*I methyltransferase binding and activity. Finally, Chapters 5 and 6 describe the development of the multiplexed, DNA-modified electrode platform for biosensing, both for the general detection of DNA-binding proteins and specific detection of methyltransferase activity.

This body of work reflects the current direction of studies on DNA CT chemistry that extends from a fundamental, multifaceted understanding of this complex process. This exciting trajectory is propelled by what was learned from the question "*How does DNA CT work?*" toward new lines of inquiry: *How does biology utilize DNA CT to coordinate proteins in their efforts to meet complex cellular challenges? How can we utilize the unique conductive properties of DNA CT in the development of nanoelectronic and biosensing devices?* What we have already learned about DNA CT indicates that the pursuit of these questions is a promising investment for the further elucidation and application of this exquisitely sensitive chemistry.

References

1. Genereux, J.G. and Barton, J.K. (2010) *Chem. Rev. 110*, 1642-1662.

2. O'Neil, M.A. and Barton, J.K. (2005) *Charge Transfer in DNA: From Mechanism to Application.* Wagenknecht, H.A. Wiley-VCH, Ed., 27.

3. Eley, D.D. and Spivey, D.I. (1962) *Trans. Faraday Soc. 58*, 411-415.

4. Georghiou, S., Bradrick, T.D., Philippetis, A., and Beechem, J. M. (1996) *Biophys. J. 70*, 1909-1922

5. Murphy, C.J., Arkin, M.R., Jenkins, Y., Ghatlia, N.D., Bossmann, S.H., Turro, N.J., and Barton, J. K. (1993) *Science 262*, 1025-1029.

6. Kelley, S.O. and Barton, J. K. (1999) *Science 283*, 375-381.

7. Kelley, S.O., Holmlin, R.E., Stemp, E.D.A., and Barton, J.K. (1997) *J. Am. Chem. Soc. 119*, 9861-9870.

8. Boon, E.M., Ceres, D.M., Drummond, T.G., Hill, M.G., and Barton, J.K. (2000) *Nature Biotechnol. 18*, 1096-1100.

9. Slinker, J.D., Muren, N.B., Gorodetsky, A.A., and Barton, J.K. (2010) *J. Am. Chem. Soc. 132*, 2769–2774.

10. Slinker, J.D., Muren, N.B., Renfrew, S.E., and Barton, J.K. (2011) *Nature Chem. 3*, 230-235.

11. Guo, X., Gorodetsky, A.A., Hone, J., and Barton, J.K. (2008) *Nature Nanotech. 3*, 163-167.

12. Boal, A.K. and Barton, J.K. (2005) *Bioconjugate Chem. 16*, 312-321.

13. Boon, E.M., Salas, J.E. and Barton, J.K. (2002) *Nature Biotechnol. 20*, 282-286.

14. Gorodetsky, A.A., Ebrahim, A., and Barton, J.K. (2008) *J. Am. Chem. Soc. 130*, 2924-2925.

15. Wang, H., Muren, N. B., Ordinario, D., Gorodetsky, A.A., Barton, J.K. and Nuckolls, C. (2012) *Chem. Sci. 3*, 62-65.

16. Liu, T. and Barton, J.K. (2005) *J. Am. Chem. Soc. 127*, 10160-10161.

17. Hall, D.B., Holmlin, E.R., and Barton, J.K. (1996) *Nature 382*, 731-735.

18. Núñez, M.E., Hall, D.B., and Barton, J.K. (1999) *Chem. Biol. 6*, 85-97.

19. Drummond, T.G., Hill, M.G., and Barton, J. K. (2004) *J. Am. Chem. Soc. 126*, 15010-15011.

20. Williams, T.T., Odom, D. T., and Barton, J.K. (2000) *J. Am. Chem. Soc 122*, 9048–9049.

21. Wan, C., Fiebig, T., Kelley, S.O., Treadway, C.R. Barton, J. K. and Zewail, A.H. (1999) *Proc. Natl. Acad. Sci. USA 96*, 6014–6019.

22. O'Neill, M.A. and Barton, J.K. (2004) *J. Am. Chem. Soc. 126*, 11471–11483.

23. Genereux, J.C., Augustyn, K.E., Davis, M.L., Shao, F., and Barton, J.K. (2008) *J. Am. Chem. Soc. 130*, 15150 -15156.

24. Genereux, J.C., Wuerth, S.M., and Barton, J.K. (2011) *J. Am. Chem. Soc. 133*, 3863-3868.

25. Genereux, J.C. and Barton, J.K. (2010) *Chem. Rev. 110*, 1642-1662.

26. Marcus, R.A. and Sutin, N. (1985) *Biochim. Biophys. Acta. 811*, 265–322.

27. Bixon, M., Giese, B., Wessely, S., Langenbacher, T., Michel-Beyerle, M.E., and Jortner, J. (1999) *Proc. Natl. Acad. Sci. U.S.A. 96*, 11713-11716.

28. Jortner, J., Bixon, M. Langenbacher, T., and Michel-Beyerle, M.E. (1998) *Proc. Natl. Acad. Sci. U.S.A. 95*, 12759-12765.

29. Jortner, J., Bixon, M., Voityuk, A.A., and Rosch, N. (2002) *J. Phys. Chem. A. 106*, 7599-7606.

30. Giese, B. (2002) *Annu. Rev. Biochem. 71*, 51-70.

31. Gorodetsky, A.A., Buzzeo, M.C., and Barton, J.K. (2008) *Bioconj. Chem. 19*, 2285-2296.

32. Gorodetsky, A.A., Green, O., Yavin, E., and Barton, J.K. (2007) *Bioconj. Chem. 18*, 1434-1441.

33. Kelley, S.O., Jackson, N.M., Hill, M.G., and Barton, J.K. (1999) *Angew. Chem. Int. Ed*. 38, 941-945.

34. Love, J.C., Estroff, L.A., Kriebel, J.K., Nuzzo, R.G., and Whitesides, G.M. (2002) *Chem. Rev. 105*, 1103-1169.

35. Drummond, T.G., Hill, M.G., and Barton, J.K. (2003) *Nature Biotechnol*. *21*, 1192-1199.

36. Bard, A.J. and Faulkner, L.R. (2002) *Electrochemical Methods*, 2nd ed., John Wiley & Sons, New York.

37. Kelley, S.O. and Barton, J.K. (1997) *Bioconj. Chem*. *8*, 31-37.

38. Gorodetsky, A.A. and Barton, J.K. (2006) *Langmuir 22*, 7917-7922.

39. Kelley, S.O., Barton, J.K., Jackson, N.M., McPherson, L.D., Potter, A.B., Spain, E.M., Allen, M.J., and Hill, M.G. (1998) *Langmuir 14*, 6781-6784.

40. Boon, E.M., Sam, M., Barton, J.K., Hill, M.G., and Spain, E.M. (2001) *Langmuir 17*, 5727-5730.

41. Ceres, D.M. and Barton, J.K. (2003) *J. Am. Chem. Soc. 125*, 14964-14965.

42. Kelley, S.O., Boon, E.M., Barton, J.K., Jackson, N.M., and Hill, M.G. (1999) *Nucleic Acids Res. 27*, 4830-4837.

43. Boon, E.M., Jackson, N.M., Wightman, M.D., Kelley, S.O., Barton, J.K., and Hill, M.G. (2003) *J. Phys. Chem. B. 107*, 11805-11812.

44. Boon, E.M. and Barton, J.K. (2003) *Bioconjugate Chem*. *14*, 1140-1147.

45. Boon, E.M., Barton, J.K., Pradeepkumar, P.I., Isaksson, J., Petit, C., and Chattopadhyaya, J. (2002) *Angew. Chem. Int. Ed*. *41*, 3402-3405.

46. Gorodetsky, A.A. and Barton, J.K. (2007) *J. Am. Chem. Soc. 129*, 6074-6075.

47. Buzzeo, M.C. and Barton, J.K. (2008) *Bioconjugate Chem. 19*, 2110-2112.

48. Boon, E.M., Livingston, A.L., Chmiel, N.H., David, S.S., and Barton, J.K. (2003) *Proc. Natl. Acad. Sci. U.S.A. 100*, 12543-12547.

49. DeRosa, M.C., Sancar, A., and Barton, J.K. (2005) *Proc. Natl. Acad. Sci. U. S. A. 102*, 10788-10792.

50. Boal, A.K., Yavin, E., Jukianova, O.A., O'Shea, V.L., David, S.S., and Barton, J.K. (2005) *Biochemistry 44*, 8397-8407.

51. Gorodetsky, A.A., Boal, A.K., and Barton, J.K. (2006) *J. Am. Chem. Soc. 128*, 12082-12083.

52. Genereux, J.C., Boal, A.K., and Barton, J.K. (2010) *J. Am. Chem. Soc. 132,* 891-905.

53. Romano, C.A., Sontz, P.A., and Barton, J.K. (2011) *Biochemistry 50,* 6133-6145.

54. Feldman, A.K., Steigerwald, M.L., Guo, X., Nuckolls, C. (2008) *Acc. Chem. Res. 41,* 1731-1741.

55. Fink, H.W. and Schonenberger, C. (1999) *Nature 398,* 407–410.

56. Porath, D., Bezryadin, A., de Vries, S., and Dekker, C.S. (2000) *Nature 403,* 635–638.

57. Storm, A.J., van Noort, J., de Vries, S., and Dekker, C.S. (2001) *Appl. Phys. Lett. 79,* 3881–3883.

58. Kasumov, A.Y., Kociak, M., Gueron, S., Reulet, B., Volkov, V.T., Klinov, D.V., and Bouchiat, H. (2000) *Science 291,* 280–282.

59. Gohen, H., Nogues, C., Naaman, R., and Porath, D. (2005) *Proc. Natl Acad. Sci. U.S.A. 102,* 11589–11593.

60. Hihath, J. Xu, B., Zhang, P., and Tao, N. (2005) *Proc. Natl Acad. Sci. U.S.A. 102,* 16979–16983.

61. Wierzbinski, E., Arndt, J., Hammond, W., Slowinski, K. (2006) *Langmuir 22,* 2426–2429.

62. Guo, X., Small, J.P., Klare, J.E., Wang, Y., Purewal, M.S., Tam, I.W., Hong, B.H., Caldwell, R., Huang, L., O'Brien, S., Yan, J., Breslow, R., Wind, S.J., Hone, J., Kim, P., and Nuckolls, C. (2006) *Science 311,* 356-359.

Chapter 2

Multiplexed DNA-Modified Electrodes

Adapted from Slinker, J. D., Muren, N. B., Gorodetsky, A. A., and Barton J. K. (2010) *J. Am. Chem. Soc. 132*, 2769-2774.

J.D. Slinker and N.B. Muren developed and fabricated multiplexed chips, prepared DNA, and performed multiplexed electrochemistry experiments. A.A. Gorodetsky assisted with chip development and performed electrochemistry on conventional rod electrodes.

Introduction

Multiplexed detection of biomarkers, such as DNA, RNA, and proteins, is of utility for laboratory assays as well as clinical and point-of-care disease diagnostics (1–4). Toward these ends, electrical and electrochemical devices are under development for biosensing applications, offering low cost, portability, and multiplexed capability (5–7). Carbon nanotubes (8, 9), functionalized nanowires (10–12) and nanoparticles (13), aptamers (14, 15), and redox or impedance schemes involving DNA (16–25) or other mediators (26) have all served as electrical and electrochemical biosensing platforms. However, despite this proliferation of electrical biosensors, few examples of multiplexed molecular diagnostics have been reported (12, 16, 18–21). Furthermore, still fewer electrical sensors have the sensitivity to distinguish single base mismatches within nucleic acid targets, and many are not suitable for sensing DNA-binding proteins. The electrochemical format we describe here offers robust, label-free, and sensitive detection in these applications, and is now multiplexed.

Electrochemical detection by DNA-mediated charge transport (DNA CT) is an emerging technology for clinical diagnostics and laboratory assays, showing great promise for sensitive and selective recognition of DNA and protein targets (27–41). Numerous studies have established that well-ordered, fully base-paired DNA facilitates electronic charge transport through the DNA π-stack over long distances, but that disruption of the base pair stack, such as by mismatched bases or bending of the duplex by proteins, greatly attenuates charge transport (27–29, 41–45). Due to this sensitivity to perturbation, DNA CT electrochemistry can be used to distinguish between targets with single base mismatches (27, 28) and subtle base lesions (35). Additionally,

electrochemistry through DNA monolayers and molecular junctions has been utilized for sensitive and selective detection of DNA (27, 28, 34–36, 41) and DNA binding proteins (29, 30, 32, 33, 38, 40, 41). Since DNA serves as a natural and specific recognition element for DNA-binding proteins, protein sensing by DNA CT makes use of DNA as both the recognition element and transducer. The result is a rational, sensitive, and selective platform that can be easily modulated to specifically detect a variety of unlabeled proteins.

Here we describe the fabrication and application of 16-electrode silicon chips with DNA-modified electrodes (DME chips) employing DNA-mediated electrochemistry for multiplexed detection of DNA and DNA-binding protein targets (Figure 2.1). Four DNA sequences may be interrogated simultaneously on one DME chip with four-fold redundancy, allowing for more meaningful comparisons and controls to be run side by side on the same gold surface. DME chips were used to demonstrate sensitivity to single base mismatches and electrochemically monitor sequence-specific DNA cleavage by the restriction enzyme *Alu*I. The quality of monolayer formation was investigated by statistical comparison of DME chips to commercially available rod electrodes, and the sizes of the working electrodes on the DME chips were scaled to investigate microelectrode effects. These experiments show that DME chips facilitate sensitive and selective detection of DNA and DNA-binding protein targets, and make it possible to utilize DNA CT in more complex experiments and applications.

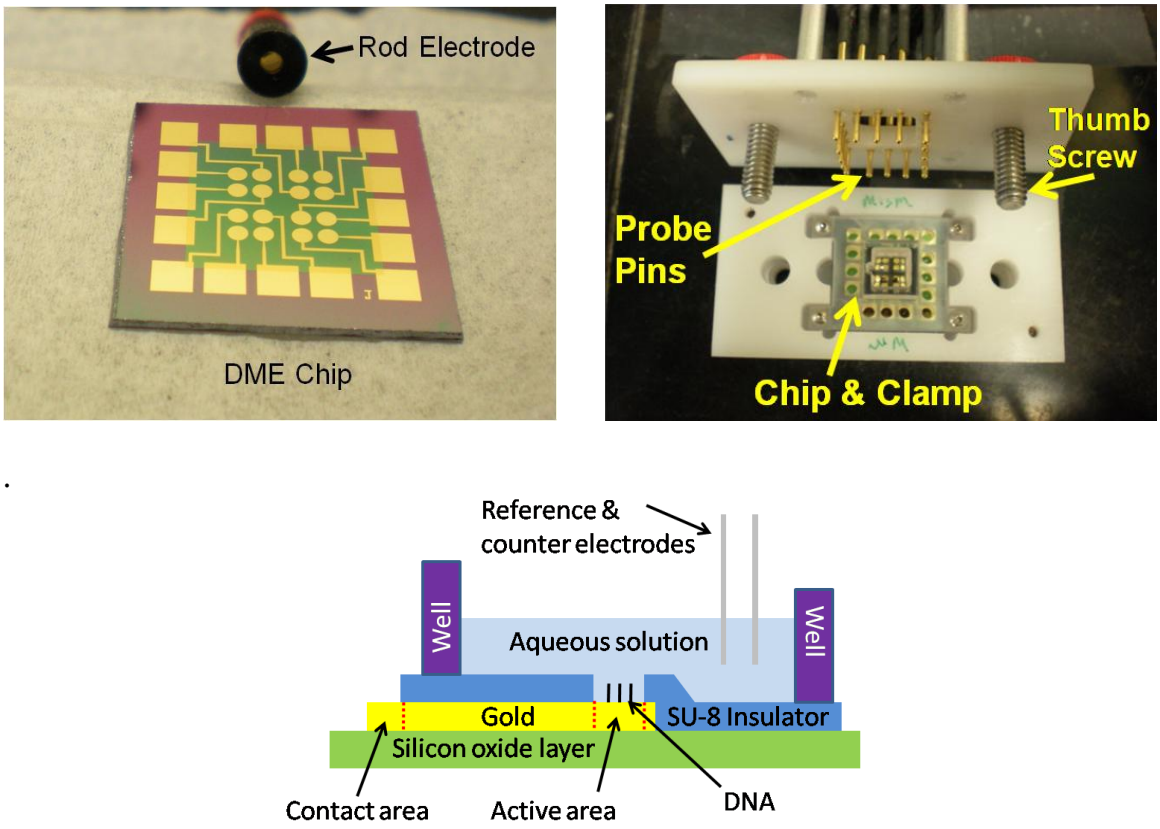

Figure 2.1 Design of the DME chip. Top left: a DME chip with sixteen 2 mm^2 gold working electrodes shown with a conventional 2 mm^2 gold rod electrode. Top right: the DME chip in a testing mount with a clamp that splits the chip into four quadrants of four electrodes and forms a well for a common buffer solution. Electrical contact is made to the chip with spring contact probe pins that are secured into contact with the chip by the thumb screws. Bottom center: side-view illustration of one electrode in a fully-assembled DME chip. The working electrode area is defined and separated from the contact area by the SU-8 insulating layer. The solution of interest is confined over the chip by the well, and external reference and counter electrodes complete the circuit.

Materials and Methods

Materials

All standard and modified phosphoramidites were purchased from Glen Research. Nile Blue perchlorate (laser grade) was purchased from Acros. All other chemicals for the preparation of buffers and DNA-modified electrodes were purchased from Sigma-Aldrich and used as recieved. Silicon wafers were purchased from Silicon Quest and reagents for DME chip fabrication were purchased from Microchem. *Alu*I was purchased from New England Biolabs and stored at -20°C. Prior to use, aliquots were exchanged into tris buffer containing 50 mM Tris-HCl, 10 mM EDTA, and 10 mM $MgCl_2$, pH 7.8, using a Pierce Slide-A-Lyzer mini dialysis kit at 4°C with overnight stirring.

DNA Sequences

For experiments on the isolation of DNA with different probes, electrodes were modified with the sequence 5′-HS-$(CH_2)_6$-ACTT*C*AGCTGAGACGCA-3′ with a Redmond Red-modified, Nile Blue-modified, or unmodified complement. Redmond Red complements were modified on the 3′ terminus while Nile Blue complements were modified on the 5′ terminus. To introduce a single base mismatch, a Nile Blue complement was prepared with an *A* opposite the italicized *C* in the sequence above. Well matched Nile Blue-modified DNA of this sequence was also used for microelectrode experiments and in *Alu*I restriction experiments as the DNA substrate with the *Alu*I restriction site (5′-AGCT-3′), which is underlined in the above sequence. For the DNA substrate without the *Alu*I restriction site, the sequence 5′-HS-$(CH_2)_6$-GAGATATAAAGCACGCA-3′ was utilized. Although this sequence does not contain

the specific *Alu*I restriction site, it does contain a pseudosite that differs by one base (5′-AGAT-3′) which is underlined. This Nile Blue-modified 17-mer without the *Alu*I site was also used for the comparison of DME chips and conventional rod electrodes.

DNA Synthesis

DNA was synthesized by standard methods on solid supports using an Applied Biosystems 3400 DNA synthesizer. For thiolated strands, the 5′ end was modified with a Thiol Modifier C6 S-S phosphoramidite. DNA modified with Redmond Red on the 3′ terminus was prepared on Epoch Redmond Red CPG columns with ultramild phosphoramidites and reagents. DNA for Nile Blue coupling was prepared with ultramild phosphoramidites and a NHS-carboxy dT phosphoramidite at the 5′ terminus. To prepare the Nile Blue-coupled DNA, the DNA on the solid support was reacted with a 10 mg/mL solution of Nile Blue perchlorate in 9:1 dichloromethane/DIEA solution for approximately 24 hrs. Excess reagents were then removed by washing with dichloromethane, methanol, and acetonitrile. Unmodified and thiolated DNA was cleaved from the solid support and deprotected by treating with concentrated ammonium hydroxide for 8 hrs. at 60 °C. Redmond Red- and Nile Blue- modified DNA strands were cleaved from the support and deprotected according to ultramild conditions with 0.05 M potassium carbonate in methanol at ambient temperature for 8 hrs.

DNA Purification

Oligonucleotides were purified by high performance liquid chromatography (HPLC) on a reversed phase C-18 column (Agilent). Following HPLC purification of the

products, the DNA was treated to remove the dimethoxytrityl (DMT) protecting group. For thiolated DNA, the disulfide of the thiolated linker was reduced to the free thiol in 100 mM dithiothreitol in 100 mM Tris-HCl buffer pH 8.3 at room temperature for 45 minutes. The DMT group was removed from the unmodified, Nile Blue, and Redmond Red DNA strands by treating with an 80% solution of glacial acetic acid for 20 min, followed by quenching of the reaction with an excess of ethanol. All oligonucleotides were then dried and purified with a second round of HPLC. The products were characterized by HPLC, matrix assisted laser desorption ionization time-of-flight mass spectrometry, and UV-visible (UV-vis) spectrophotometry.

All DNA was subsequently desalted and quantified by UV-vis spectrophotometry according to their extinction coefficients (IDT Oligo Analyzer). Duplexes were formed by thermally annealing equimolar amounts (50 μM) of complementary oligonucleotides at 90 °C for 5 min in deoxygenated phosphate buffer (5 mM phosphate, 50 mM NaCl, pH 7) followed by slow cooling to ambient temperature.

DME Chip Fabrication

One millimeter thick Si wafers with a 10,000 Å thick oxide layer were used for DME chip fabrication. Chips were patterned in a two-layer process. In the first layer, the gold electrodes were deposited by a lift-off technique. For the second layer, SU-8 photoresist was patterned as an insulator isolating the gold working electrode areas from the contact pads. First, wafers were cleaned thoroughly in 1165 Remover and vapor primed with hexamethyldisilizane (HMDS). SPR 220 3.0 photoresist was spin-cast at 4000 rpm and baked. The photoresist was patterned with a Karl Suss MA6 contact

aligner and a chrome photomask. Following postexposure baking, wafers were developed in AZ 300 MIF developer for 1 min and rinsed thoroughly with deionized water. A 15 Å Ti adhesion layer and a 1000 Å Au layer were deposited on the chips with a CHA Mark 50 electron beam evaporator. Wafers were then immersed in 1165 Remover overnight and sonicated as needed to complete metal lift-off. Subsequently, the wafers were thoroughly baked and cleaned by UV ozone treatment. SU-8 2002 was spin-cast at 3000 rpm, baked, and photopatterned as above. Wafers were developed in SU-8 Developer for 1 min and baked for a permanent set of the photoresist. The wafers were subsequently diced into 1-in. by 1-in. chips by hand with a diamond scribe and stored under vacuum until use.

Preparation of DNA Monolayers

Immediately prior to DNA monolayer assembly, gold surfaces were cleaned by sonication for 15 min in acetone and 5 min in 2-propanol, followed by treatment with UV ozone for 3 min. Multilevel wells were placed over the chip, defined by a custom-made Viton rubber gasket and a polypropylene clamp secured by screws to a test mount, providing a compression seal over the chip (Figure 2.1). This allowed for application of up to four distinct sequences of 25 μM duplex DNA solutions in phosphate buffer with 100 mM $MgCl_2$ added. Monolayer formation was allowed to proceed in a humidified environment for a period of 16-20 hrs. Upon completion of film formation, the cell was backfilled with 0.5 mM 1-mercaptohexanol in a 5% glycerol solution in phosphate buffer for 60 min. The electrodes and cells were rinsed thoroughly prior to electrochemistry experiments to ensure removal of residual 1-mercaptohexanol.

Electrochemical Analysis

Cyclic voltammetry (CV) experiments were performed by automated measurement with a CH760B Electrochemical Analyzer and a 16-channel multiplexer module (CH Instruments). The chips were interfaced with these instruments with a custom-built device mount bearing springloaded probe pins. Chips were tested with a common Pt auxiliary electrode and a common silver/silver chloride (Ag/AgCl) reference electrode. Alternatively, reference and counter electrodes can be patterned on the chip surface, though including other metals for a stable reference would increase the complexity of chip fabrication. Electrochemistry was recorded at ambient temperature in either phosphate buffer supplemented with 4 mM $MgCl_2$, 4 mM spermidine, 50 μM ethylenediaminetetraacetic acid (EDTA) and 10% glycerol at pH 7.0 or Tris buffer containing 50 mM Tris-HCl, 10 mM EDTA, and 10 mM $MgCl_2$, at pH 7.8. Electron transfer kinetics were obtained by Laviron analysis (46).

Electrochemical Measurement of Restriction Activity

For the preparation of DME chips to measure restriction activity, $MgCl_2$ was excluded from the DNA assembly solution in order to produce a lower density monolayer and grant greater access to the restriction enzyme. Dialyzed *Alu*I in Tris buffer was titrated onto the chip with test concentrations ranging from 0–50 nM (0–2000 units/mL). The reaction was allowed to equilibrate at each point of the titration for approximately 30 min. before scanning the chip. The integrated CV peak areas were recorded at each concentration

Results and Discussion

Design of DME Chip and Testing Assembly

Figure 2.1 shows a DME chip with 16 macroscale, 2 mm^2 gold working electrodes for multiplexed analysis. The DME chips are designed as a multiplexed extension of a conventional 2 mm^2 commercially available rod electrode, which is also shown for comparison in Figure 2.1. Each chip is patterned with four quadrants of four electrodes each so that four distinct DNA sequences can be simultaneously tested with four-fold redundancy. Isolation of the quadrants is accomplished with a gasket and clamp assembly having four shallow wells surrounded by a larger well. The shallow wells, each with a maximum volume of approximately 25 μL, are used for deposition of different DNA solutions to form distinct monolayers, while the larger well, with minimum and maximum working volumes of 150 and 600 μL, respectively, enables all 16 electrodes to share a common analyte solution as well as common reference and counter electrodes.

The active area of each working electrode of the DME chip is defined by the SU-8 layer. Each working electrode is connected to a square contact pad on the periphery of the DME chip. These contact pads are connected to a computer-controlled multiplexer module and electrochemical analyzer through spring contact probe pins on a testing mount secured with thumb screws. This allows for rapid electrical connection and interchange of each DME chip. In this configuration, multiplexed electrochemical testing of all 16 electrodes could be performed sequentially with common reference and counter electrodes.

Multiplexed Detection of Diverse DNA Types

Multiplexed electrochemical analysis of four types of DNA with different redox signatures was accomplished with the DME chip. The analyzed 17-mers share the same sequence but are distinct in either the choice of redox probe or the inclusion of a mismatch. The redox probes Nile Blue and Redmond Red were used as they have been previously demonstrated for sensitive detection of proteins (40) and abasic sites (47), respectively. As illustrated (Figure 2.2), these DNA substrates include (i) a well matched duplex with a proximal 3′ Redmond Red redox probe (48), (ii) a well matched duplex with no redox probe, (iii) a well matched duplex with a distal 5′ Nile Blue redox probe, and (iv) a duplex modified with a 5′ Nile Blue redox probe and containing a single base-pair (CA) mismatch. The choice of these four diverse DNA types illustrates the versatility of the detection technique, the generality of redox probes used, the selectivity to specific DNA sequences, and the ability to isolate four monolayers with fidelity on the chip.

The CV data resulting from these four DNA monolayers are shown in Figure 2.2. The monolayer prepared with well matched, Nile Blue-modified DNA gives a large CV peak area of 5.2 nC at -320 mV versus an Ag/AgCl reference (cathodic wave). Similarly, the well matched monolayer with a Redmond Red redox probe exhibits a large CV peak area of 6.2 nC located at the distinct potential of -340 mV (cathodic wave). These results reveal that high density DNA monolayers can be prepared on DME chips. In contrast, the monolayer prepared with a well matched complementary strand containing no redox probe shows no discernible CV peak, highlighting that no cross-contamination of the monolayers occurs between DME chip quadrants.

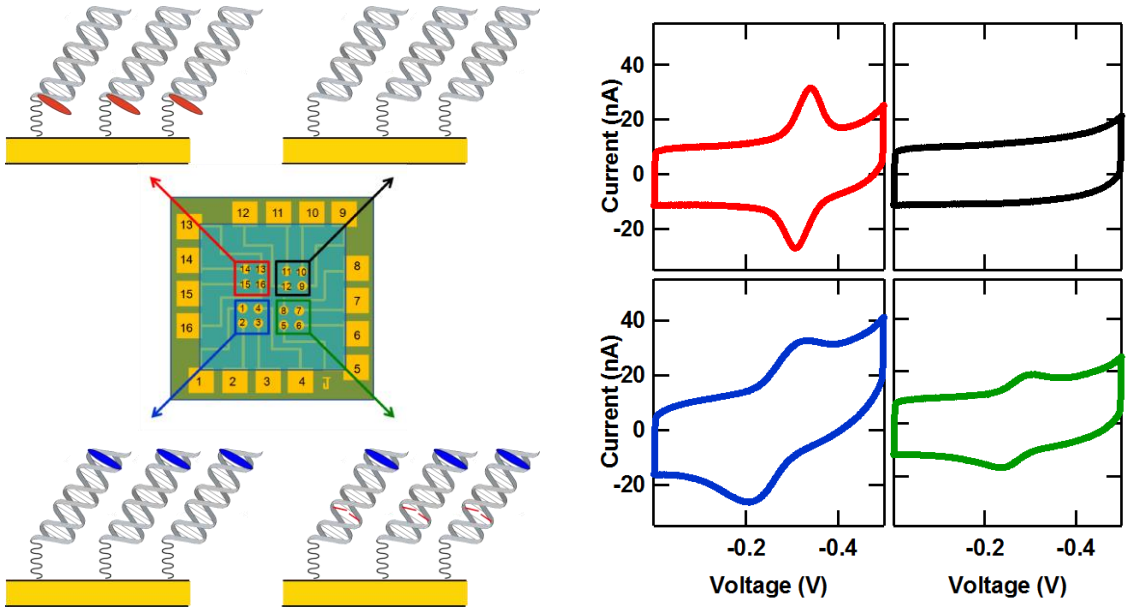

Figure 2.2 Multiplexed measurement of four different DNA types on a DME chip. Left: illustration of a DME chip modified with four DNA types with distinct redox signatures including (clockwise from top left): a well matched strand with a proximal 3′ Redmond Red probe, a well matched strand with no redox probe, a 5′ Nile Blue-labeled strand containing a single base-pair (CA) mismatch, and a well matched strand with a distal 5′ Nile Blue redox probe. All DNA was composed of the same thiolated strand: 5′-HS-$(CH_2)_6$-ACTTCAGCTGAGACGCA-3′, where the italicized *C* is the location of the CA mismatch. Right: CV data for each DNA type with plot orientation corresponding to the chip illustration. The potentials are reported versus Ag/AgCl with a CV scan rate of 100 mV/s, and each curve represents an average over the four electrodes in each chip quadrant.

It has previously been demonstrated that DNA-modified electrodes which report DNA CT redox processes can be used to distinguish single base mismatches and other subtle lesions due to distortion imposed on the DNA base pair π-stack (27, 28, 35). Notably, the CV signals on DME chips are significantly attenuated for electrodes modified with the Nile Blue 17-mer that contains a single CA mismatch. The CV peak area from these mismatched duplexes was 1.9 nC (cathodic wave), a factor of 2.7 lower than that found for the well matched complement. Thus, DME chips support probe reduction by a DNA CT pathway and can thus be used for precise discernment of specific DNA and RNA targets, even distinguishing single base mismatches. Note that here DME chips provide a direct measurement of mismatch discrimination, as both well matched and mismatched films are formed under identical experimental conditions and the comparison may be made side-by-side within the same experiment.

Overall, three DME chips were prepared identically to that of Figure 2.2. The ratios of integrated charge for well matched to mismatched Nile Blue strands across these three chips were 2.8 and 3.1 for the anodic and cathodic sweeps, respectively. The variation in signal size (integrated cathodic peak ± standard deviation) among electrodes modified with the same type of DNA within a chip was 5.1 ± 1.6 nC for the well matched Nile Blue monolayer, 2.1 ± 0.1 nC for the mismatched Nile Blue monolayer, and 6.3 ± 0.4 nC for the well matched Redmond Red monolayer. Alternatively, the variation in the average integrated cathodic CV peak charge among three chips was 1.5, 1.0, and 3.0 nC for well matched Nile Blue, mismatched Nile Blue, and well matched Redmond Red monolayers, respectively. Thus, in general, the variation across a chip was smaller than that between chips. DNA films on DME chips were found to be relatively stable under

storage at 4 °C. For example, a chip stored for 24 days at 4 °C retained over 80% of the initial integrated charge, corresponding to an average signal loss of < 1% per day.

Electron transfer kinetics from these monolayers were also estimated from the scan rate dependence of the cyclic voltammetry by Laviron analysis (46). The electronic transfer rates were 4.2, 1.0, and 2.4 s^{-1}, for well matched Redmond Red, well matched Nile Blue, and mismatched Nile Blue monolayers, respectively. These values are comparable to estimates on similarly prepared monolayers on rod electrodes (49). Notably, there is little difference in the transfer kinetics between matched and mismatched DNA, suggesting the same CT mechanism for both sequences.

It should be noted that our platform can be used for detection of unlabeled single-stranded DNA targets. To accomplish this, single-stranded DNA bearing the sequence complementary to the target is modified with a redox probe on one end and a thiol linker on the other end for assembly on the electrode. Hybridization with the unlabeled target will complete the base pair π-stack and turn on the DNA-mediated redox signal.

Monitoring Sequence-Specific Enzymatic Activity

A major advantage of the multiplexed chip format over individual electrodes is the ability to measure protein-DNA binding activity with different DNA sequences on the same chip, thus exploring site-specific activity while preserving identical experimental conditions. We demonstrate this capability by measuring the sequence-specific activity of the *Alu*I restriction endonuclease, which cleaves at the restriction site 5′-AGCT-3′, leaving blunt ends between the G and C bases (Figure 2.3). A DME chip was prepared with 17-mer Nile Blue modified DNA, where half of the electrodes were assembled with

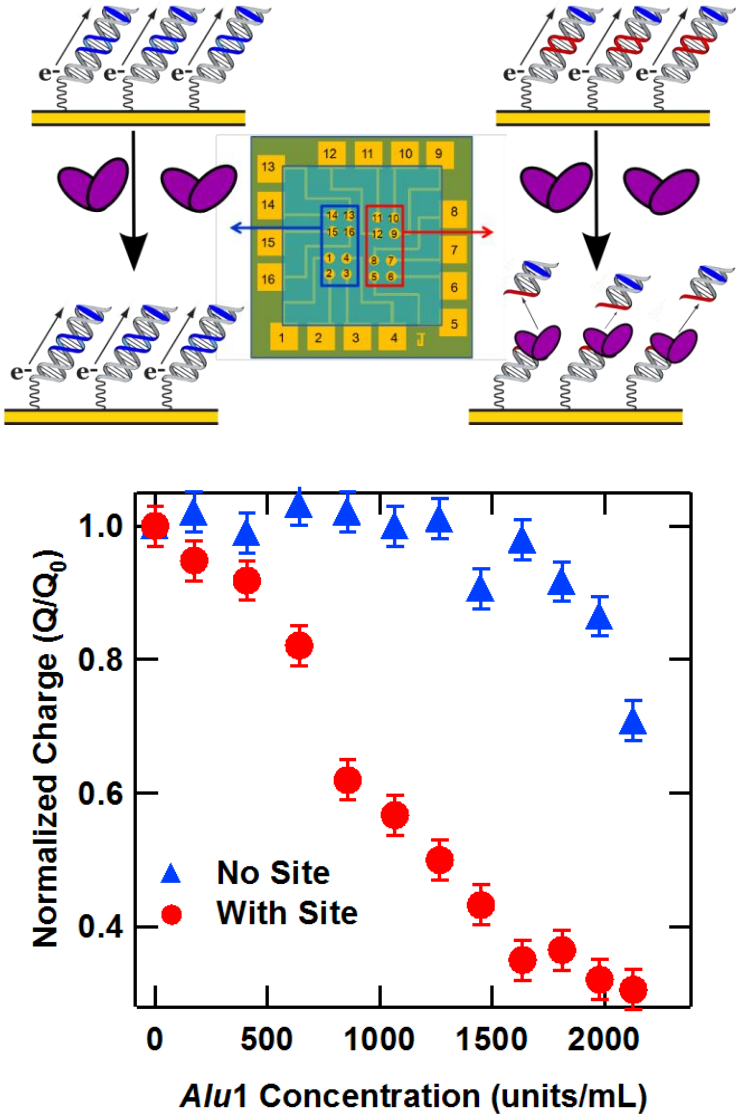

Figure 2.3 Detection of sequence-specific restriction activity on a DME chip. Top: Chips were modified on one half with the Nile Blue-modified 17-mer that lacks the *Alu*I restriction site (left, blue) and the other half with the Nile Blue-modified 17-mer that contains the *Alu*I restriction site (right, red). *Alu*I was titrated onto the chip and the restriction activity was monitored electrochemically. Bottom: plot of measured signal size (normalized against the initial signal) versus *Alu*I concentration for a DME chip modified with DNA with (Red) and without (Blue) the *Alu*I restriction site. Charge was obtained by integrating the cathodic Nile Blue CV peaks obtained at a 50 mV/s scan rate after equilibration of *Alu*I activity at each concentration.

a sequence containing the *Alu*I recognition site and the other half with a sequence lacking this site. The *Alu*I restriction enzyme was titrated onto the chip, and the integrated CV peak areas were recorded at each concentration. The resulting plot of charge (normalized against the initial signal) versus *Alu*I concentration is given in Figure 2.3.

At low concentrations, there is a definitive drop in the integrated charge at the electrodes bearing the restriction site, while the charge from the electrodes without the site remains stable. In contrast, for the DNA-modified electrode lacking the target site, there is virtually no drop in signal over this concentration range. The threshold of *Alu*I restriction activity for the sequence containing the restriction site was 400 units/mL, corresponding to a concentration of approximately 10 nM (50). As the total sample volume was 250 μL, this corresponds to 2.5 pmol of enzyme per chip, or 160 fmol of enzyme per electrode. At concentrations greater than 1600 units/mL (51) the charge at the electrodes lacking the restriction site decreases due to nonspecific restriction activity, also known as star activity. In this case, the DNA without the consensus restriction site contains a pseudosite differing by only one base (5′-ATCT-3). Thus, as expected at higher enzyme concentrations, restriction cleavage at this pseudosite is apparent.

Several important implications arise from these observations. Cleavage by the *Alu*I restriction endonuclease requires that the DNA on these chips is in its native conformation and accessible to the protein. The observation of sequence-specific cleavage indicates that protein detection with DNA-mediated electrochemistry is highly selective. Also, by extension, incorporation of multiple DNA sequences with different protein binding characteristics on a single chip indicates that DME chips can serve as a robust platform to simultaneously monitor reactions on different oligonucleotides.

Finally, this assay requires only microliter volumes of low protein concentrations, making it competitive with alternative detection methods.

Statistical Comparison of DME Chips to Rod Electrodes

We have found that electrodes from DME chips exhibit performances superior to those of conventional, commercially available rod electrodes. This is clearly revealed in the histogram of Figure 2.4, which compares the total charge obtained by integrating the cathodic CV peaks from Nile Blue-modified, 17-mer DNA monolayers prepared on DME chips and rod electrodes. The average integrated charge value of 3.5 nC from the DME chips is nearly twice that of the 1.8 nC average obtained from rod electrodes, and the relative deviation is significantly lower, 0.5 versus 0.7. This higher average integrated charge is indicative of higher surface density of DNA at the DME electrodes. In addition, on average, fewer electrode failures (charge < 0.5 nC) were observed on the DME chips (6%) versus rod electrodes (25%). Background noise is also much smaller for the DME chips, as they display a lower capacitive current (data not shown). The higher overall signals, lower standard deviation, and better signal-to-noise ratio of the DME chips are clearly preferred for sensing and diagnostic applications.

Microelectrodes

In addition to macroelectrodes, we demonstrate that DME chips can be easily prepared with microelectrodes. Microelectrodes exhibit a number of benefits for DNA and protein sensing such as high sensitivity, rapid kinetics, and lower sample volumes (18-20, 40, 52, 53). By reducing the diameter of the SU-8 layer opening over each

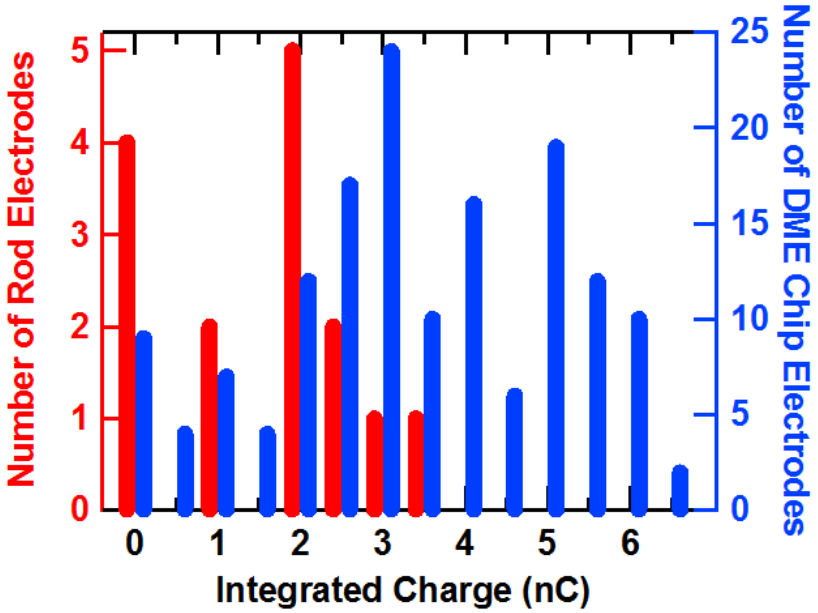

Figure 2.4 Statistical comparison of signal size on DME chips and conventional rod electrodes. A histogram of the integrated charge from DNA monolayers on the electrodes of 9 DME chips (blue) and 15 rod electrodes (red). Both types of electrodes were modified with the same well matched Nile Blue-modified 17-mer: 5′-HS-$(CH_2)_6$-GAGATATAAAGCACGCA-3′. The integrated charge was obtained by integrating the cathodic peak of the CV taken at a 50 mV/s scan rate. For ease of comparison, integrated charges have been sorted according to the nearest half coulomb. Note that, on average, much higher signals and fewer failures (signals < 0.5 nC) are found for gold electrodes on DME chips.

electrode, DME chips with the gold layout of Figure 2.1 were patterned with circular working electrodes of 300, 56, and 10 μm diameters. These electrodes were modified with the well matched 17-mer with a distally bound Nile Blue redox probe, and the CV curves for these electrodes at a 50 mV/s scan rate are given in Figure 2.5.

For the 300 μm diameter working electrodes, the conventional macroelectrode surface-bound redox peaks associated with Nile Blue are visible at a midpoint potential of -220 mV vs Ag/AgCl. However, for the 56 and 10 μm diameter electrodes, the CV curves are significantly altered from this conventional shape. The 10 μm diameter electrodes exhibit the sigmoidal curves characteristic of microelectrode effects (52, 53). This result is similar to our previous work with individual microelectrodes, where microelectrode effects were observed for devices of 25 μm diameter or less (40). This shape arises because ionic equilibration is achieved virtually instantaneously with the sweep of the voltage due to the small size of the electrode relative to the abundance of ions in the surrounding solution (52, 53). As seen previously, the midpoint potential is shifted negatively by over 100 mV, while the limiting current and capacitive current are each higher by a factor of 5–6. These increases may be due to more dense DNA monolayers and/or the presence of oxygen. Alternatively, the 56 μm diameter electrodes yield a CV curve that is intermediate to the macroelectrode and microelectrode regimes. Microelectrode effects can thus be observed on DME chips, combining the benefits of high sensitivity and rapid equilibration to this multiplexed platform.

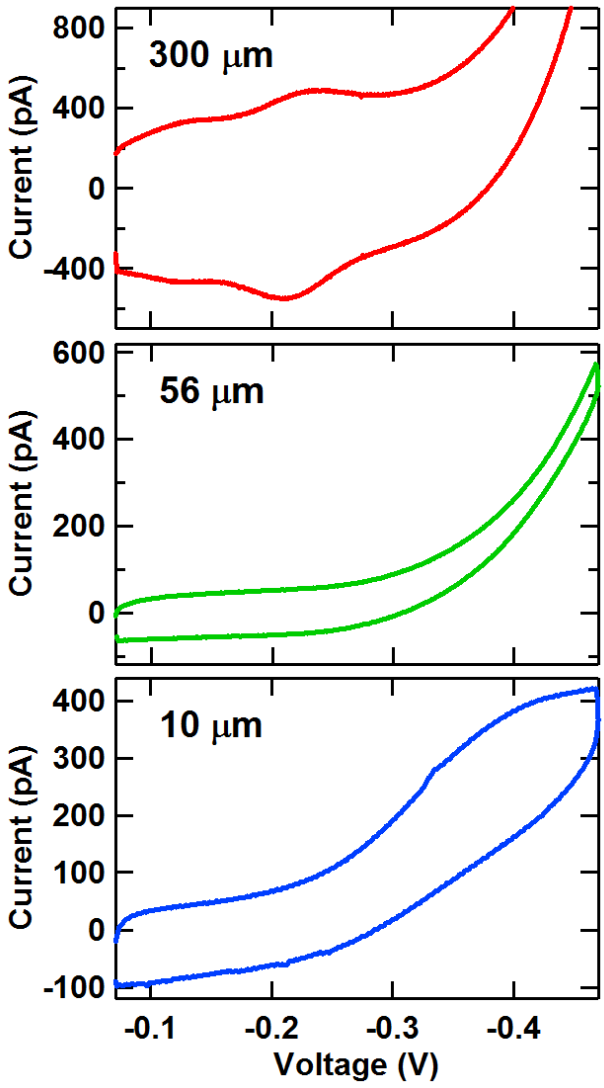

Figure 2.5 Electrochemistry of microelectrodes on DME chips. Electrodes of 300 μm (top), 56 μm (center), and 10 μm (bottom) diameter were modified with a Nile Blue-modified 17-mer on the same chip and averaged CV scans are shown for each. The sequence for all DNA was: 5′-HS-$(CH_2)_6$-ACTTCAGCTGAGACGCA-3′. The potentials are reported versus Ag/AgCl with a CV scan rate of 50 mV/s, and each curve represents an average over four electrodes. The 300 μm electrodes show the conventional surface-bound macroelectrode redox peak, while the 10 μm electrodes show a sigmoidal CV curve, reflecting microelectrode effects.

Summary and Conclusions

We have developed a multiplexed DME chip platform that employs DNA CT chemistry for the sensitive, electrochemical detection of DNA and DNA-binding protein targets. Four electrochemically distinct types of DNA were simultaneously distinguished on a single DME chip with 4-fold redundancy, demonstrating the capacity of this platform isolate DNA monolayers for complex comparisons and controls on the same electrode surface. Side-by-side analysis of well matched DNA and DNA with a single base mismatch showed significant signal attenuation of the mismatched DNA. Thus DME chips support probe reduction by a DNA CT mechanism and as such, are highly sensitive and selective detection devices.

DME chips also allow for the study of DNA-protein interactions and specifically here, sequence-specific restriction activity by *Alu*I was measured on a single chip surface. Uniform signal sizes were measured among electrodes on the same chip, and in general these chips display larger, more consistent signals with less electrode failures than commercially available rod electrodes. In addition to studies with macroelectrodes on DME chips, the working electrode areas on the chips were reduced to 10 μm to achieve microelectrode behavior that is useful for high sensitivity and rapid kinetic detection. DME chips thus offer a new and sensitive platform for the multiplexed, electrochemical detection of DNA and DNA-binding protein targets.

References

1. Darnell, J.E. (2002) *Nat. Rev. Cancer 2*, 740.

2. Libermann, T.A. and Zerbini, L.F. (2006) *Curr. Gene Ther. 6*, 17.

3. Bell, J. (2004) *Nature 429*, 453–456.

4. Ludwig, J.A. and Weinstein, J.N. (2005) *Nat. Rev. Cancer 5*, 845–856.

5. Drummond, T.G., Hill, M.G., and Barton, J.K. (2003) *Nat. Biotechnol. 21*, 1192.

6. Liu, J., Cao, Z., and Lu, Y. (2009) *Chem. Rev. 109*, 1948.

7. Sadik, O.A., Aluoch, A.O., and Zhou, A. (2009) *Biosens. Bioelectron. 24*, 2749.

8. Wong, S.S., Joselevich, E., Woolley, A.T., Cheung, C.L., and Lieber, C.M. (1998) *Nature, 394*, 52.

9. Chen, R.J., Bangsaruntip, S., Drouvalakis, K.A., Kam, N.W.S., Shim, M., Li, Y.M., Kim, W., Utz, P.J., and Dai, H.J. (2003) *Proc. Natl. Acad. Sci. U.S.A. 100*, 4984.

10. Cui, Y., Wei, Q., Park, H., and Lieber, C.M. (2003) *Science 293*, 1289.

11. Gao, Z., Agarwal, A., Trigg, A.D., Singh, N., Fang, C., Tung, C. H., Fan, Y., Buddharaju, K.D., and Kong, J. (2007) *Anal. Chem. 79*, 3291.

12. Zheng, G., Patolsky, F., Cui, Y., Wang, W.U., and Lieber, C.M. (2005) *Nat. Biotechnol. 23*, 1294.

13. Park, S.-J., Taton, T.A., and Mirkin, C.A. (2002) *Science 295*, 1503.

14. Zuo, X., Xiao, Y., and Plaxco, K.W. (2009) *J. Am. Chem. Soc. 131*, 6944.

15. Xu, D., Xu, D., Yu, X., Liu, Z., He, W., and Ma, Z. (2005) *Anal. Chem. 77*, 5107.

16. Yu, C.J., Wan, Y., Yowanto, H., Li, J., Tao, C., James, M.D., Tan, C.L., Blackburn, G.F., and Meade, T.J. (2001) *J. Am. Chem. Soc. 123*, 11155.

17. Fan, C., Plaxco, K.W., and Heeger, A.J. (2003) *Proc. Natl. Acad. Sci. U.S.A. 100*, 9134.

18. Li, X., Zhou, Y., Sutherland, T.C., Baker, B., Lee, J.S., and Kraatz, H.-B. (2005) *Anal. Chem. 77*, 5766.

19. Li, X., Lee, J.S., and Kraatz, H.-B. (2006) *Anal. Chem. 78*, 6096.

20. Elsholz, B., Worl, R., Blohm, L., Albers, J., Feucht, H., Grunwald, T., Jurgen, B., Schweder, T., and Hintsche, R. (2006) *Anal. Chem. 78*, 4794.

21. Fang, Z., Soleymani, L., Pampalakis, G., Yoshimoto, M., Squire, J.A., Sargent, E.A., and Kelley, S.O. (2009) *ACS Nano 3*, 3207.

22. Cash, K.J., Ricci, F., and Plaxco, K.W. (2009) *J. Am. Chem. Soc. 131*, 6955.

23. Ghindilis, A.L., Smith, M.W., Schwarzkopf, K.R., Roth, K.M., Peyvan, K., Munro, S.B., Lodes, M.J., Stover, A.G., Bernards, K., Dill, K., and McShea, A. (2007) *Biosens. Bioelectron. 22*, 1853.

24. Liao, J.C., Mastali, M., Gau, V., Suchard, M.A., Møller, A.K., Bruckner, D.A., Babbitt, J.T., Li, Y., Gornbein, J., Landaw, E.M., McCabe, E.R.B., Churchill, B.M., Haake, D.A. (2006) *J. Clin. Microbiol. 44*, 561.

25. Anne, A., and Demaille, C. (2008) *J. Am. Chem. Soc. 130*, 9812.

26. Karasinski, J., Andreescu, S., Sadik, O.A., Lavine, B., and Vora, M.N. (2005) *Anal. Chem. 77*, 7941.

27. Kelley, S.O., Boon, E.M., Barton, J.K., Jackson, N.M., and Hill, M.G. (1999) *Nucleic Acids Res. 27*, 4830.

28. Boon, E.M., Ceres, D.M., Drummond, T.G., Hill, M.G., and Barton, J. K. (2000) *Nat. Biotechnol. 18*, 1096.

29. Boon, E.M., Salas, J.E., and Barton, J.K. (2002) *Nat. Biotechnol. 20*, 282.

30. Boon, E.M., Livingston, A.L., Chmiel, N.H., David, S.S., and Barton, J.K. (2003) *Proc. Natl. Acad. Sci. U.S.A. 100*, 12543.

31. Drummond, T.G., Hill, M.G., and Barton, J.K. (2004) *J. Am. Chem. Soc. 126*, 15010.

32. Boal, A.K., Yavin, E., Lukianova, O.A., O'Shea, V.L., David, S.S., and Barton, J.K. (2005) *Biochemistry 44*, 8397.

33. DeRosa, M.C., Sancar, A., and Barton, J.K. (2005) *Proc. Natl. Acad. Sci. U.S.A. 102*, 10788.

34. Inouye, M., Ikeda, R., Takase, M., Tsuri, T., and Chiba, J. (2005) *Proc. Natl. Acad. Sci. U.S.A. 102*, 11606.

35. Boal, A.K. and Barton, J.K. (2005) *Bioconjugate Chem. 16*, 312.

36. Okamoto, A., Kamei, T., and Saito, I. (2006) *J. Am. Chem. Soc. 128*, 658.

37. Gorodetsky, A.A. and Barton, J.K. (2006) *Langmuir 22*, 7917.

38. Gorodetsky, A.A., Boal, A.K., and Barton, J.K. (2006) *J. Am. Chem. Soc. 128*, 12082.

39. Wong, E.L.S. and Gooding, J.J. (2007) *J. Am. Chem. Soc. 129*, 8950.

40. Gorodetsky, A.A., Ebrahim, A., and Barton, J.K. (2008) *J. Am. Chem. Soc. 130*, 2924.

41. Guo, X., Gorodetsky, A.A., Hone, J., Barton, J.K., and Nuckolls, C. (2008) *Nat. Nanotechnol. 3*, 163.

42. Kelley, S.O., Jackson, N.M., Hill, M.G., and Barton, J.K. (1998) *Angew. Chem. Int. Ed. 38*, 941.

43. Nuñez, M.E., Hall, D.B., and Barton, J.K. (1999) *Chem. Biol. 6*, 85.

44. Kelley, S.O. and Barton, J.K. (1999) *Science 283*, 375.

45. Schuster, G.B. (2000) *Acc. Chem. Res. 33*, 253.

46. Laviron, E. (1979) *J. Electroanal. Chem. 101*, 19.

47. Buzzeo, M.C. and Barton, J.K. (2008) *Bioconjugate Chem. 19*, 2110.

48. Redmond Red in the proximal position has been used to differentiate protein effects on DNA CT when compared to a distal probe. See: Gorodetsky, A.A., Dietrich, L.E.P., Lee, P.E., Demple, B., Newman, D.K., and Barton, J.K. (2008) *Proc. Natl. Acad. Sci. U.S.A. 105*, 3684.

49. Gorodetsky, A.A., Green, O., Yavin, E., and Barton, J.K. (2007) *Bioconjugate Chem. 18*, 1434.

50. A conversion factor of 1 million units per milligram *Alu*1 was used (New England Biolabs, personal communication).

51. One unit is defined as the amount of enzyme required to digest 1 μg of λ DNA in 1 hr. at 37 °C in a total reaction volume of 50 μL.

52. Bard, A.J. and Faulkner, L.R. (2001) *Electrochemical Methods*, 2nd ed.; John Wiley & Sons: New York

53. Heinze, J. (1993) *Angew. Chem., Int. Ed. 32*, 1268.

Chapter 3

DNA Charge Transport over 34 nm

Adapted from Slinker, J. D., Muren, N. B., Renfrew, S. E., Barton, J. K. (2011) *Nature Chem. 3*, 230-235.

J.D. Slinker and N.B. Muren fabricated multiplexed chips, prepared DNA, and performed multiplexed electrochemistry experiments and analysis. S.E. Renfrew assisted with DNA preparation and data collection.

Introduction

Extensive research has focused on charge transport (CT) through conjugated molecules in an effort to use these molecules as components in the construction of nanoscale circuits (1, 2). Molecular wires provide a unique opportunity to study CT in one and two dimensions and are promising materials for electronic applications, such as optoelectronics, energy storage devices, logic circuits and sensors (3). Thus, many efforts have been directed toward the fabrication of long, linear conjugated molecules for these purposes (1–9). However, the synthesis of functional molecular wires is challenging, as these wires must have precisely defined, uniform lengths and functionalized terminal groups to bond to electrodes or electroactive moieties. These requirements limit the effective length of the conjugated molecules to ~10–20 nm (1–9). Alternatively, DNA satisfies easily the synthetic requirements of molecular wires (2, 10, 11). Unlike other conjugated bridges and molecular monolayer assemblies, DNA synthesis is mastered to the point of automation. The unique structure and directionality of DNA mean that modification of both the 3′- and 5′-DNA termini can be executed selectively and with high yield to endow it with a variety of functionalities. Reaction products may be characterized precisely using mass spectrometry, measurements of melting behavior, and spectroscopy.

The challenge that surrounds the use of DNA as a molecular wire, in contrast, arises not in the synthesis, but in obtaining consistent electrical properties from DNA. A wide range of conductivities are reported, from insulating to superconducting (12–22). However, for those studies that utilized well characterized connections to the DNA and preserved the duplex conformation in buffered solution without damaging the bases, high

conductivities were achieved consistently (14, 19–22). In our laboratory, recently we measured single molecule conductivities for 15-mer DNA duplexes that bridged a carbon nanotube gap, and we observed resistances through the stacked DNA bases comparable to those expected perpendicular to graphite planes (19). Also, in these experiments attenuation in conductivity was seen in duplexes that contained a single base-pair mismatch, as expected from photophysical studies (23). These studies and work by other groups have established that well ordered, fully base-paired DNA facilitates electronic CT through the DNA π-stack (19–30).

Beyond the basic questions of conductivity, achieving long-range CT in DNA is particularly attractive because of its inherent biological recognition capabilities (10, 11) and its unmatched capacity to be patterned into precise, nanoscale shapes (31, 32), ideal for nanoelectronics such as integrated circuits and sensors. The characterization of factors that govern DNA conductivity on scales of increasing length would not only facilitate the incorporation of DNA into complex nanoscale devices, but also its utilization for applications in biotechnology. Solution-based photooxidation studies showed long-range oxidative DNA damage through DNA CT over 20 nm (26). DNA electrochemistry provides a direct measure of ground-state CT through a well-ordered molecular assembly and is of great utility for electrical device applications (10, 33). However, efficient DNA CT through molecular assemblies over long distances has not been demonstrated, and electrochemical observation of DNA CT is limited typically to a range of 5 nm (15 base pairs) (10). Here we probe CT through 34 nm DNA monolayers (100 base pairs) electrochemically.

Materials and Methods

Materials

All standard and modified phosphoramidites were purchased from Glen Research. Nile Blue perchlorate (laser grade) for coupling was purchased from Acros. All other chemicals for the preparation of buffers and DNA-modified electrodes were purchased from Sigma-Aldrich and used as recieved. The restriction enzyme *Rsa*I was purchased from New England Biolabs and stored at -20°C. Prior to use, an aliquot of *Rsa*I was exchanged into Tris buffer containing 10 mM Tris, 50 mM NaCl and 4 mM spermidine, pH 8.0, using a Pierce Slide-A-Lyzer mini dialysis kit at 4°C with overnight stirring. Multiplexed chips were fabricated at Caltech as described previously (34).

DNA Sequences

Each 100-mer duplex was assembled from five single-stranded segments that were annealed to form the complete sequence 5′-HS-$(CH_2)_6$-AGT ACT GCA GTA GCG ACG TCA TAG GAC ATC AGT CTG CGC CAT TCA TGA CAT AC*G TAC* GCA GTA GGT GA**A** TCG TGG CAG GTC AGT CAT GTA TAC TGC ACT A-3′. The 5′ terminus opposite the thiol linker was modified with a covalent Nile Blue redox probe. For experiments with mismatched 100-mer duplexes, a single base-pair mismatch (CA) was incorporated primarily at the bold **A** in the sequence above. For analysis of different mismatch locations, experiments were also carried out with a CA mismatch generated at the underlined bases. The italicized bases 5′-*GTAC*-3′ mark the location of the *Rsa*I restriction site. The Nile Blue-modified 17-mer duplexes were prepared with the sequences 5′-HS-$(CH_2)_6$-GA GAT ATA AAG CAC GCA-3′ for the 17-mer without the

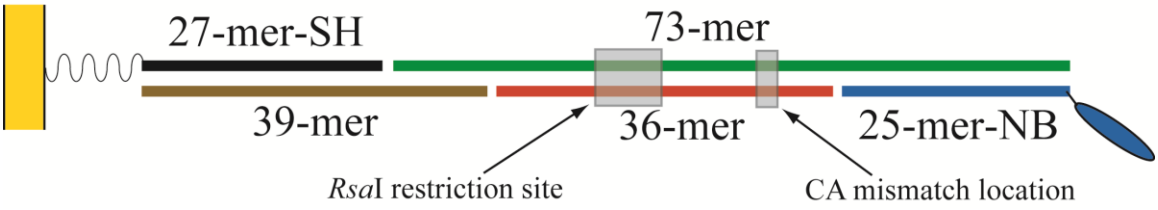

Figure 3.1 Assembly of the well matched 100-mer DNA duplex. The overall duplex is composed of five single stranded DNA segments. The 73-mer (green) and 39-mer (brown) help to stabilize the duplex by pairing at a 12 base overlap region. The positions of the *Rsa*I restriction site and CA mismatch, both within the central 36-mer, are indicated.

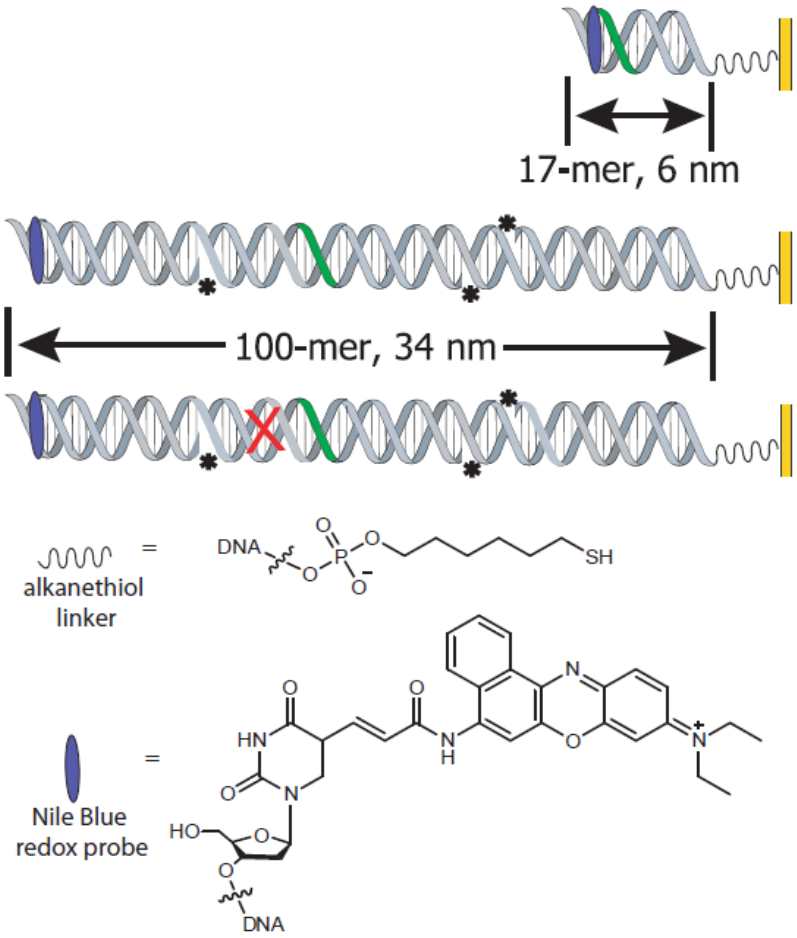

Figure 3.2 Illustration of the DNA, with redox probe and linker structures, used to modify the electrodes. Shown are (top to bottom) a well matched 17-mer, a well matched 100-mer, a 100-mer with a single mismatched base pair, the six carbon alkanethiol linker, and the Nile Blue redox probe coupled through a uracil. The green sections of the 100-mer mark the approximate location of the *Rsa*I restriction enzyme binding site, and the X notes the approximate location of the single CA mismatch, 69 bases from the thiolated end of the duplex. The asterisks on the sugar phosphate backbone of the 100-mers indicate the location of nicks. The specific sequences are given in the methods section.

*Rsa*I binding site and 5′-HS-$(CH_2)_6$-GA GAT ATA AA*G TAC* GCA-3′ for the 17-mer with the *Rsa*I binding site (shown in italics).

DNA Synthesis and Purification

Oligonucleotides were synthesized on an Applied Biosystems 3400 DNA Synthesizer. For thiolated strands, the 5′ end was modified with a Thiol Modifier C6 S-S phosphoramidite. Thiolated DNA was cleaved from the solid support and deprotected by treating with concentrated ammonium hydroxide for 8 hrs. at 60 °C. DNA for Nile Blue coupling was prepared with ultramild phosphoramidites and a NHS-carboxy dT phosphoramidite at the 5′ terminus. Covalent Nile Blue coupling was carried out as described previously (34, 35). Briefly, DNA on the solid support was reacted with a 10 mg/mL solution of Nile Blue perchlorate in 9:1 dichloromethane/DIEA for approximately 24 hrs, followed by washing with dichloromethane, methanol, and acetonitrile. Nile Blue- modified DNA strands were cleaved from the support and deprotected according to ultramild conditions with 0.05 M potassium carbonate in methanol at ambient temperature for 8 hrs.

Each single strand was purified by high-performance liquid chromatography (HPLC) on a reversed phase C-18 column (Agilent) with a 50 mM ammonium acetate buffer/acetonitrile gradient according to the reported protocol (34). For the 73-mer strand, the HPLC column was heated to 40 °C to discourage the formation of a secondary structure. Subsequently, the purified oligonucleotides were desalted and quantified by ultraviolet-visible spectrophotometry according to their extinction coefficients (IDT Oligo Analyzer). Duplexes were formed by thermally annealing equimolar (50 μM)

amounts of oligonucleotides at 90 °C for five minutes in deoxygenated phosphate buffer (5 mM phosphate, 50 mM NaCl, pH 7) followed by slow cooling to ambient temperature. The integrity of each strand was verified by HPLC, matrix-assisted laser desorption/ionization time of flight mass spectrometry and ultraviolet-visible spectroscopy, and full hybridization and stoichiometry of double-stranded DNA solutions were confirmed through ultraviolet analysis of melting temperature.

Preparation of DNA Monolayers and Electrochemical Analysis

DNA monolayers were formed by assembly on chips bearing 16 gold electrodes described previously (34). Each chip was prepared with up to four sequences of 25 mM duplex DNA solutions in phosphate buffer that contained 100 mM $MgCl_2$. Typically, monolayer formation was allowed to proceed in a humidified environment for a period of 16–20 hours. Upon completion of film formation, the cell was backfilled with 0.5 mM 1-mercaptohexanol in a 5% glycerol in phosphate buffer for 60 minutes. The electrodes were rinsed thoroughly prior to the electrochemistry experiments to ensure removal of residual 1-mercaptohexanol. Cyclic voltammetry (CV) scans were performed by automated measurement with a CH760B Electrochemical Analyzer and a 16-channel multiplexer module (CH Instruments). Chips were tested with a common Ag/AgCl reference electrode and Pt auxiliary electrode. Unless otherwise noted, electrochemistry was recorded at ambient temperature in Tris buffer containing 10 mM Tris, 50 mM NaCl, 10 mM $MgCl_2$ and 4 mM spermidine at pH 7.1. Electron transfer kinetics were estimated by Laviron analysis (40).

Electrochemistry of Partial DNA Assemblies

To demonstrate that probe reduction is DNA-mediated and not due to direct surface contact, the electrochemistry of partial DNA assemblies was compared to that of the 17-mer and 100-mer duplexes. In addition to annealing the Nile Blue-modified, well matched 100-mer and well-matched 17-mer (without the *Rsa*I binding site) as described in previous sections, an aliquot of the 100-mer without the 36-mer segment added was also annealed. These samples (diluted to 25 μM) and a 25 μM sample of the ssNB-25-mer directly from the stock were assembled with 100 mM Mg^{2+} in separate quadrants on chips using the same conditions described in the previous section. After thorough rinsing, the chip was backfilled with 1 mM 1-mercaptohexanol for 45 min. CV scans were performed at a scan rate of 100 mV s^{-1} in buffer containing 5 mM phosphate, 50 mM NaCl, 4 mM $MgCl_2$, 4 mM spermidine, 50 μM EDTA, 10% glycerol, pH 7.

*Rsa*I *Restriction Assays*

For the analysis *Rsa*I restriction activity on partial DNA assemblies, chips were treated with 1,500 units/mL *Rsa*I in 10 mM Tris-HCl, 50 mM NaCl, 4 mM spermidine, pH 8.0 with 10 mM $MgCl_2$ added. Restriction activity was allowed to occur for 15 min. at room temperature. CV scans were performed before and after the addition of *Rsa*I in buffer containing 5 mM phosphate, 50 mM NaCl, 4 mM $MgCl_2$, 4 mM spermidine, 50 μM EDTA, 10% glycerol, pH 7. For analysis of the 100-mer over time with and without *Rsa*I treatment, chips were also treated with 1,500 units/mL *Rsa*I in the described buffer but 10 mM $MgCl_2$, which is necessary to activate *Rsa*I was not added until after the *Rsa*I solution had been added to the chip and allowed to fully equilibrate (~1 hr.).

Measurements were carried out on chips with the standard, single-well set up as well as with a custom-built well clamp bearing a control quadrant with a separate well to maintain one quadrant free of enzyme. For this clamp, the reference and counter electrodes were thoroughly rinsed with deionized water when transferring between wells.

Results and Discussion

Preparation of DNA Monolayers

Figures 3.1 and 3.2 show the various features of double-stranded DNA used in monolayers for DNA electrochemistry. To make the 100-mer, five single-stranded oligonucleotides were synthesized and purified (34). Duplexes were prepared by annealing a 27-mer strand with a six carbon thiol linker at its 5′-terminus and a 73-mer strand to complementary strands that included a 39-mer, a 36-mer and a 25-mer with a Nile Blue redox probe covalently attached through a uracil at its 5′-terminus. This piecewise synthesis, which involves assembly of the double-stranded 100-mer from these overlapping single-stranded DNA segments, was employed to improve synthetic yield. Although duplexes prepared in this manner contain nicks in the sugar-phosphate backbone, DNA-mediated CT occurs through the π-stack and not through the backbone (36), so these duplexes remain fully functional for DNA CT. The fully assembled 100-mer duplexes were designed such that the Nile Blue redox probe was positioned at one 5′-terminus of the duplex and the thiol linker extended from the other 5′-end.

To investigate restriction-enzyme activity, 100-mers were designed with the binding site of the *Rsa*I restriction enzyme near the center of the DNA duplex. Likewise, those 100-mers that contained a single CA mismatch also had the mismatch located near

the center of the duplex. Well matched 17-mer strands were prepared with the same modifications, the Nile Blue redox probe at one 5′-end and thiol linker at the other 5′-end. The DNA monolayers were assembled on silicon chips bearing sixteen 2 mm^2 gold electrodes, which enabled simultaneous comparison of up to four distinct monolayers on a single chip with fourfold redundancy (34). All monolayers were assembled as duplex DNA and, prior to testing, the electrodes were backfilled with mercaptohexanol to passivate against direct electrochemistry with the gold surface. Previously, the morphology of DNA monolayers on gold electrodes was investigated with atomic force microscopy (37, 38); at negative potentials the duplexes were repelled from the surface to a near-vertical orientation.

Electrochemistry of Well Matched and Mismatched 100-mers

First, we explored the general electrochemical characteristics of DNA as a 34 nm molecular bridge between the gold electrode and Nile Blue redox probe. Cyclic voltammetric (CV) signals from these monolayers are given in Figure 3.3. The CV measurements from well matched 100-mer monolayers exhibit large peaks associated with the Nile Blue redox probe, indicative of effective CT at a midpoint potential of –240 mV versus an Ag/AgCl reference. The integrated cathodic and anodic peak areas for these well matched monolayers were 1.7 ± 0.1 nC and 3.6 ± 0.1 nC, respectively, which correlate with a surface coverage of approximately 1 pmol cm^{-2}; some variations arose with buffer and adventitious oxygen. The surface coverage and the CV peak areas were comparable to those observed with 17-mers. For instance, the average CT signal size through well-matched 17-mers modified by Nile Blue was 3.5 ± 0.5 nC, as averaged

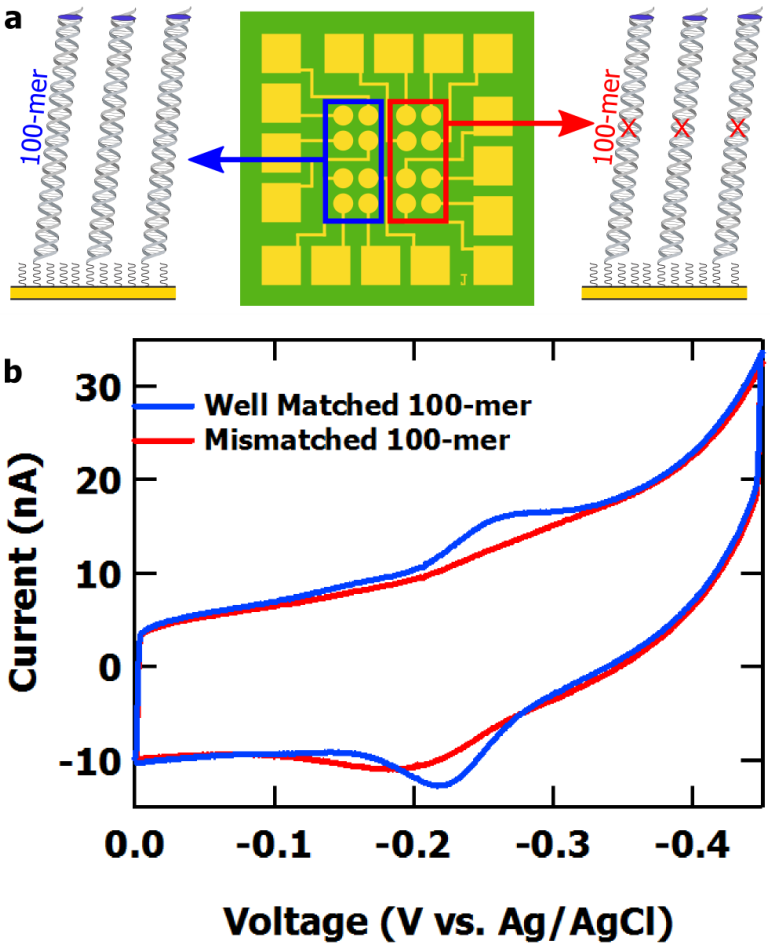

Figure 3.3 Electrochemistry from 100-mer well matched and mismatched monolayers. **a**, The chip layout used to compare monolayer electrochemistry between well matched 100-mers and 100-mers with a single base-pair mismatch. A mismatch (CA) is generated in the 36-mer segment by substitution of a C for a T at the position 69 bases from the thiolated end of the duplex. **b**, Average CV curves from well matched (blue) and mismatched (red) 100-mer DNA, each modified with a Nile Blue redox probe. Data were obtained at a 50 mV/s scan rate in Tris buffer (10 mM Tris-HCl, 50 mM NaCl, 10 mM $MgCl_2$ and 4 mM spermidine, pH 7) and averaged over the similar electrodes on the chip.

over 100 electrodes (34). Therefore, the 34 nm DNA was comparably as effective a surface-to-probe bridge as smaller oligonucleotides.

To verify that the charge was passing through the DNA, we also measured the electrochemistry of well matched DNA duplexes against duplexes that contained a single mismatched base pair (CA) on the same chip (Figure 3.3a). Mismatched bases have been shown to attenuate DNA CT through perturbations of the π-stack (24, 25, 34, 39). Comparing well matched and mismatched DNA monolayers on the same chip ensured that both were subjected to the same processing conditions. As seen, the mismatch clearly attenuates the CT signal, as the average CV peak area was significantly lower, measuring only 0.8 ± 0.1 nC and 1.8 ± 0.2 nC for the cathodic and anodic peaks, respectively. This is a factor of two or more lower than that of the well matched monolayer in each case. The mismatched peaks exhibit slightly larger splitting, although this difference does not hold at higher scan rates. This effect is independent of mismatch position; placement of the mismatch at positions that differed by up to 20 base pairs in the 100-mer, through single base changes in the central 36-mer segment, resulted in similar signal attenuation (data not shown). The mismatch inhibited the transport capability of the DNA bridge regardless of its position in the 100-mer.

To establish the reproducibility of mismatch attenuation, we tested DNA CT of well-matched and mismatched 100-mer monolayers side-by-side across six chips, which represented over 40 electrodes of each type of monolayer (configuration as illustrated in Figure 3.3a). We found that the ratios of the cathodic CV peak areas of well-matched to mismatched monolayers were 2.3 ± 0.4. A *t*-test of this ratio distribution in comparison to the null ratio of 1 had a *p*-value of 0.0005. By comparison, this well matched to

mismatched ratio is 1.9 to 3.5 for various intercalating redox probes in 15-mer DNA (24) and 2.7–2.8 for 17-mer DNA with a Nile Blue redox probe (34). The consistency of this measured attenuation for mismatches with prior measurements of mismatched monolayers demonstrates that charge flow depends on the integrity of the DNA π-stack, a strong argument that transport occurs through the 100-mer DNA. Furthermore, that a single defect in a 100-mer produced an effect similar to one in much shorter DNA is remarkable given the substantial length disparity.

Kinetics of DNA CT Through 100-mer Monolayers

Electron transfer kinetics were estimated by measuring the scan-rate dependence of the peak splitting between the anodic and cathodic Nile Blue CV peaks of these DNA monolayers. At high scan rates (> 1 Vs^{-1}), the voltammetry enters the totally irreversible reaction regime and the peak splitting becomes linear with scan rate. By applying Laviron analysis (40) in this regime, the electron transfer rate k can be estimated. Interestingly, the electron transfer kinetics of well matched and mismatched 100-mer DNA monolayers were virtually identical, as with prior measurements of 17-mers (Figure 3.4) (34). For the well-matched 100-mer, k_{100} = 39 s^{-1}, and similarly the mismatched 100-mer yielded k_{100} = 40 s^{-1}.

Although slow, these transfer rates are significantly faster than those expected for tunnelling across 34 nm from the electrode directly to the redox probe (41–43). These figures are also indistinguishable (given the analysis) from those obtained from the 17-mer monolayer on the same chip, for which k_{17} = 25 s^{-1}, consistent with our previous studies of DNA of similar lengths (34, 44–47). Thus, the electron transfer rates of these

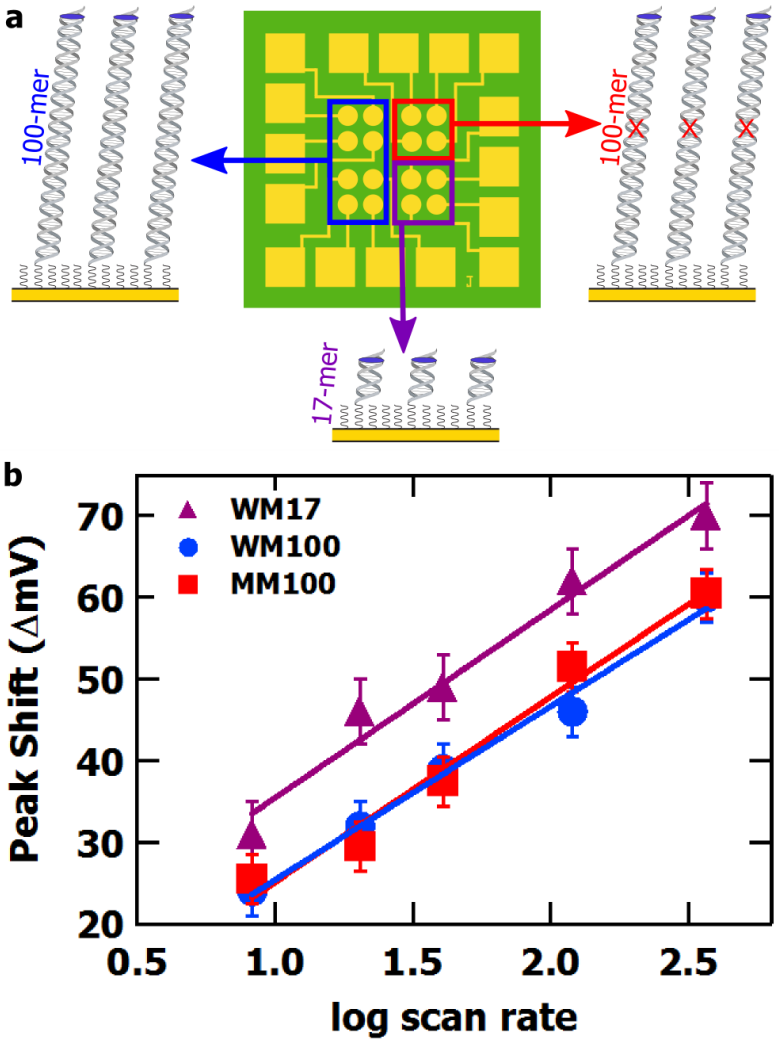

Figure 3.4 Kinetics of CT through 100-mer and 17-mer monolayers**. a**, The chip layout for testing electron transfer kinetics. **b**, CV peak splitting versus scan rate for well matched (WM) and mismatched (MM) 100-mer DNA monolayers along with well matched 17-mer monolayers as averaged over four devices on a single chip. Data were obtained in Tris buffer (10 mM Tris-HCl, 50 mM NaCl, 10 mM $MgCl_2$ and 4 mM spermidine, pH 7). By applying Laviron analysis in this linear regime, the electron transfer coefficient and electron transfer rate were obtained. Values are $\alpha = 0.6$ and $k =$ 30–40 s^{-1} for well matched 100-mer, mismatched 100-mer, and well matched 17-mer monolayers.

monolayers exhibit essentially no variation with length over this regime. Previous transfer-kinetic studies of DNA monolayers with 16-mer sequences showed an exponential dependence of the electron transfer rate with linker length with a coefficient for the electronic coupling, β = 1 Å^{-1}, consistent with values expected for tunnelling through a saturated carbon linker (47); the extrapolated transfer rate through the 16-mer DNA in the absence of the linker was ~10^8 s^{-1}. It appears that the rate-limiting step is not CT through the DNA duplex, but rather transport through the alkanethiol linker. Thus, the estimated rates are also fully consistent with rapid transfer through the 100-mer DNA assembly.

To provide further evidence that CT in the 100-mer is DNA-mediated and does not involve direct interaction of the Nile Blue probe with the surface, we prepared a chip with the well matched 100-mer, a well matched 17-mer, the 100-mer assembly without the central 36-mer single-stranded segment, and the single-stranded, Nile Blue-modified 25-mer (ssNB 25-mer) alone without complement (Figure 3.5). The ssNB 25-mer was included as a clear control for direct contact of the redox probe with the surface. Since this single-stranded segment of DNA lacks a thiol, the only mode by which it may adhere to the electrode is by adsorption onto the gold through direct interactions of the bases and redox probe with the surface. Thus, probe reduction must necessarily be due to direct surface contact and not DNA CT.

Consistent with this, it is evident in Figure 3.5 that the CV of the 100-mer differs significantly from that of the adsorbed ssNB 25-mer, not only with respect to the signal intensity and peak shape, but also with respect to peak splitting and midpoint potential. The CV of the 100-mer instead resembles that of the 17-mer, for which CT is DNA-

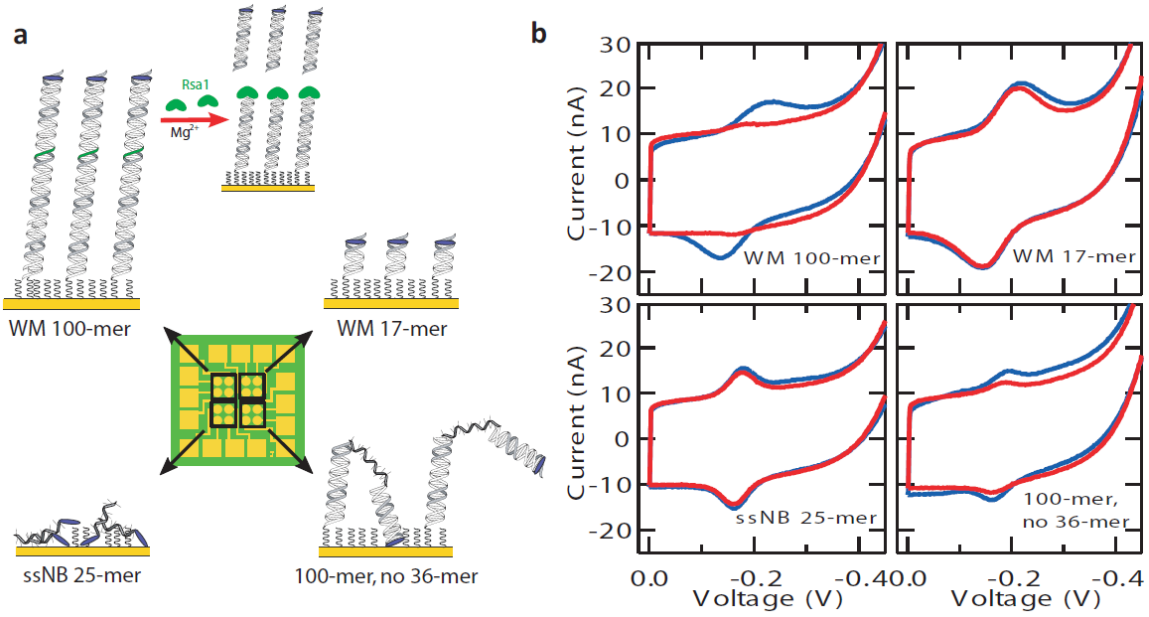

Figure 3.5 Electrochemistry and enzymatic activity on fully and partially assembled DNA films. **a**, The chip layout used to measure the electrochemical characteristics and *Rsa*I activity with four DNA films (from top left to bottom right) including the well matched 100-mer which contains the *Rsa*I binding site, a well matched 17-mer that does not contain the *Rsa*I binding site, the single stranded 25-mer modified with Nile Blue (ssNB), and the 100-mer without the central 36-mer segment. As illustrated, the ssNB 25-mer and 100-mer without the central 36-mer are expected to be reduced through direct surface adsorption and contact. Figure (**a**) also illustrates restriction of the well matched 100-mer DNA films upon addition of *Rsa*I and Mg^{2+}. **b**, CV scans of the four DNA films before (blue) and after (red) the addition of *Rsa*I. The enzyme reaction was carried out in Tris buffer (10 mM Tris-HCl, 50 mM NaCl, 10 mM $MgCl_2$, 4 mM spermidine, pH 7.9). Scans were taken before and after the enzyme reaction in phosphate buffer (5 mM phosphate, 50 mM NaCl, 4 mM $MgCl_2$, 4 mM spermidine, 10% glycerol, pH 7). CV scans were measured versus Ag/AgCl at a scan rate of 100 mV s-1. For the 100-mer, 17-mer and single stranded 25-mer, respectively, the peak splittings are 80 mV, 60 mV, and 15mV, the midpoint potentials are -180 mV, -180mV, and -170mV, and $k_{100} = k_{17} = 1/39\ k_{ss25}$. Values could not be determined accurately for the 100-mer without the 36-mer segment.

mediated. Moreover, although direct surface reduction of the Nile Blue probe on the ssNB 25-mer yields a sharp CV peak that shows only minor splitting at fast scan rates, DNA-mediated reduction of the Nile Blue probe through the well matched 100-mer and 17-mer yield a broad peak that is split significantly and further broadened at fast scan rates. These pronounced, visible differences in the electrochemistry can be attributed to the greater kinetic barrier associated with charge transfer through the DNA as compared to direct contact and reduction at the electrode surface. This kinetic difference is highlighted further by the measured CT rates for these samples: surface reduction of the Nile Blue probe on the ssNB 25-mer occurs at a nearly 40-fold faster rate than charge transfer through the 100-mer and 17-mer DNA, based on Laviron analysis for these chips. Although kinetic comparisons can be made between these assemblies, signal intensities are hard to compare because of the substantial differences in mode of adherence to the surface and the resultant packing densities.

Also shown in Figure 3.5, omission of the central 36-mer to create a duplex with a central single-stranded segment that can easily bend and sway also yields drastic electrochemical changes. Not only is its redox peak significantly smaller than that of the fully assembled 100-mer (cathodic peak size of 0.7 nC versus 2 nC, respectively), the decreased peak splitting and sharper peak shape much more closely resemble those of the ssNB 25-mer. Thus, the Nile Blue redox signal of the 100-mer DNA missing the 36-mer segment is probably caused by direct contact of the probe with the surface, just as for the single-stranded 25-mer. Interestingly, the signal for this disordered jumble of DNA on the surface is much smaller than the signal from either the ssNB 25-mer or the fully assembled, well matched 100-mer.

*Rsa*I Restriction Activity on 100-mer Monolayers

Restriction enzyme activity on these 100-mer-modified electrodes provided another probe of the DNA-mediated reaction. To facilitate restriction, the restriction site must be accessible for protein binding and in a biologically recognizable conformation. If the restriction site is below the Nile Blue redox probe and if the duplex is upright and does not contact the surface, successful cutting releases the probe into solution. This activity on a DNA-modified electrode destroys the pathway of DNA CT to the probe to yield significant loss of the redox signal.

To test for restriction-enzyme activity, chips with partial assemblies as shown in Figure 3.5 were exposed to the restriction enzyme *Rsa*I, which cuts the sequence 5′-GTAC-3′ with high specificity and leaves blunt ends on the resulting DNA segments. For these chips, the 100-mer is the only DNA assembly with a viable *Rsa*I restriction site. After incubation of the enzyme with 10 mM Mg^{2+} for 15 minutes on the chip, substantial signal attenuation (90% by the cathodic peak area of the CV) is observed for the 100-mer, while the other quadrants remain essentially unchanged. This result demonstrates clearly that the DNA in these 100-mer monolayers is accessible to the protein and in a biologically recognizable conformation. Moreover, in the 100-mer, CT is necessarily DNA-mediated. For the quadrant containing the ssNB 25-mer which directly contacts the surface, exposure to *Rsa*I caused no change in the signal. For the quadrant containing the 100-mer without the central 36-mer segment, the minimal signal loss (10% by the cathodic peak of the CV) is probably due to the instability of this assembly to the electrode rinsing and buffer-exchange steps required for this experiment. For the 17-mer duplex, there is no restriction site and therefore no expectation of signal attenuation. For

the 100-mer, then, the attenuation we observed must reflect that CT to the Nile Blue probe is DNA-mediated; if the Nile Blue redox probe of the 100-mer were directly adsorbed to the surface, no response to *Rsa*I treatment would be expected.

Restriction-enzyme activity was also monitored as a function of time in the well matched 100-mer alongside other DNA duplexes that contain the *Rsa*I binding site (Figure 3.6). These included a well matched 17-mer (with a different sequence than that which was used in the partial assembly experiment) and the 100-mer with a single base-pair mismatch (not at the restriction site). As these three types of DNA all contain the *Rsa*I binding site, successful cutting will result in detachment of the Nile Blue redox probe and attenuation of the electrochemical signal. As a negative control, one well of the chip was modified with the well matched 100-mer, but was not treated with *Rsa*I. Initially, before the enzyme was added, the signals from all the monolayers were stable in the buffer solution. Subsequently, *Rsa*I was added to the quadrants that contained the well matched 100-mer, well matched 17-mer, and mismatched 100-mer. The fourth quadrant, which was modified with the well matched 100-mer, was isolated in a separate well maintained free of enzyme. While activation of the enzyme with Mg^{2+} triggers a rapid decrease in integrated charge on the *Rsa*I-exposed quadrants, the signal from the quadrant not treated with enzyme increases slightly. The loss of Nile Blue signal for the three *Rsa*I-treated quadrants is consistent with *Rsa*I cleavage activated by divalent cations. In the isolated quadrant where the DNA is intact, Mg^{2+} enhances the signal. The observation of enzymatic activity in these monolayers demonstrates that the DNA is in its native conformation and is biologically accessible and active.

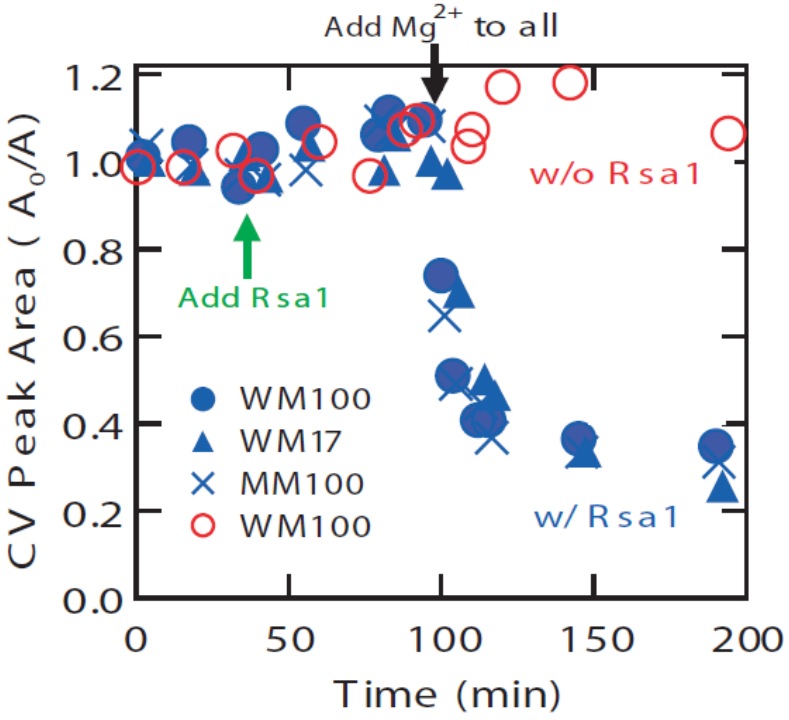

Figure 3.6 Enzymatic activity on 100-mer monolayers as a function of time. Integrated cathodic CV peak area versus time for various DNA monolayers exposed to *Rsa*I (red) and 100-mer DNA in the absence of enzyme (blue). The types of DNA tested include the well matched (WM) 100-mer, a well matched (WM) 17-mer, and the mismatched (MM) 100-mer, all of which contain the *Rsa*I binding site. The charge was obtained by integrating the cathodic Nile Blue CV peaks obtained at a 100 mV s^{-1} scan rate.

Summary and Conclusions

DNA-mediated electrochemistry through 100-mer monolayers revealed large signals for well matched duplexes, comparable to those observed with shorter duplexes. This result indicates that CT through DNA is robust in these long DNA films. Nonetheless, attenuation by single base mismatches illustrates the delicacy of this process and strongly argues that the integrity of the base pair π-stack is crucial. That a single mismatch within a 100-mer of otherwise well matched bases causes signal attenuation equal to that seen in mismatched DNA that is ~20% of the length establishes a new point of reference for the sensitivity of DNA CT to minor perturbations. Cutting with the *Rsa*I restriction endonuclease demonstrates the biological integrity of the monolayers and also illustrates the utility of these longer DNA assemblies for sensing DNA-binding protein reactions. The ability to construct these CT-active assemblies using smaller oligonucleotides may be particularly useful for associated nanoelectronics applications. All of these results document that DNA can efficiently facilitate CT over 100 base pairs, or 34 nm, close to the persistence length of duplex DNA in solution. This remarkable distance for CT surpasses those in other reports of long-range transport through conjugated molecular wires (8, 9), and is among the longest distances reported for a molecular monolayer (4, 5, 7, 48).

From our estimates of electron transfer rates, which are essentially the same for the 100-mer and 17-mer, the rate-limiting step must still be tunneling through the alkanethiol linker. This puts a lower bound on the rate of electron transfer through the 100-mer DNA itself. In our previous studies of a 16-mer, in which we saw significant variations in rate caused by linker length, we could extrapolate that the rate of electron

transfer through the 16-mer must be > 10^8 s^{-1}. Given our lower bound for the 100-mer, k_{100} = 10^2 s^{-1}, that is no faster than that through the linker, we obtain an estimate for β of 0.05 $Å^{-1}$ through the DNA. This conservative estimate is in the range of conventional conjugated molecular wires (0.001-0.2 $Å^{-1}$) (2-9). Simply put, even for this 34 nm DNA wire, the small alkanethiol linker is still rate-limiting.

The full mechanism associated with this DNA-mediated electrochemistry is still elusive, and this study highlights several observations that are difficult to reconcile. Despite a wide range of redox potentials, various redox probes are compatible with DNA electrochemistry as long as the probes are electronically well coupled to the DNA base-pair stack (28). For all of these probes we found that they are reduced at potentials near their free redox potentials. However, the reduction potentials of the individual bases were all significantly higher than the redox potentials of the probes. In this study, the reduction potential of Nile Blue (-250 mV versus Ag/AgCl) is substantially more positive than that of any of the free bases (less than -1 V versus Ag/AgCl) (49). To date, direct reduction of DNA has not been observed at the potentials of these redox probes, nor would it be consistent with the parameters involved. This conundrum could be reconciled if the stacked DNA duplex forms a delocalized band structure, different from individual bases, that has a low-lying lowest unoccupied molecular orbital from the overlapping π-orbitals of the bases. Although such a band structure is plausible, to date an equilibrium band structure has not been observed experimentally. Our group thus postulated that DNACT is conformationally gated and that the CT-active state or states are transient, nonequilibrium states (50). Experimental evidence suggests that in solution these states, which we consider to be delocalized domains of the π-stacked bases, extend

over about four base pairs (50). Whether these domains are more extended or less transient within the DNA film versus within solution is unclear. Unlike conventional molecular wires, which exhibit inherent rigidity, DNA undergoes motions on time scales of picoseconds to milliseconds. The fleeting alignment of the bases creates a delicate π-network with CT states that are active only transiently. The observation that a single mismatch in a 100-mer is resolved with the same degree of signal attenuation as seen in much shorter DNA further underscores how remarkably small perturbations in this system profoundly influence the global orbital network. A poorly stacked single base-pair mismatch may block the formation of the potential band structure.

Is DNA a molecular wire? In this experiment, clearly it bridged the electrode and redox probe over 34 nm. DNA not only fulfils many of the requirements of molecular wires, but also it surpasses conventional wires in its ease of synthesis and flexibility of design. However, this is a transient and fragile wire, as it must be maintained in buffered solution, and effective conduction over its length is extraordinarily sensitive to subtle structural variations. Indeed, the DNA bridge may be considered instead as an extension of the gold electrode, a sensor 34 nm long to detect solution-borne targets. Although the sensitivity to base stacking presents a challenge for the use of DNA as a molecular wire for integrated circuits, the ability to make long, well coupled DNA assemblies in circuits is a clear benefit. On the other hand, this exquisite electronic sensitivity to structural perturbations actually makes the DNA wire ideal for biosensing under physiological conditions.

References

1. Robertson, N. and McGowan, C.A. (2003) *Chem. Soc. Rev. 32*, 96–103.

2. Chen, F. and Tao, N. J. (2009) *Acc. Chem. Res. 42*, 429–438.

3. Malliaras, G. and Friend, R. (2005) *Phys. Today 58*, 53–58.

4. Tuccitto, N. et al. (2009) *Nat. Mater. 8*, 41–46.

5. Choi, S.H., Kim, B., and Frisbie, C.D. (2008) *Science 320*, 1482–1486.

6. Liu, L. and Frisbie, C.D. (2010) *J. Am. Chem. Soc. 132*, 8854–8855.

7. Søndergaard, R. *et al*. (2009) *J. Mater. Chem. 19*, 3899–3908.

8. Hu, W. *et al*. (2006) *Phys. Rev. Lett. 96*, 027801.

9. Vura-Weis, J. *et al*. (2010) *Science 328*, 1547–1550.

10. Drummond, T.G., Hill, M.G., and Barton, J.K. (2003) *Nat. Biotechnol. 21*, 1192–1199.

11. Liu, J., Cao, Z. and Lu, Y. (2009) *Chem. Rev. 109*, 1948–1998.

12. Endres, R.G., Cox, D.L. and Singh, R.R.P. (2004) *Rev. Mod. Phys. 76*, 195–214.

13. Roy, S. *et al*. (2008) *Nano Lett. 8*, 26–30.

14. Murphy, C.J. *et al*. (1993) *Science 262*, 1025–1029.

15. Fink, H.W. and Schoenberger, C. (1999) *Nature 398*, 407–410.

16. de Pablo, P.J. *et al*. (2000) *Phys. Rev. Lett. 85*, 4992–4995.

17. Kasumov, A. *et al*. (2001) *Science 291*, 280–282.

18. Storm, A.J., van Noort, J., de Vries, S. and Dekker, C. (2001) *Appl. Phys. Lett. 79*, 3881–3883.

19. Guo, X., Gorodetsky, A.A., Hone, J., Barton, J.K. and Nuckolls, C. (2008) *Nat. Nanotech. 3*, 163–167.

20. Kelley, S.O. and Barton, J.K. (1999) *Science 283*, 375–381.

21. Cohen, H., Nogues, C., Naaman, R., and Porath, D. (2005) *Proc. Natl Acad. Sci. USA 102*, 11589–11593.

22. Xu, B., Zhang, P., Li, X., and Tao, N. (2004) *Nano Lett. 4*, 1105–1108.

23. Kelley, S.O., Holmlin, R.E., Stemp, E.D.A. and Barton, J.K. (1997) *J. Am. Chem. Soc. 119*, 9861–9870.

24. Kelley, S.O., Boon, E.M., Barton, J.K., Jackson, N.M. and Hill, M.G. (1999) *Nuc. Acids Res. 27*, 4830–4837.

25. Boon, E.M., Ceres, D.M., Drummond, T.G., Hill, M.G. and Barton, J.K. (2000) *Nat. Biotechnol. 18*, 1096–1100.

26. Nuñez, M.E., Hall, D.B. and Barton, J.K. (1999) *Chem. Biol. 6*, 85–97.

27. Boon, E.M., Salas, J.E., and Barton, J.K. (2002) *Nat. Biotechnol. 20*, 282–286.

28. Genereux, J.C. and Barton, J.K. (2010) *Chem. Rev. 110*, 1642–1662.

29. O'Neil, M.A. and Barton, J.K. (2005) *Charge Transfer in DNA: From Mechanism to Application.* Wagenknecht, H.A. Wiley-VCH, Ed., 27.

30. Kawai, K., Kodera, H., Osakada, Y., and Majima, T. (2009) *Nat. Chem. 1*, 156–159.

31. Douglas, S.M. *et al*. (2009) *Nature 459*, 414–418.

32. Rothemund, P.W.K. (2006) *Nature 440*, 297–302.

33. Soleymani, L. *et al*. (2010) *Nat. Nanotech. 4*, 844–848.

34. Slinker, J.D., Muren, N.B., Gorodetsky, A.A., and Barton, J.K. (2010) *J. Am. Chem. Soc. 132*, 2769–2774.

35. Gorodetsky, A.A., Ebrahim, A., and Barton, J.K. (2008) *J. Am. Chem. Soc. 130*, 2924–2925.

36. Liu, T. and Barton, J.K. (2005) *J. Am. Chem. Soc. 127*, 10160–10161.

37. Kelley, S.O. *et al*. (1998) *Langmuir 14*, 6781–6784.

38. Sam, M., Boon, E.M., Barton, J.K., Hill, M.G., and Spain, E.M. (2001) *Langmuir 17*, 5727–5730.

39. Boal, A.K. and Barton, J.K. (2005) *Bioconj. Chem. 16,* 312–321.

40. Laviron, E. (1979) *J. Electroanal. Chem. 101,* 19–28.

41. Weber, K., Hockett, L. and Creager, S. (1997) *J. Phys. Chem. B 101*, 8286–8291.

42. Huang, K. *et al*. (2009) *ChemPhysChem 10*, 963–971.

43. Yu, H.Z., Shao, H.B., Luo, Y., Zhang, H.L. and Liu, Z.F. (1997) *Langmuir 13*, 5774–5778.

44. Boon, E.M. and Barton, J.K. (2003) *Langmuir 19*, 9255–9259.

45. Kelley, S.O., Jackson, N.M., Hill, M.G., and Barton, J.K. (1999) *Angew. Chem. Int. Ed. 38*, 941–945.

46. Gorodetsky, A.A., Green, O., Yavin, E., and Barton, J.K. (2007) *Bioconj. Chem. 18*, 1434–1441.

47. Drummond, T.G., Hill, M.G., and Barton, J.K. (2004) *J. Am. Chem. Soc. 126*, 15010–15011.

48. Arikuma, Y., Nakayama, H., Morita, T., and Kimura, S. (2010) *Angew. Chem. Int. Ed. 49*, 1800–1804.

49. Steenken, S., Telo, J.P., Novais, H.M., and Candeias, L.P. (1992) *J. Am. Chem. Soc. 114*, 4701–4709.

50. Genereux, J.C., Augustyn, K.E., Davis, M.L., Shao, F., and Barton, J.K. (2008) *J. Am. Chem. Soc. 130*, 15150–15156.

Chapter 4

DNA Charge Transport in Single Molecules: Length Dependence Measurements and Detection of Methyltransferase Binding and Activity

Adapted from Wang, H., Muren, N. B., Ordinario, D., Gorodetsky, A. A., Barton J. K., and Nuckolls, C. (2012) *Chem. Sci*. *3*, 62-65.

H. Wang, D. Ordinario, and A.A. Gorodetsky prepared CNT-DNA devices and collected conductivity data. N.B. Muren synthesized DNA and assisted with data analysis and interpretation.

Introduction

Carbon nanotube (CNT)-based devices, in which single molecules span an oxidatively cut gap in the CNT, provide a versatile platform with well defined electrical contacts that has previously been used to measure the electrical properties of a variety of small molecule bridges (1–9). Importantly, these measurements can be carried out in aqueous solution, making them useful for measurements involving biomolecules. Previously, this platform was shown to be highly effective for single molecule measurements of DNA-mediated charge transport (DNA CT) through DNA duplexes that covalently bridge the CNT gap (Figure 4.1) (9). In these studies, the path of CT through the device was confirmed to be DNA-mediated because of the dramatic loss of current flow induced by single base mismatches in the bridging duplex, a result that is consistent with measurements of DNA CT in ensemble electrochemical studies (10–13). Additionally the single DNA duplex that is wired into the device was shown to be readily bound and cut by a restriction endonuclease, indicating that it is maintained in a biologically recognizable and accessible conformation (9).

This previous work suggests that CNT-DNA devices may be utilized for other measurements and applications of DNA CT that have previously been limited to bulk solution and electrochemical studies. Though challenging, single molecule measurements provide more direct information about the fundamental electronic properties of a molecule than do ensemble measurements (14). Additionally, the inherent responsiveness of single molecule platforms and the extreme sensitivity of DNA CT to structural perturbations enhance each other when combined for biosensing applications.

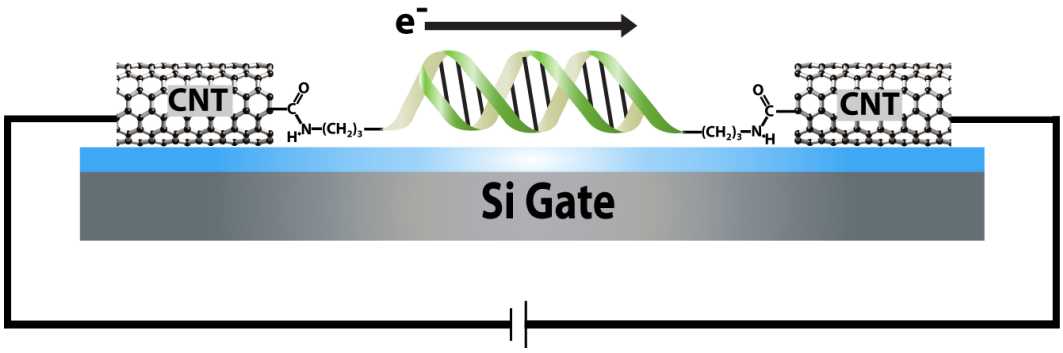

Figure 4.1 Electronic integration of DNA into a CNT device. Oxidative cutting of the CNT creates a gap with carboxylic acid point contacts on the cut ends. Amine-modified DNA is then covalently attached to these point contacts by peptide coupling to form an electronic bridge across the gap. The resulting DNA-mediated path for current flow through the device is sensitive to structural perturbations that disrupt DNA CT.

Here, we show work to extend this single molecule, CNT-DNA platform to measurements of the distance dependence of DNA CT and to electrical detection of methyltransferase binding and activity.

The characterization of long-range CT in DNA is an important goal not only for our fundamental understanding of this process but also to determine how this property might be exploited for nanoelectronics and biotechnology applications. Additionally, basic rate and distance dependence measurements will be key for the interpretation of growing evidence that DNA CT may be utilized in living organisms for long-range signaling toward the coordination of complex cellular activities (15). Previous measurements in solution and with surface electrochemical platforms indicate that the distance dependence of DNA CT is very shallow and puts DNA within the conductive range of other molecular wires (16–19).

In electrochemical, ground state measurements of DNA CT over 34 nm (100 bp), for example, CT was limited not by the DNA length but by the C6 alkanethiol linker used to attach the DNA to the electrode surface (19). Although this limit prevents the direct calculation of β—a parameter that describes the distance dependence of the CT rate—the dominance of the linker, even over 34 nm, provides compelling support for a shallow distance dependence. An estimated β value of 0.05 $Å^{-1}$ from these measurements agrees with previous work in solution (16, 17), putting DNA among the longest molecular wires reported to date (19). Here we investigate this distance dependence further with ground state, single molecule measurements of DNA CT. We fabricate and characterize CNT-DNA devices with DNA bridges of varying length (up to 34 nm) and also investigate the effect of linker length (C3 vs. C6) on these measurements.

In general for the detection of biomolecules, CNTs and nanowires incorporated into field-effect transistors offer valuable electrical detection platforms because their conductivity is modulated by binding of analytes (20–24). One drawback of these devices is that the conductivity changes are not specific and depend upon the characteristics of the analyte and its mode of interaction with the CNT (25, 26). Interference caused by nonspecific binding of analytes presents a significant challenge for specific detection, particularly in single molecule measurements. The electronic integration of DNA into these devices, with its dual function as recognition element and transducer, helps to overcome this challenge, especially for the detection of DNA-binding proteins. The programmable sequence of DNA imparts specific recognition by protein targets, and the structural sensitivity of DNA CT facilitates the direct conversion of protein binding into an electrical signal.

The use of DNA CT for the sensitive and specific detection of proteins has already been demonstrated on electrochemical platforms (27, 28). Proteins that distort the structure of the DNA π-stack upon binding, such as methyltransferases which bind DNA and flip a base completely out of the duplex (29, 30), have been shown electrochemically to cause a sharp attenuation of DNA CT (27). In this study, we use the CNT-DNA platform to detect single molecule binding and activity by the methyltransferase *Sss*I which binds the sequence 5′-CG-3′ and, with the methyl donor S-adenosyl methionine (SAM), methylates the cytosine base (31). This methyltransferase is considered the bacterial analog to human methyltransferases, which also recognize and methylate the same site (31). We show that CNT-DNA devices can be used to detect binding and base flipping by single molecules of *Sss*I based on the resulting disruption of

DNA CT and thus current flow through the device. Additionally, methylation of the devices by *Sss*I alters the binding potential of the bridging DNA substrate and this effect may be monitored electrically.

Materials and Methods

Materials

All standard and modified phosphoramidites were purchased from Glen Research. All other chemicals for the preparation of DNA, buffers, and CNT-DNA devices were purchased from Sigma-Aldrich and used as recieved. The methyltransferase *Sss*I and BSA were purchased from New England Biolabs, stored at -20°C, and used as received.

DNA Sequences

For distance dependence studies, the 15-mer, 40-mer, 60-mer, 80-mer, and 100-mer were designed such that one strand in each duplex carried a C3 amine linker at each end and the complementary strand was unmodified. For the 15-mer, the sequence was: 5'-H_2N-$(CH_2)_3$-GAC AGT CGA CAT GTC-$(CH_2)_3$-NH_2-3'. For the 100-mer, the sequence was: 5'-H_2N-$(CH_2)_3$-AGT ACT GCA GTA TCG ACG TCA TAG GAC ATT GGA GCG CTC CAG CTG TGA CAT ATA AAA GTA GTG AGT CAA TCG TGT ACT GTA GTC CAT GTA TAC TGC ACT A-$(CH_2)_3$-N_2H-3'. For the 40-mer, 60-mer, and 80-mer the sequences were identical to the 100-mer but with 30, 20, and 10 bases, respectively, removed from each end.

For *Sss*I binding and activity studies, 15-mers with one or more *Sss*I binding sites (5′-<u>CG</u>-3′, shown underlined) were used including: H_2N-$(CH_2)_3$-5′-GAC AGT <u>CG</u> ACA

TGT C-3′-$(CH_2)_3$-NH_2 and H_2N-$(CH_2)_3$-5′-CG GCC CG GC CG CG CG-3′-$(CH_2)_3$-NH_2. A 15-mer without the *Sss*I binding site was also used: H_2N-$(CH_2)_3$-5′-ATTAAATTAATATAT-3′-$(CH_2)_3$-NH_2.

DNA Synthesis and Purification

Oligonucleotides were synthesized on an Applied Biosystems 3400 DNA Synthesizer using standard reagents. The amine-modified strands were synthesized with 3'-PT-amino-modifier C3 CPG beads to modify the 3' end and a 5'-amino-modifier C3-TFA phosphoramidite to modify the 5' end. The unmodified complement was synthesized using standard reagents and procedures. Both amine-modified and unmodified DNA were cleaved from the solid support and deprotected by treating with concentrated ammonium hydroxide for 8 hrs. at 60 °C. All DNA was purified by high-performance liquid chromatography (HPLC) on a polymeric PLRP-S column (Agilent) with a 50 mM ammonium acetate buffer/acetonitrile gradient. For the 40-mer, 60-mer, 80-mer, and 100-mer strands, the column was heated to 60 °C to discourage the formation of secondary structures. At least two rounds of HPLC were performed on each DNA type to achieve highly pure samples. After purification, samples were characterized by matrix-assisted laser desorption/ionization time of flight mass spectrometry. DNA stocks were then desalted, resuspended in phosphate buffer (5 mM phosphate, 50 mM NaCl, pH 7), and quantified by UV/Vis absorption at 260 nm according to their extinction coefficients (IDT Oligo Analyzer). Equimolar amounts (50 μM) of complementary strands were combined and thermally annealed.

CNT-DNA Device Preparation

Devices with electronically wired CNT point contacts were prepared as described previously (4–9, 32, 33). Briefly, chemical vapor deposition was used to grow sparse single walled CNTs on a doped silicon wafer containing 300 nm of native oxide on its surface. The surface was then coated with PMMA photoresist (Microchem) and conventional photolithography was used to pattern gold source and drain electrodes over the CNTs with a grid shadow mask (SPI Supplies). For each device, electron beam lithography was then used to remove the PMMA coating from a section of the nanotube. The exposed portion was then cut with an oxidative plasma etch, leaving carboxylic acids on the two termini of the cut nanotube. Importantly, the size of the gap cut in the nanotube was adjusted to fit precisely the length of a given DNA bridge. To prepare the devices for reconnection with DNA, the nanotubes were treated with a 2-(*N*-morpholino) ethansulfonic acid (MES) buffer solution (0.1 M) with EDCI (5 mM) and Sulfo-NHS (10 mM) overnight to activate the carboxylic acid termini inside the CNT gap. Following this, the devices were rinsed with MES buffer, dried, and treated with 5 μM DNA in phosphate buffer to reconnect the devices with DNA.

Electrical Measurements of DNA Length Dependence and SssI Binding

Electrical measurements for all devices were performed under ambient, buffered conditions with the silicon wafer serving as a global back gate. A mechanical probe station was used to make electrical contact to each device and a semiconductor device analyzer (Agilent) was used to collect and process electrical data. For DNA length dependence studies, the resistance of devices connected with various lengths of DNA was

measured over a rage of gating voltages (-3 V to 1 V). The highest resistance measured over this range was taken as the resistance of the device and a plot of resistance vs. DNA length was compiled. From this plot, the distance dependence parameter β was extrapolated by fitting the plot with the exponential shown in equation 1:

$$R = R_0 e^{\beta L} \quad (1)$$

where R is the device resistance, R_0 is the y-intercept, and L is the DNA bridge length.

For measurements of *Sss*I binding, reconnected devices with or without the recognition site were treated with 6 nM *Sss*I and 300 μM SAM in *Sss*I reaction buffer (10 mM Tris-HCl, 50 mM NaCl, 10 mM $MgCl_2$, 1 mM Dithiothreitol, pH 7.9). The conductance of each device was measured over a range of gating voltages (-3 V to 1 V), before and after *Sss*I treatment as well as after rinsing away the bound protein. The highest conductance measured in this range for a given condition was taken to represent the device conductance for that condition, and all conductance values for a device were normalized with respect to the overall highest conductance measured for the device.

Results and Discussion

Single Molecule Length Dependence Measurements of DNA CT

For DNA length dependence measurements, CNT-DNA devices were prepared with bridging DNA segments of varying length including a 15-mer (5 nm), 40-mer (14 nm), 60-mer (20 nm), 80-mer (27 nm), and 100-mer (34 nm), all with C3 amine linkers. For each DNA length, the resistance of 3–5 different reconnected devices was measured These data were plotted (Figure 4.2) and fit to equation 1. The line of best fit for these data gives a β value of 0.01 $Å^{-1}$. This shallow distance dependence is in agreement with

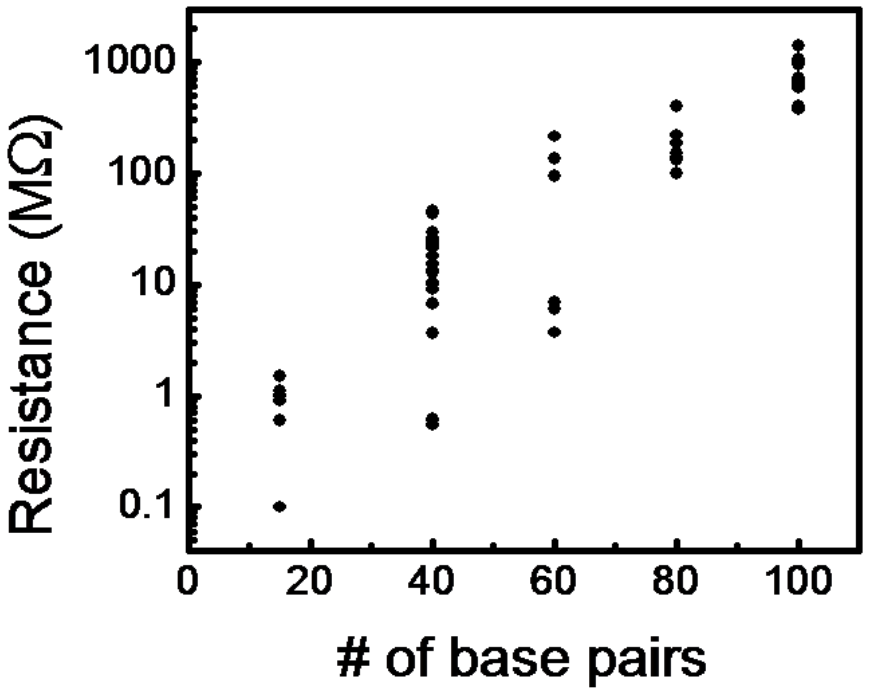

Figure 4.2. Resistance of DNA spanning a carbon nanotube gap as a function of DNA length. Data shown are for DNA attached to the CNT device by a C3 linker. The highest resistance measured over a rage of gating voltages (-3 V to 1 V) for each device was taken as the resistance of the device. Measurements from multiple devices are shown for each DNA length. The data are fit to equation 1 to give a β value of 0.01 $Å^{-1}$.

previous ensemble measurements on DNA-modified electrode surfaces in which a conservative estimate of β was made at 0.05 $Å^{-1}$ (19).

In contrast to ensemble electrochemistry measurements in which the C6 alkanethiol linker, not the DNA length, limits the rate of DNA CT over 34 nm, it appears here that the C3 linker may not be limiting. If the C3 linker limited DNA CT in this case, the same resistance value—the resistance contribution of the two C3 linkers—would be expected for each DNA length. Although the variation in the measured resistance for each progressively longer DNA segment does overlap and thus makes it difficult to rule out a contribution from the linker, there is a clear trend toward increased resistance with increased DNA length. In particular, the average resistance for the 100-mer DNA bridge is statistically greater than the average resistance for the 15-mer. As a control, and to gain more information about the contribution of the alkane linker to these measurements, DNA duplexes of the various DNA lengths with C6 amine linkers are currently being studied.

Single Molecule Detection of *Sss*I Methyltransferase

The scheme for a typical *Sss*I binding experiment on a DNA-bridged device is given in Figure 4.3, and the corresponding conductance-voltage characteristics are given in Figure 4.4. For these initial experiments, a DNA bridge with more than one 5′-CG-3′ *Sss*I binding site was used. However, given the footprint of *Sss*I, which spans at least 6 base pairs on each side of the binding site (34), the 15-mer DNA segment is likely to only accommodate binding by a single *Sss*I protein at a central site. For devices reconnected with this DNA (3 devices), an average conductance of 1.4 ± 0.8 μS was observed (Figure

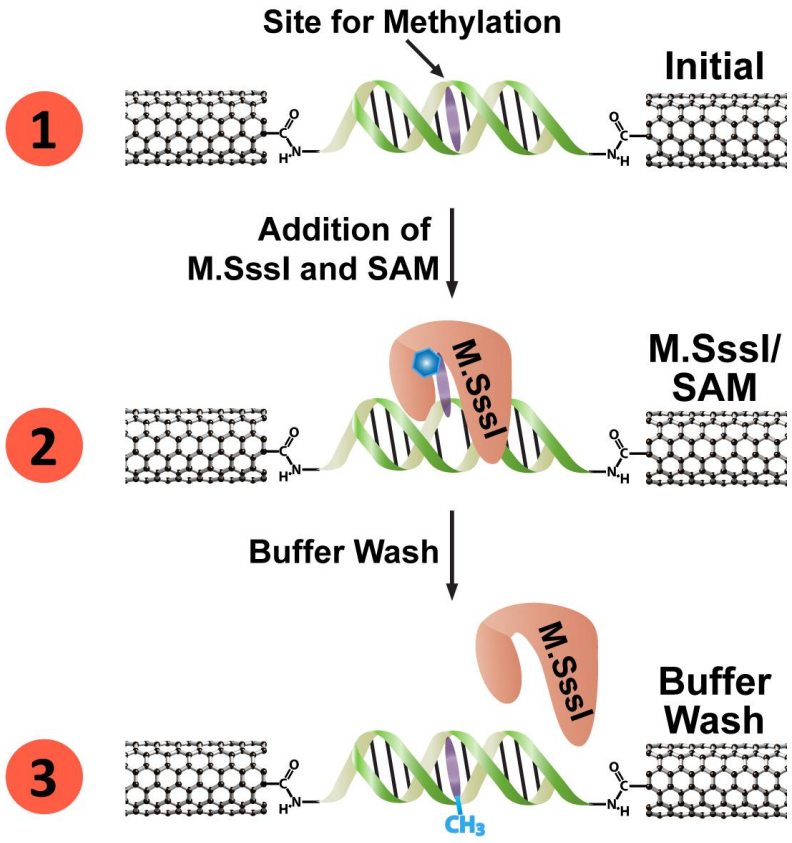

Figure 4.3 Electrical detection of *Sss*I binding at a DNA-bridged CNT device. All DNA for these experiments is attached to the CNT device by a C3 linker. (1) Duplex DNA containing the *Sss*I binding site (with target base to be methylated shown in purple) forms a conductive bridge between the two ends of a gap cut in a CNT device. (2) Upon addition of *Sss*I and SAM cofactor (represented by the blue hexagon), the methyltransferase binds the DNA at its recognition site, and flips the base to be methylated out of the DNA π-stack, thereby cutting off DNA CT. *Sss*I remains bound with the base flipped even after the methylation reaction is complete. (3) Upon rinsing, *Sss*I dissociates from the DNA; the methylated base re-inserts into the DNA π-stack and restores CT through the device.

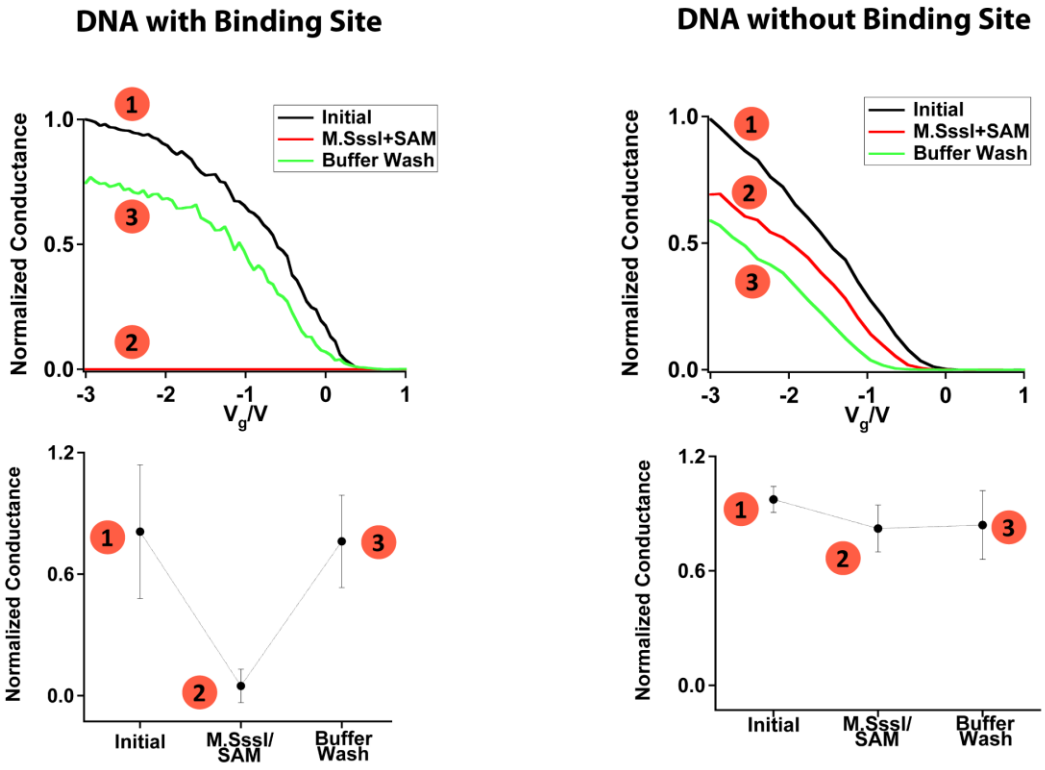

Figure 4.4 Sequence-specific, *Sss*I-DNA binding and disruption of DNA CT through the CNT device. Left column: *Sss*I binding at a DNA-bridged device containing the *Sss*I recognition site. The DNA sequence was H_2N-$(CH_2)_3$-5′-CGGCCCGGCCGCGCG-3′-$(CH_2)_3$-NH_2. Right column: lack of *Sss*I binding at a DNA-bridged device that does not contain the *Sss*I recognition site. The DNA sequence was H_2N-$(CH_2)_3$-5′-ATTAAATTAATATAT-3′-$(CH_2)_3$-NH_2. Typical normalized conductance curves (top row) and average relative conductance values (bottom row) are shown for the respective DNA-bridged devices. For each, the numbered points correspond to measurements at the numbered steps illustrated in Figure 4.3: (1) buffer before addition of *Sss*I, (2) buffer with *Sss*I and SAM, and (3) buffer after *Sss*I has been rinsed away. The buffer conditions were 10 mM Tris-HCl, 50 mM NaCl, 10 mM $MgCl_2$, 1 mM Dithiothreitol, pH 7.9. The conductance of each device was normalized with respect to the highest conductance value.

4.4, left column). Upon incubation of these devices with 6 nM *Sss*I and 300 μM of the requisite SAM cofactor, a 91% ± 15% reduction in the conductance was observed. Notably, the *Sss*I concentration utilized for our experiments is just below the binding affinity of this enzyme (K_d = 11 nM) (35). The crystal structure of the similar methyltransferase *Hha*I bound to methylated DNA shows that base flipping occurs even when the protein is bound to this substrate (30), although the binding affinity is reduced (36–38). In these single molecule devices, it is apparent that the protein remains bound with the base flipped out, even after the methylation reaction is complete. Washing these devices with buffer is necessary to dissociate the enzyme and recover the conductance to close to the initial value.

Sequence Specificity and SAM Dependence of *Sss*I Detection

To test for sequence-specific binding of *Sss*I, the nanotube gap was bridged with a sequence that lacks the *Sss*I binding site (Figure 4.4, right column). Before treatment with the methyltransferase, the devices showed an average conductance of 1.5 ± 0.4 μS. Even after extended incubation (>1 h) of these devices with *Sss*I and the SAM cofactor, no changes in the conductance of these devices was observed. Clearly, the specific recognition sequence is necessary for *Sss*I binding and subsequent base flipping that shuts off current flow through the device.

The cofactor SAM is required for methyltransferase activity, because it is the source of the electrophilic methyl group and is necessary for the specific binding of the enzyme to the substrate (31). Thus, to further confirm that the decrease in conductance is due to the specific binding and methyltransferase activity of *Sss*I, we investigated the

SAM-dependence of this decrease (Figure 4.5). To simplify the analysis, devices that were reconnected with DNA containing only one, centrally located 5′-CG-3′ binding site for *Sss*I were utilized. When these DNA-bridged devices were incubated with *Sss*I in the absence of the SAM cofactor, only a slight attenuation in conductance was observed. This may be due to the introduction of more scattering sites in the channel of the device upon nonspecific protein binding (5). However, when the same devices were subsequently incubated with *Sss*I in the presence of the SAM cofactor, a >90% attenuation of their conductance was observed. In turn, the conductance of the devices could be recovered to their original value with a buffer wash.

_Sss_I-catalyzed Device Methylation

Finally, the effect of methylation of the *Sss*I binding site on the measurement of subsequent activity by *Sss*I was investigated. To address this question, devices with a single *Sss*I binding site were again utilized. The devices were first exposed to *Sss*I and SAM in order to catalyze methylation of the DNA bridge. Similar to the experiments described above, a large decrease in the current flow through the device is observed, but the original conductivity is nearly recovered when the protein is washed away (Figure 4.5, steps 1–4). If this, now methylated, device is then re-subjected to *Sss*I and SAM treatment, no change in the conductance is observed (Figure 4.5, steps 5–7). This result reflects the reduced affinity of *Sss*I for methylated DNA. Initially, the 6 nM concentration of *Sss*I is high enough for binding and base flipping to occur at the non-methylated substrate. With the protein washed away, the added methyl group itself does

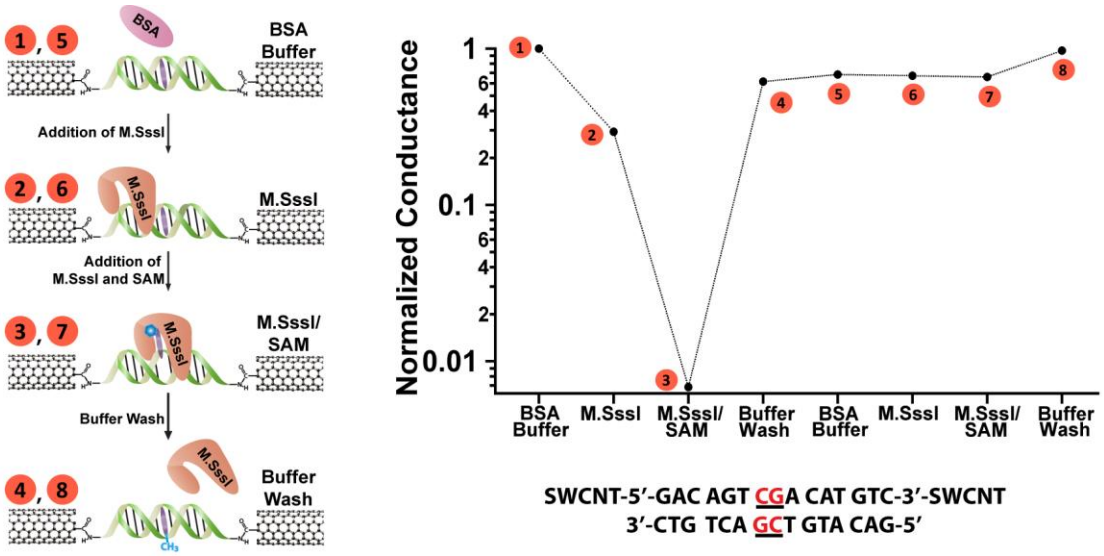

Figure 4.5 *Sss*I-catalyzed DNA methylation alters the protein-binding affinity of the device. A device containing a single *Sss*I binding site was taken through the illustrated and numbered steps (left) and the corresponding relative conductances (right) were measured in (1) buffer containing 10 nM BSA before addition of *Sss*I, (2) buffer and *Sss*I without SAM, (3) buffer and *Sss*I with SAM (represented by the blue hexagon), and (4) buffer after *Sss*I has been rinsed away. Note that current attenuation is only observed for step (3). After device methylation, the device was taken through the same sequence of steps 5-8 with no current attenuation observed. The sequence was H_2N-$(CH_2)_3$-5′-GACAGTCGACATGTC-3′-$(CH_2)_3$-NH_2, with the single 5′-CG-3′ site located at the center of the duplex. The buffer conditions were 10 mM Tris-HCl, 50 mM NaCl, 10 mM $MgCl_2$, 1 mM Dithiothreitol, pH 7.9.

not inhibit DNA CT as this modification does not perturb the π-stack. When the device is re-subjected to 6 nM *Sss*I, however, this concentration is no longer high enough to initiate binding to the now methylated DNA. These changes in the binding potential of the DNA are sensitively translated here from the single molecule level as an electrical output; chemical modification of the DNA wire by the protein alters subsequent protein binding and the resulting electrical response.

Summary and Conclusions

The experiments described here demonstrate the versatility of applications for which CNT-DNA devices may be used to measure DNA CT at the single molecule level. Using this platform, the distance dependence of DNA CT was investigated by preparing devices with DNA bridges of varying length and measuring current flow through these devices. For data collected at five different bridge lengths (15-mer, 40-mer, 60-mer, 80-mer, and 100-mer) a β value of 0.01 $Å^{-1}$ was derived. This shallow distance dependence measurement agrees strongly with the conservative estimate of β for DNA CT derived from ensemble measurements on DNA-modified electrode surfaces (β = 0.05 $Å^{-1}$) (19). Unlike previous ensemble measurements where β could not be measured directly, these data suggest that CNT-DNA devices allow for the direct measurement of the distance dependence of DNA CT. Continued work to support the characterization of this fundamental property of DNA is currently underway. In order to understand the contribution of the alkane linker to these measurements, DNA duplexes with C6 amine linkers, in addition to C3 amine linkers, are being studied at the various DNA lengths.

Work to detect DNA binding and DNA methylation by the methyltransferase *Sss*I with CNT-DNA devices represents the first report of an electrical strategy to monitor these activities on the single molecule level. These experiments demonstrate that DNA in these devices, which forms a covalently wired bridge, is simultaneously a sensitive recognition element and transducer of methyltransferase binding. Base flipping by *Sss*I at its specific recognition sequence disrupts CT through the DNA bridge and causes nearly complete attenuation of the device conductance. These devices can be used to sensitively distinguish DNA that lacks the 5′-CG-3′ binding site, as *Sss*I does not induce

base flipping and the disruption of DNA CT at DNA without this site. These studies represent the next step up in complexity from previous work in which these devices were used to detect DNA cutting by a restriction enzyme (9). Unlike these previous studies, in which detection was achieved by irreversible destruction of the device, here the sequence-specific binding and activity of *Sss*I is detected in a way that leaves the device intact, yet reports on the enzymatic reaction. Methylation of the DNA bridge by *Sss*I is readily observed because this activity alters the subsequent protein binding affinity of the device, but not its conductivity.

Thus, this work generalizes the CNT-DNA platform for fundamental, single molecule measurements of DNA CT as well as for the detection of proteins that bind DNA and disrupt DNA CT. Completed investigations of the distance dependence of DNA CT with this platform will provide, for the first time, a direct measure of this property. This information will help to inform nanoelectronic applications that utilize DNA CT as well as provide insight about how DNA CT may be used for long-distance signaling in living organisms. The specific, electrical monitoring of single molecule protein-DNA interactions with CNT-DNA devices may be extended to the wide variety of other proteins that disrupt DNT CT upon DNA binding. This strategy shows promise by providing a unique perspective from which to detect and characterize protein-DNA interactions, and allowing these activities to be sensitively monitored at the single molecule level.

References

1. Liu, S., Zhang, X., Luo, W., Wang, Z., Guo, X., Steigerwald, M.L., and Fang, X. (2011) *Angew. Chem., Int. Ed. 50*, 2496.

2. Liu, S., Clever, G.H., Takezawa, Y., Kaneko, M., Tanaka, K., Guo, X. and Shionoya, M. (2011) *Angew. Chem., Int. Ed. 50*, 8886.

3. Roy, S., Vedala, H., Roy, A.D., Kim, D., Doud, M., Mathee, K., Shin, H., Shimamoto, N., Prasad, V., and Choi, W. (2008) *Nano Lett. 8*, 26.

4. Guo, X., Small, J.P., Klare, J.E., Wang, Y., Purewal, M.S., Tam, I.W., Hong, B.H., Caldwell, R., Huang, L., O'Brien, S., Yan, J., Breslow, R., Wind, S.J., Hone, J., Kim, P., and Nuckolls, C. (2006) *Science 311*, 356.

5. Whalley, A.C., Steigerwald, M.L., Guo, X., and Nuckolls, C. (2007) *J. Am. Chem. Soc. 129*, 12590.

6. Guo, X., Whalley, A., Klare, J.E., Huang, L., O'Brien, S., Steigerwald, M.L., and Nuckolls, C. (2007) *Nano Lett. 7*, 1119.

7. Feldman, A., Steigerwald, M.L., Guo, X., and Nuckolls, C. (2008) *Acc. Chem. Res. 41*, 1731.

8. Guo, X. and Nuckolls, C. (2009) *J. Mater. Chem. 19*, 5470.

9. Guo, X., Gorodetsky, A.A., Hone, J., Barton, J.K., and Nuckolls, C. (2008) *Nat. Nanotechnol. 3*, 163.

10. Kelley, S.O., Holmlin, R.E., Stemp, E.D.A., and Barton, J.K. (1997) *J. Am.Chem. Soc. 119*, 9861.

11. Kelley, S.O., Boon, E.M., Barton, J.K., Jackson, N.M., and Hill, M.G. (1999) *Nuc. Acids Res. 27*, 4830.

12. Kelley, S.O. and Barton, J.K. (1999) *Science 283*, 375.

13. Genereux, J.C. and Barton, J.K. (2010) *Chem. Rev. 110*, 1642.

14. Feldman, A.K., Steigerwald, M.L., Guo, X., Nuckolls, C. (2008) *Acc. Chem. Res. 41*, 1731.

15. Genereux, J.C., Boal, A.K., and Barton, J.K. (2010) *J. Am. Chem. Soc. 132*, 891.

16. Murphy, C. J., Arkin, M.R., Jenkins, Y., Ghatlia, N.D., Bossmann, S. H., Turro, N.J., Barton, J. K. (1993) *Science 262,* 1025.

17. Kelley, S. O., Barton, J. K. (1999) *Science 283,* 375.

18. Nuñez, M.E., Hall, D.B. and Barton, J.K. (1999) *Chem. Biol. 6,* 85.

19. Slinker, J.D., Muren, N.B., Renfrew, S.E., and Barton, J.K. (2011) *Nat. Chem. 3,* 230.

20. Zheng, G., Patolsky, F., Cui, Y., Wang, W.U. and Lieber, C.M. (2005) *Nat. Biotechnol. 23,* 1294.

21. Chen, R.J., Bangsaruntip, S., Drouvalakis, K.A., Kam, N.W.S., Shim, M., Li, Y., Kim, W., Utz, P.J., and Dai, H. (2003) *Proc. Natl. Acad. Sci. U.S.A. 100*, 4984.

22. Patolsky, F., Zheng, G., and Lieber, C.M. (2006) *Anal. Chem. 78,* 4260.

23. Sorgenfrei, S., Chiu, C.-Y., Gonzalez, R.L., Yu, Y.-J., Kim, P., Nuckolls, C. and Shepard, K.L. (2011) *Nat. Nanotechnol. 11,* 1093.

24. Kauffman, D. and Star, A. (2008) *Chem. Soc. Rev. 37*, 1197.

25. Balasubramanian, K. and Burghard, M. (2006) *Anal. Bioanal. Chem. 385*, 452.

26. Jacobs, C.B., Peairs, M.J., and Venton, B.J. (2010) *Anal. Chim. Acta. 662*, 105.

27. Boon, E.M., Salas, J.E. and Barton, J.K. (2002) *Nature Biotechnol. 20*, 282.

28. Gorodetsky, A.A., Ebrahim, A., and Barton, J.K. (2008) *J. Am. Chem. Soc. 130*, 2924

29. Klimasauskas, S., Kumar, S., Roberts, R.J., and Cheng, X. (1994) *Cell 76*, 357.

30. O'Gara, M., Klimasauskas, S., Roberts, R. and Cheng, X. (1996) *J. Mol. Biol. 261*, 634.

31. Renbaum, P., Abrahamove, D., Fainsod, A., Wilson, G., Rottem, S., and Razin, A. (1990) *Nuc. Acids Res. 18,* 1145.

32. Guo, X., Xiao, S., Myers, M., Miao, Q., Steigerwald, M., and Nuckolls, C. (2009) *Proc. Natl. Acad. Sci. U.S.A. 106,* 691.

33. Guo, X., Myers, M., Xiao, S., Lefenfeld, M., Steiner, R., Tulevski, G., Tang, J., Baumert, J., Leibfarth, F., Yardley, J., Steigerwald, M., Kim, P., and Nuckolls, C. (2006) *Proc. Natl. Acad. Sci. U.S.A. 103*, 11452.

34. Razin, A. and Renbaum, P. (1995) *J. Mol. Biol. 248*, 19.

35. Darii, M.V., Kirsanova, O.V., Drutsa, V.L., Kochetkov, S.N., and Gromova, E.S. (2007) *J. Mol. Biol. 41*, 110.

36. Roberts, R.J. and Klimasauskas, S. (1995) *Nuc. Acids Res. 23*, 1388.

37. Klimasauskas, S., Weinhold, E., Serva, S., Merkiene, E., and Vilkaitis, G. (2001) *J. Biol. Chem., 276*, 20924.

38. Dubey, A.K. and Roberts, R.J. (1992) *Nuc. Acids Res. 20*, 3167.

Chapter 5

Electrochemical Detection of Protein-DNA Binding

Introduction

Binding interactions between proteins and DNA are critical to many cellular processes including transcriptional regulation, replication, DNA modification, and DNA repair. As such, significant efforts have been made towards the development of effective assays to characterize protein-DNA interactions as well as towards exploiting these events for disease detection and drug targeting. Of particular interest is DNA binding by transcription factors and methyltransferases—two different classes of proteins that can significantly influence gene expression. While transcription factors directly regulate gene expression by binding DNA (1), methyltransferases alter methylation patterns in the genome, upon DNA binding, that epigenetically direct gene expression (2). Overexpression and aberrant activity of transcription factors and methyltransferases can lead to abnormal gene expression and thus many of these proteins have been identified as primary indicators of cancer and other disease processes (3-7).

Unfortunately, current technologies for the detection of these proteins are not amenable for use in the clinic due to cost, complexity, lengthy analysis times, or lack of portable equipment, all of which impede their use as diagnostic markers for disease (8, 9). Several prominent techniques for protein detection and the study of protein-DNA interactions include western blotting, chromatin immunoprecipitation on microarrays (ChIP-chip) (10, 11), protein binding microarrays (11), Dam methylase fusion proteins (DamID) (12), and molecular beacons (13). As these techniques rely on fluorescence, they are prone to the errors and sensitivity limitations inherent with this platform (14, 15). In addition, they often involve multiple labeling steps, protein-specific antibodies, expensive reagents, bulky detection instrumentation, and complex data analysis, and thus

are not feasible for routine clinical use (14, 15).

Electrochemistry offers an appealing alternative to fluorescence-based detection schemes as this transduction method is inherently inexpensive, requires minimal sample preparation, involves straightforward data analysis, may utilize portable equipment, and has the potential for multiplexing (15–17). Electrochemical assays which rely on the sensitivity of DNA-mediated charge transport (DNA CT) chemistry show particular promise for rapid and facile biosensing (16, 18). As DNA CT is mediated through the base pair π-stack formed by the double helix, this chemistry has unmatched structural sensitivity to perturbations of the π-stack (19, 20). The DNA-modified electrode platform has been used to readily detect all base mismatches (21, 22), and a variety of base lesions (23) and DNA-binding proteins (24, 25) that structurally distort the DNA.

In this detection scheme, thiol-modified DNA duplexes bearing a covalent redox probe are assembled on a gold electrode surface (21, 22). When a potential is applied to the electrode, DNA CT facilitates reduction of the probe, producing an electrochemical signal. DNA with a structural distortion to the π-stack shows an attenuated signal, relative to unperturbed DNA, thereby allowing for sensitive detection of the structural distortion. As most DNA-binding proteins bind specific DNA sequences, this property may be exploited to specifically detect a protein of interest. Electrodes can easily be modified with customized DNA containing binding sites aimed at the specific detection of target proteins (Figure 5.1). Thus DNA may be utilized in these electrochemical sensors of protein-DNA interactions as both the recognition element and the transducer.

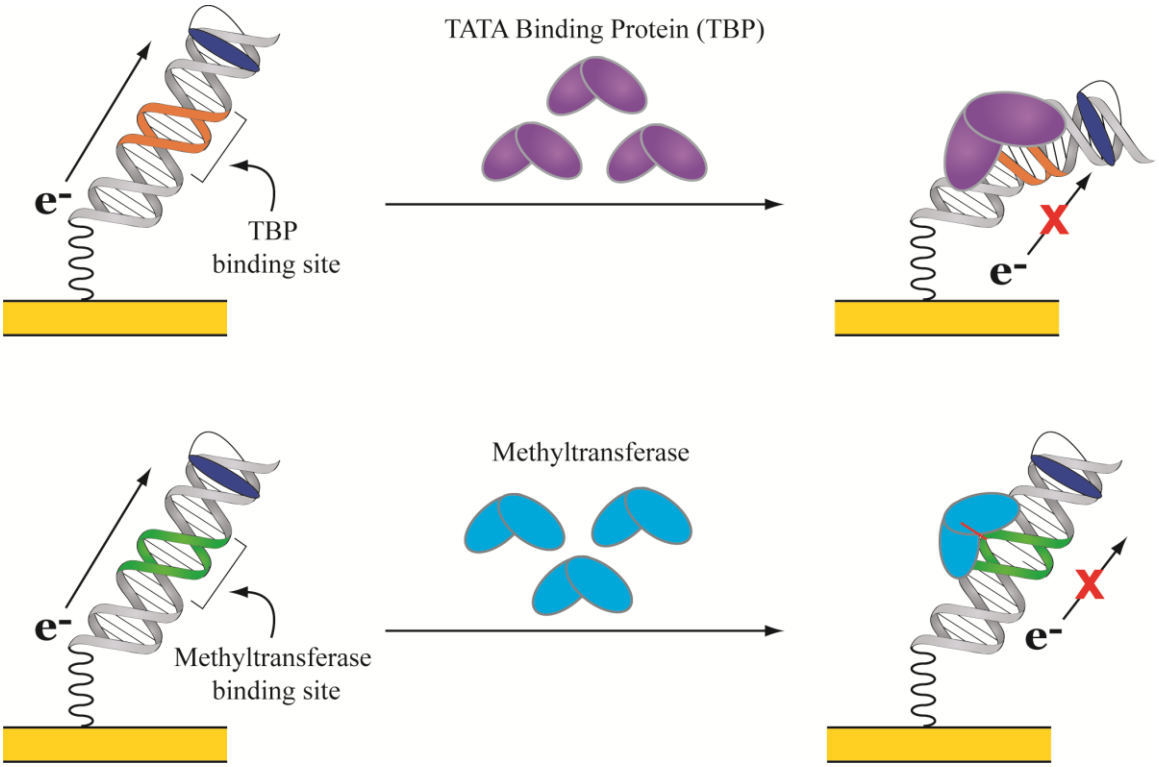

Figure 5.1 Detection of protein binding on DNA-modified gold electrodes. DNA bearing a covalent redox probe (blue oval) and thiol linker (wavy line) is assembled on a gold electrode surface. Top row: for DNA containing the TBP binding site, treatment of the electrode with TBP results in DNA binding and bending by 90°. Bottom row: for DNA containing a methyltransferase binding site, treatment of the electrode with the methyltransferase results in DNA binding and base flipping. Both binding events distort the structure of the DNA π-stack and severely impede DNA CT to the redox probe. The resulting attenuation of the measured redox signal allows for the detection of protein binding.

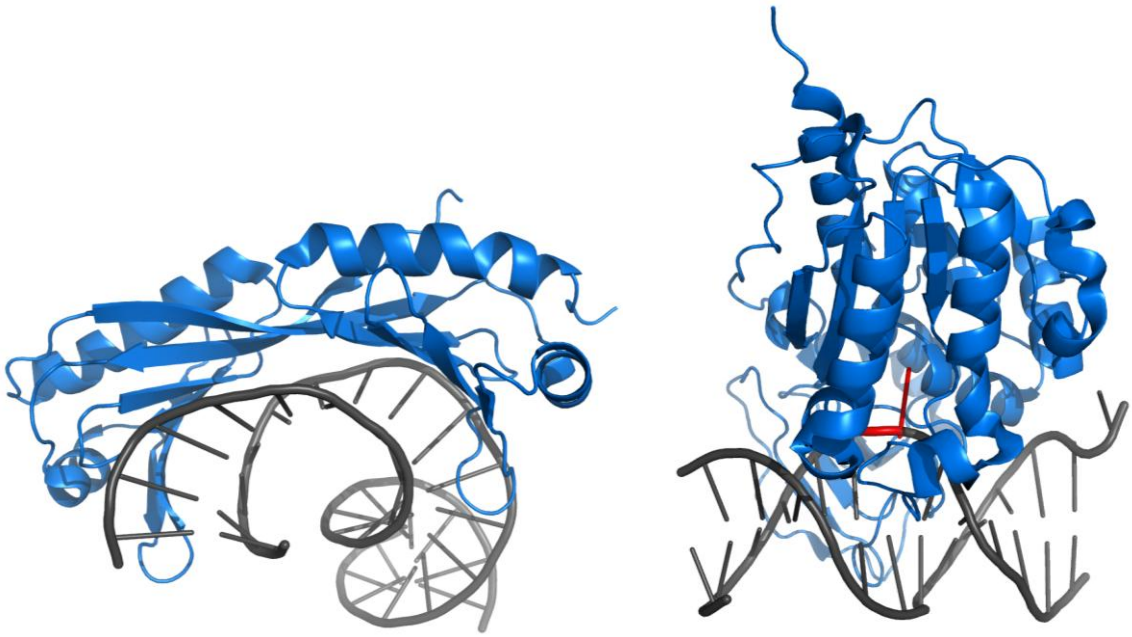

TATA Binding Protein (TBP) **Methyltransferase**

Figure 5.2 Distortion of the DNA π-stack by DNA-binding proteins. Proteins are shown in blue and DNA is shown in grey. (Left) Crystal structure of TBP bound to DNA (PDB ID: 1NH2) (30). TBP binds the recognition site 5′-TATAAAG-3′ and kinks the DNA 90° upon binding. (Right) Crystal structure of *Hha*I methyltransferase bound to DNA (PDB ID: 1FJX) (28). *Hha*I binds the recognition site 5′-G<u>C</u>GC-3′ and flips the underlined cytosine out of the base stack, shown in red.

Proteins detected previously with this platform include DNA methyltransferases and the transcription factor TBP (TATA binding protein) which both significantly disrupt the π-stack of DNA upon binding by very different modes (Figures 5.1, 5.2). While DNA methyltransferases flip a base completely out of the DNA helix in order to catalyze the transfer of a methyl group (26–28), TBP kinks the DNA by 90° upon binding (29, 30). For the detection of these proteins, DNA bearing the covalently crosslinked intercalator daunomycin was utilized in a single electrode format (24). Though effective, this redox reporter has several significant drawbacks, including instability and sequence restrictions, which limit its versatility and prospects for use in a simple diagnostic assay. Beyond the probe, a more effective detection scheme also requires the switch to a multiplexed format to increase statistics, decrease assay time and labor, and allow for the side-by-side measurement of multiple samples and controls on the same device.

Here we describe work to improve this DNA CT-based platform for the rapid, electrochemical detection of DNA-binding proteins. This work centers specifically on the need for large, consistent signals from a stable, DNA-mediated redox reporter, in a multiplexed electrode format. Using TBP and the bacterial methyltransferase *Sss*I as targets, properties of the covalent redox probes Nile Blue and Methylene Blue (Figure 5.3) were investigated on multiplexed chips. The effects of protein buffer components on signal size and shape were evaluated as well as the response to protein binding. Upon establishing optimal buffer conditions and determining that the Methylene Blue probe is more responsive to protein binding, *Sss*I binding was examined in greater detail. This work provides insight on the parameters that must be considered for the continued development of DNA CT-based electrochemical strategies for protein detection.

Materials and Methods

Materials

All standard and modified phosphoramidites were purchased from Glen Research. Nile Blue perchlorate (laser grade) for coupling was purchased from Acros. Modified Methylene Blue dye for coupling was synthesized as described previously (31). Sinefungin was purchased in dry form from Sigma-Aldrich and solutions were prepared in 10 mM HCl and stored at -20°C. Lambda DNA was purchased in solution from New England Biolabs and used as received. All other chemicals for the preparation of protein buffers and DNA-modified electrodes were purchased from Sigma-Aldrich and used as recieved. Multiplexed chips were fabricated at Caltech as described previously (32).

Protein Preparation

All proteins were purchased from commercial sources and used as received. BSA was purchased from New England Biolabs and stored at -20°C. Human TBP was purchased from ProteinOne and aliquots were stored at -80°C. *Sss*I methylase was purchased from New England Biolabs and stored at -20°C.

DNA Sequences

All DNA sequences used in these experiments are summarized in Table 5.1. For experiments on running buffer effects and TBP binding, electrodes were modified with the sequence 5′-HS- $(CH_2)_6$ -GAGATATAAAG*C*ACGCA-3', where the TBP binding site is underlined, with a Nile Blue- or Methylene Blue-modified complement. For mismatch

Table 5.1 DNA sequences used for electrochemistry. The TBP and *Sss*I binding sites are indicated in red. The site of a CA mismatch for mismatch discrimination experiments is bolded. For all DNA, the Nile Blue or Methylene Blue redox probe is covalently attached to the terminal 5′-T.

Experiment	Sequence
Buffer effects, TBP binding, mismatch discrimination	5'-HS- $(CH_2)_6$ - GAGA**TATAAAG****C**ACGCA -3' CTC T**ATATTTC****G**TGCGT
*Sss*I binding, Unmethylated	5'-HS- $(CH_2)_6$ - GACTGAC**CG**TGGACTGA -3' CTGACTG**GC**ACCTGACT
*Sss*I binding, Fully Methylated	5'-HS- $(CH_2)_6$ - GACTGAC^{m}**CG**TGGACTGA -3' CTGACTG**G**^{m}**C**ACCTGACT
*Sss*I binding, No site	5'-HS- $(CH_2)_6$ - GACTGACTGTGGACTGA -3' CTGACTGACACCTGACT

discrimination experiments a CA mismatch was inserted into this sequence at the italicized *C* base. For experiments to measure *Sss*I binding, the sequence 5′-HS-$(CH_2)_6$-GACTGAC<u>CG</u>TGGACTGA-3' was used with either an unmethylated or methylated *Sss*I binding site (underlined). A Methylene Blue-modified complement, with an unmethylated or methylated site, was employed to form duplexes with an unmethylated or fully methylated *Sss*I binding site, respectively. A sequence in which a T replaces the 5′-C in the *Sss*I binding site was also utilized to measure binding on a nonspecific DNA substrate: 5′-HS-$(CH_2)_6$-GACTGACTGTGGACTGA-3′.

DNA Synthesis

All DNA was synthesized on an Applied Biosystems 3400 DNA Synthesizer. Thiolated strands were prepared with a C6-S-S phosphoramidite at the 5′ terminus. Strands containing methylated cytosine were synthesized with a 5-methyl dC-CE phosphoramidite. DNA for Nile Blue coupling was prepared with ultramild phosphoramidites and a NHS-carboxy dT phosphoramidite at the 5′ terminus. DNA for Methylene Blue coupling was prepared with regular phosphoramidites and an amino-C6-dT phosphoramidite at the 5′ terminus. All DNA was purified by reverse-phase HPLC with a polymeric PLRP-S column (Agilent) and characterized by mass spectrometry. All DNA stocks were desalted, resuspended in phosphate buffer (5 mM phosphate, 50 mM NaCl, pH 7), and quantified by UV/Vis absorption at 260 nm. Equimolar amounts (50 μM) of complementary strands were combined and thermally annealed.

For Nile Blue-modified DNA, coupling was carried out on the solid support as described previously (25). Briefly, a saturated solution of Nile Blue perchlorate (10

mg/mL) in 10% DIEA in dichloromethane was applied to the DNA by syringe (1mL per column) and allowed to shake overnight (18 hours) at room temperature. The DNA was then washed with dichloromethane, methanol, and acetonitrile, dried, deprotected and cleaved from the solid support (50 mM potassium carbonate in methanol overnight at room temperature), and purified by reverse-phase HPLC. For Methylene Blue-modified DNA, coupling was carried out in solution as described previously (31). Briefly, DNA that had been purified by reverse-phase HPLC with the dimethoxy trityl group removed was suspended in 0.1 M $NaHCO_3$ and combined with an equimolar amount of modified Methylene Blue dye in DMSO. The mixture was allowed to shake overnight at room temperature. The coupled DNA was then purified from the free dye using a Nap-5 size exclusion column (GE Healthcare) before further purification by HPLC. The final structures of Methylene Blue- and Nile Blue-modified DNA are illustrated in Figure 5.3. For thiolated DNA, after initial HPLC purification, the disulfide was reduced to the free thiol in 100 mM dithiothreitol in 100 mM Tris-HCl buffer pH 8.3 at room temperature for 45 minutes, purified on a Nap-5 column, and further purified by HPLC.

Multiplexed Chip Preparation and Assembly

Prior to application of DNA solutions, chips were cleaned with acetone and isopropanol, dried, and further cleaned by exposure to UV ozone for 5 minutes. The chips were then assembled with a rubber gasket and clamp, and a solution of 25 µM DNA in phosphate buffer was immediately applied to each quadrant of the chip (25 µL DNA per quadrant). The DNA was allowed to assemble on the chip overnight in a humidified environment at room temperature.

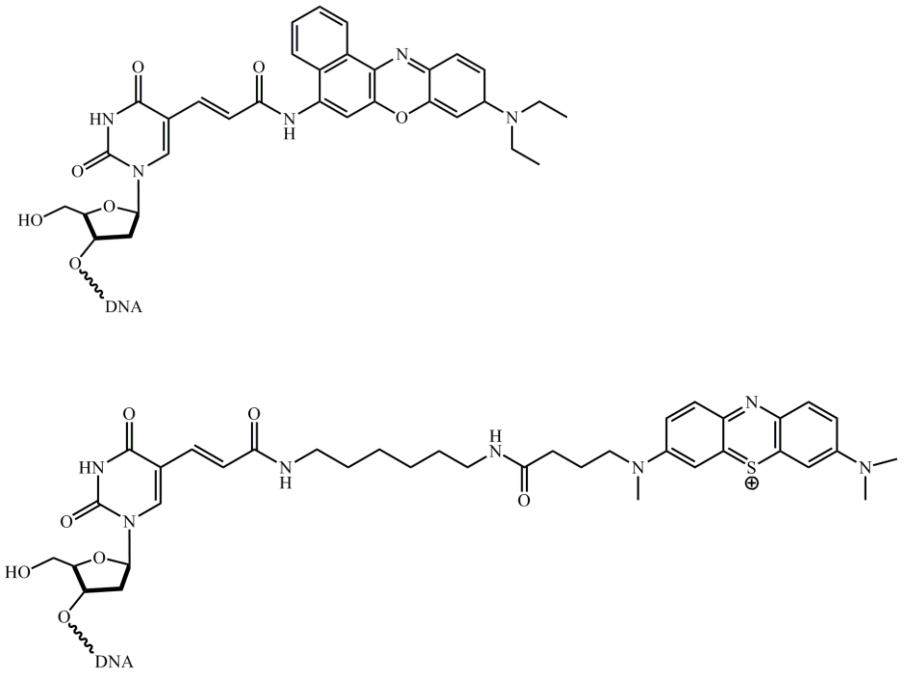

Figure 5.3 Covalent redox probes for the detection of protein binding. Structures of Nile Blue (top) and Methylene Blue (bottom) redox probes covalently attached to DNA.

Electrochemistry

All electrochemistry was carried out with a standard potentiostat and multiplexer console (CH Instruments). A three-electrode system was employed including a Pt wire auxiliary electrode and Ag/AgCl reference electrode (Cypress Systems). Chips were first backfilled with 1 mM mercaptohexanol in phosphate buffer with 5% glycerol for 45 minutes at room temperature. For all electrochemistry, cyclic voltammetry (CV) scans were performed at a 100 mV/s scan rate over the potential window of 0 mV to -500 mV. Squarewave voltammetry (SWV) was performed at 15 Hz over the same potential range. Signal size was measured as the CV cathodic peak area or the SWV peak area, as indicated. For experiments to determine the effects of different buffer components, after backfilling and thorough rinsing by buffer exchange, scans were performed in a variety of buffers. These include phosphate buffer, TBP-binding buffer (5 mM phosphate, 50 mM NaCl, 4 mM $MgCl_2$, 4 mM spermidine, 50 μM EDTA, 10% glycerol, pH 7) and variations that isolate different components.

For all protein binding experiments, after backfilling with mercaptohexanol, electrodes were backfilled with 3 μM BSA in phosphate buffer for 45 minutes at room temperature. After thorough rinsing by buffer exchange, background scans were performed in the specific binding buffer for the protein of interest. TBP-binding buffer was used for TBP while *Sss*I-binding buffer (10 mM Tris-HCl, 50 mM NaCl, 10 mM $MgCl_2$, pH 7.9) was used for *Sss*I. After removing this blank buffer from the common well over the electrodes, a solution of the target protein in binding buffer was then added (200 μL total volume).

For experiments with *Sss*I, the inactive cofactor analog sinefungin (160 µM) was added to the reaction solution. Scans were performed in this solution at various time points to measure binding over time. For protein titrations, the reaction solution was serially exchanged for solutions of increasing protein concentration and binding was allowed to occur for 30 minutes before scanning. To measure the effect of competitor DNA, scans were taken after complete binding of the protein (30 minutes). A solution of Lambda DNA in protein-binding buffer was then added directly into the protein solution on the electrode, mixed thoroughly, and scans were performed over time. To investigate the importance of the cofactor for *Sss*I binding, electrodes were treated with 50 nM *Sss*I without any cofactor, allowed to incubate for 45 minutes, and then scanned. Chips were then rinsed thoroughly, exposed to a new solution of 50 nM *Sss*I with 160 µM sinefungin, allowed to incubate for 45 minutes, and then scanned. To evaluate *Sss*I binding on DNA with a fully methylated binding site or without a binding site, chips were modified on one half with the DNA substrate for specific binding (unmethylated with 5′-CG-3′ site) and on the other half with the DNA substrate for nonspecific binding (fully methylated or with the sequence 5′-TG-3′). *Sss*I binding to these substrates was then performed side-by-side on the same surface.

Results and Discussion

Effect of Running Buffer on Signal Size and Shape

In this electrochemical protein detection scheme, the protein binding buffer is also the electrochemical running buffer. Thus, it is critical to establish how various buffer components affect the electrochemical signal in order to both ensure conditions that allow

for protein binding and maximize signal size. Drastic differences in signal size and peak sharpness were observed for DNA-modified electrodes scanned in phosphate buffer followed by TBP-binding buffer (Figure 5.4). For these electrodes, there is an approximately 10-fold increase in the CV cathodic peak size when scanned in TBP-binding buffer as compared to phosphate buffer. Upon this buffer change, the redox peaks also change from extremely broad and split to sharp with reduced splitting. This effect is reversible with buffer exchange and was observed for the same 17-mer DNA sequence with either the covalent Nile Blue or Methylene Blue redox probe.

As the main difference between phosphate buffer and TBP-binding buffer is the presence of spermidine and $MgCl_2$ in the TBP-binding buffer, the individual effect of these buffer components was investigated. Electrodes modified with 17-mer Nile Blue were scanned in phosphate buffer followed by phosphate buffer with added 4 mM spermidine or 4 mM $MgCl_2$. Scans were taken in phosphate buffer between each exchange to ensure complete signal reversal back to the baseline (Figure 5.5). From this experiment, it is clear that both magnesium and spermidine contribute to the signal enhancement, with spermidine contributing most significantly. Indeed, the combined signals from phosphate buffer with spermidine or $MgCl_2$ alone nearly approximate the signal size and shape when the electrode is scanned in TBP-binding buffer.

It is important to determine if the enhanced signals caused by spermidine and $MgCl_2$ in the running buffer are DNA-mediated or if these buffer components induce an alternate mode of probe reduction. To do this, a single CA mismatch was incorporated into the 17-mer Nile Blue DNA and the well matched and mismatched duplexes were assembled side-by-side on the same chip. Scans of the chip in TBP-binding buffer show

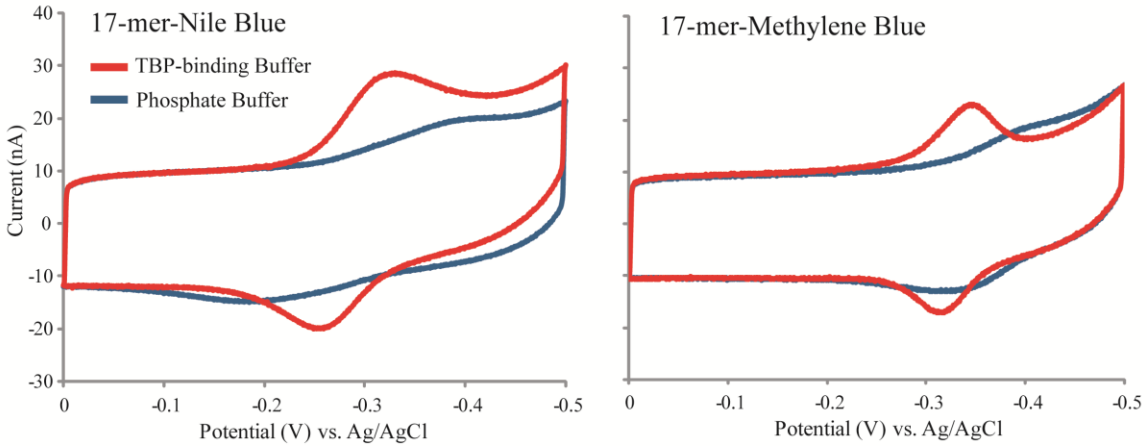

Figure 5.4. Running buffer conditions influence the signal size and shape from multiplexed, DNA-modified electrodes. Electrodes were modified with (left) Nile Blue- and (right) Methylene Blue-modified 17-mer DNA of the same sequence. CVs from the electrodes scanned first in phosphate buffer (5 mM phosphate, 50 mM NaCl, pH 7) (red trace), followed by TBP-binding buffer (5 mM phosphate, 50 mM NaCl, 4 mM $MgCl_2$, 4 mM spermidine, 50 µM EDTA, 10% glycerol, pH 7) (blue trace) are shown for representative electrodes. Scans were performed at a 100 mV/s scan rate with an Ag/AgCl reference electrode.

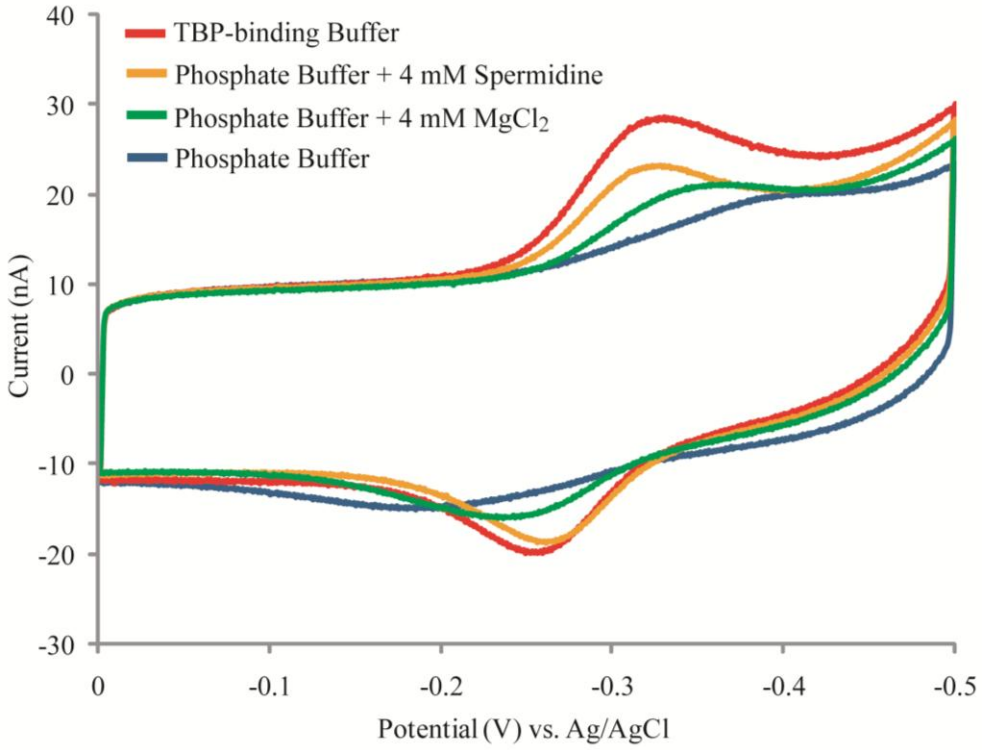

Figure 5.5 Spermidine and $MgCl_2$ in running buffer cause signal enhancement. The well matched Nile Blue-modified 17-mer was assembled on multiplexed chips and scanned in a variety of buffers including phosphate buffer (5 mM phosphate, 50 mM NaCl, pH 7) (blue trace), phosphate buffer with 4 mM $MgCl_2$ added (green trace), phosphate buffer with 4 mM spermidine added (orange trace), and TBP-binding buffer (5 mM phosphate, 50 mM NaCl, 4 mM $MgCl_2$, 4 mM spermidine, 50 µM EDTA, 10% glycerol, pH 7) (red trace). Scans were taken in phosphate buffer between each new solution to ensure that the signal reversed completely back to the initial phosphate buffer baseline scan. CVs for a representative electrode are shown overlaid. Scans were performed at a 100 mV/s scan rate with an Ag/AgCl reference electrode.

clear mismatch discrimination with a mismatched: well matched CV cathodic peak size ratio of 0.2 ± 0.1 across 20 electrodes for each DNA type (3 chips) (Figure 5.6). This result is consistent with previous measurements of DNA-mediated electrochemical signal attenuation in the presence of a CA mismatch (21, 22), confirming that the buffer-enhanced signals are still DNA-mediated.

Mg^{2+} and spermidine have previously been shown to facilitate DNA packing as their positive charge helps to neutralize the negatively charged phosphate backbone of DNA and decrease interstrand repulsions (33–35). The increased peak sharpness in TBP-binding buffer indicates a greater degree of organization and uniformity in the film, and the increased peak size indicates that the film reorganization induced by Mg^{2+} and spermidine facilitates more efficient reduction of the redox probe. Since gathering these initial results, the signal enhancing effects of Mg^{2+} and spermidine have been used for a wide range of DNA sequences and lengths on DNA-modified electrodes (31, 36, 37).

Response to TBP-Binding by Nile Blue- vs. Methylene Blue-Modified DNA

In addition to the identification of buffer conditions that both allow for protein binding and promote strong electrochemical signals, the selection of a covalent probe that responds sensitively to protein binding is also critical. Toward this end, the response to TBP binding of two consistent and well characterized redox probes for DNA-mediated electrochemistry were compared. Nile Blue- and Methylene Blue-modified 17-mers containing the TBP binding site (5´-TATAAAG-3´) were assembled side by side on multiplexed chips and the binding of 200 nM human TBP was electrochemically monitored over time (Figure 5.7).

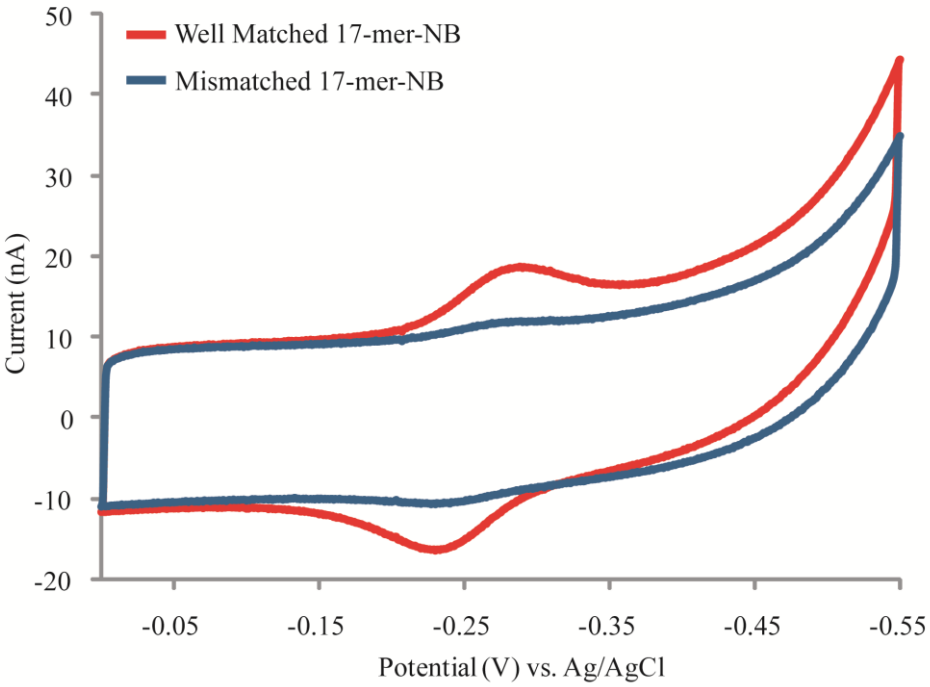

Figure 5.6 Mismatch discrimination is retained in signal-enhancing buffer conditions. The well matched (red trace) and mismatched (blue trace) Nile Blue-modified 17-mers (17-mer-NB) were assembled side by side on multiplexed chips and scanned in TBP-binding buffer. CVs for representative electrodes are shown overlaid. Scans were performed at a 100 mV/s scan rate with an Ag/AgCl reference electrode.

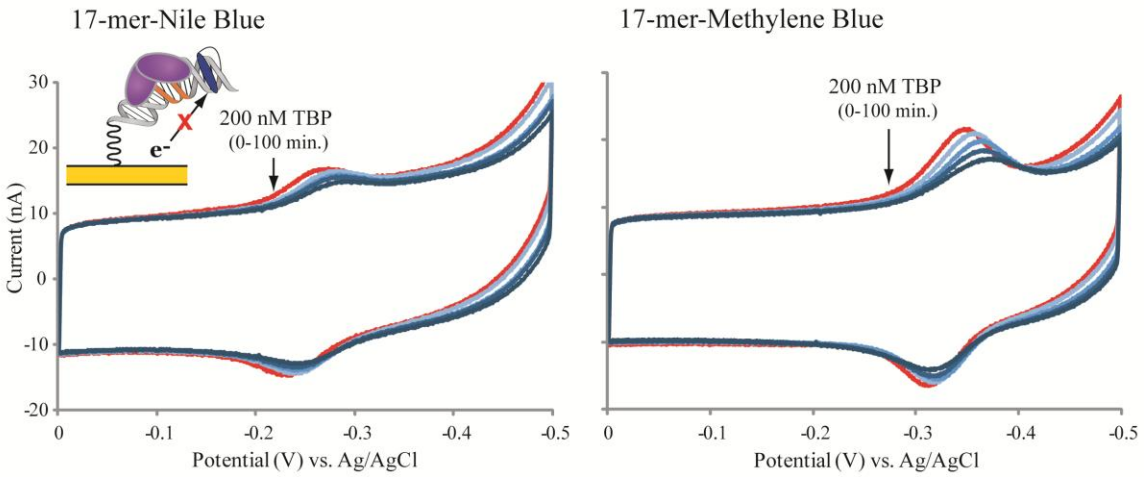

Figure 5.7 Response of Nile Blue- and Methylene Blue-modified DNA to TBP binding over time. Electrodes were modified with (left) Nile Blue- and (right) Methylene Blue-modified 17-mers containing the TBP binding site side by side on multiplexed chips. After addition of 200 nM TBP in TBP-binding buffer, the electrodes were scanned over time. CVs of representative electrodes for each DNA type are shown with traces at progressive time points overlaid: background scan (red); 200 nM TBP, initial, 20 min., 40 min., and 100 min. (light blue to dark blue). All scans were performed in the TBP-containing solution. Scans were performed at a 100 mV/s scan rate with an Ag/AgCl reference electrode.

In general, the Methylene Blue-modified 17-mer yielded larger initial signals (3 nC ± 0.2 nC for the CV cathodic peak) in TBP-binding buffer than the Nile Blue-modified 17-mer (1 nC ± 0.2 nC) across 16–24 electrodes tested for each DNA type (3 chips). This result—a generally larger signal size for methylene Blue-modified DNA—has has been consistently observed across different sequences of DNA modified with this probe (31). In monitoring the signal change over time with TBP binding, the Methylene Blue-modified DNA also showed a greater response. At the final time point (100 minutes), the Methylene Blue-modified DNA yielded a 40% ± 5% signal decrease by CV cathodic peak while the Nile Blue-modified DNA yielded a 20% ± 4% signal decrease.

The larger signal decrease for Methylene Blue-modified DNA is likely related to its overall larger signal size; with a larger initial signal there is simply more signal to lose upon TBP binding and greater potential for a signal change that may be fully measured. Signal size is also important for the dynamic range of the electrochemical sensor. A larger initial signal creates a wider range over which subtle changes in signal may be meaningfully interpreted. In DNA CT-based protein sensing this may, for example, allow for the accurate electrochemical determination of protein concentration or for the monitoring of conformational changes in protein-DNA binding that occur under changing conditions.

Time and Concentration Dependence of *Sss*I Binding

As Methylene Blue-modified DNA was shown to consistently produce large signals and respond sensitively to protein binding, this probe was used for the detection of *Sss*I methyltransferase. *Sss*I, which binds the site 5′-CG-3′ and methylates the C-5

position of the target cytosine, was selected for study because it is considered the bacterial analog to human methyltransferases, which bind and methylate the same sequence (38). Additionally, *Sss*I belongs to the same, highly conserved C-5-cytosine methyltransferase family as *Hha*I methyltransferase, the most thoroughly characterized DNA methyltransferase. Biochemical and structural analyses indicate that the characteristics of binding and activity by *Hha*I, which recognizes the site 5′-GCGC-3′ and methylates the C-5 position of the first cytosine, may be generalized across this family, with particular similarity to *Sss*I (39, 40). Thus, although a crystal structure for *Sss*I has not yet been solved, the DNA binding and base flipping of the target cytosine observed in the crystal structure of *Hha*I is considered closely homologous between these two methyltransferases (28).

For electrochemical *Sss*I detection experiments, the manufacturer-recommended buffer for *Sss*I binding was confirmed to produce sizable signals on multiplexed chips modified with Methylene Blue-modified DNA due to the high $MgCl_2$ content (10 mM). For these experiments, sinefungin, an inactive analog of the S-adenosyl-L-methionine (SAM) cofactor, was used. This cofactor analog is commonly used in methyltransferase-DNA binding experiments to prevent DNA methylation and protein dissociation and to trap *Sss*I in the bound state.

To characterize the binding activity, the electrochemical response of Methylene Blue-modified DNA to *Sss*I binding was first measured over time (Figure 5.8). To reach the maximum signal response, a high concentration of *Sss*I (100 nM) was tested. These timecourse experiments show that the majority of the signal loss (22% ± 4% by CV cathodic peak) occurs in the first 20 minutes, with the maximum response (32% ± 4%)

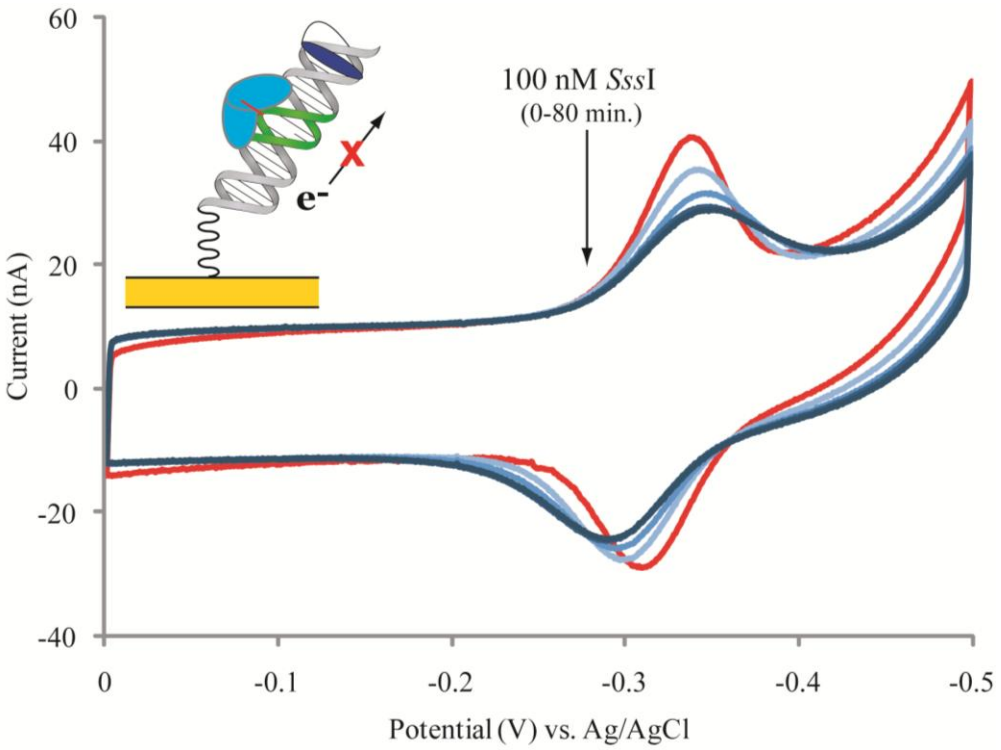

Figure 5.8 Time dependent response to *Sss*I binding. Electrodes were modified with the Methylene Blue-modified 17-mer containing the *Sss*I binding site. After addition of 100 nM *Sss*I with 160 μM sinefungin in *Sss*I-binding buffer, the electrodes were scanned over time. CV scans for a representative electrode are shown with traces at progressive time points overlaid: background scan (red); 100 nM *Sss*I, initial, 20 min., 50 min., and 80 min. (light blue to dark blue). All scans were performed in the *Sss*I-containing solution. CV scans were performed at a 100 mV/s scan rate with an Ag/AgCl reference electrode.

reached by 50 minutes. In addition to signal loss, there is significant peak broadening associated with *Sss*I binding, a result also observed for TBP binding. This is likely due to increased disorder and heterogeneity in the DNA film upon protein binding that decreases the uniformity of probe reduction. Because this peak broadening translates directly into decreased peak size as measured by SWV, this technique may be used to more sensitively report changes in the electrochemical signal from protein binding. In this case, analysis of the SWV data shows a signal loss of 48% ± 3% by the first 20 minutes and a maximum signal loss of 60% ± 1% by 50 minutes.

After the timescale of *Sss*I binding had been established, the concentration dependence of the electrochemical response was measured (Figure 5.9). *Sss*I concentrations from 15 nM to 100 nM were measured by titration. Since it was determined that the maximum response to binding is reached between 20-45 minutes after treatment, protein binding was allowed to proceed for 30 minutes before scanning. From these titration experiments, it is clear that the electrochemical response to *Sss*I binding is concentration dependent over the tested range. Consistent with the result measured from the time dependence study, a maximum signal loss of 62% ± 1% (by SWV peak area) was observed for 100 nM *Sss*I.

By compiling data from two separate titration experiments in which different *Sss*I concentrations were measured, a binding curve can be approximated (Figure 5.10). This curve suggests that half of the total signal loss from binding occurs between 40-50 nM *Sss*I. This concentration range cannot be directly compared to the reported K_d for *Sss*I bound to DNA in solution (11 nM) (41) for several reasons: *Sss*I binding in this system is likely not at equilibrium, not all DNA strands in the film are equally accessible, and the

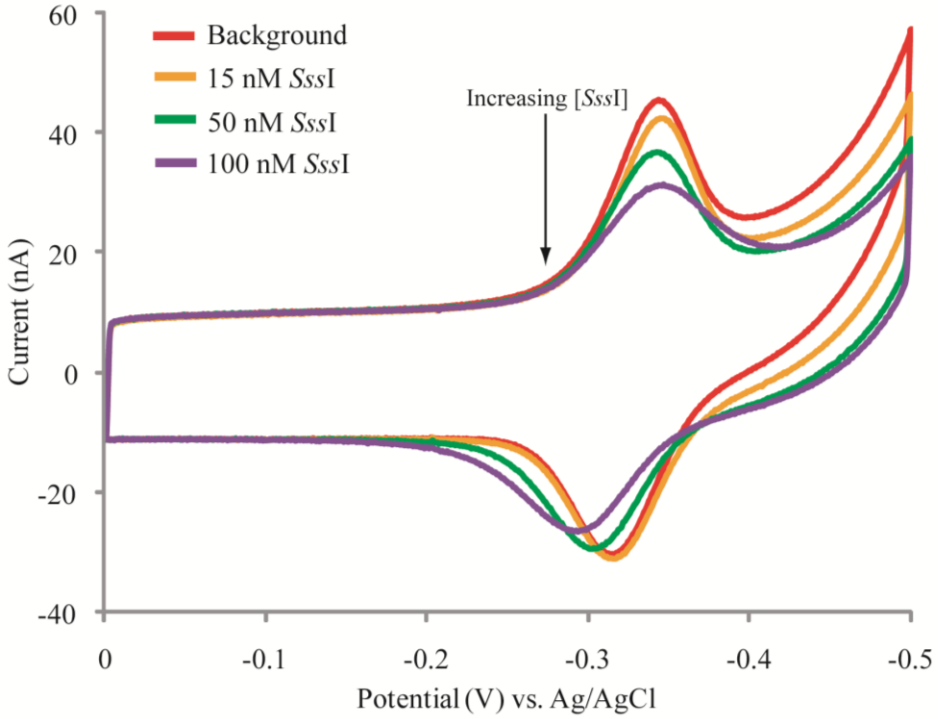

Figure 5.9 Concentration dependent response to *Sss*I binding. Electrodes were modified with the Methylene Blue-modified 17-mer containing the *Sss*I binding site. *Sss*I was titrated into *Sss*I-binding buffer with 160 μM sinefungin, starting at 15 nM. Each increasing *Sss*I concentration was allowed to bind on the electrode for 30 min. before scanning. CV scans for a representative electrode are shown with traces at increasing concentrations of *Sss*I overlaid: background scan (red), 15 nM *Sss*I (orange), 50 nM *Sss*I (green), and 100 nM *Sss*I (purple). All scans were performed in the *Sss*I-containing titration solution. CV scans were performed at a 100 mV/s scan rate with an Ag/AgCl reference electrode.

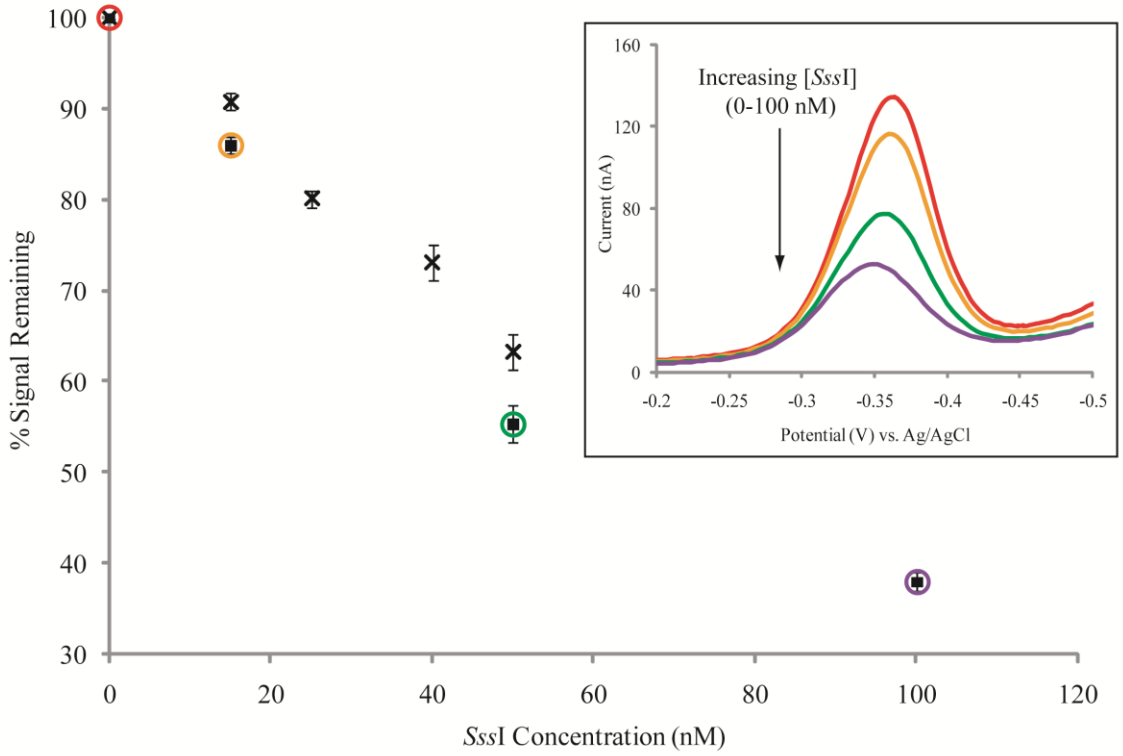

Figure 5.10 Binding curve for *Sss*I from electrochemical titration experiments. Data shown are a compilation of two separate titration experiments, corresponding to the filled square or X marker shapes. Electrodes were modified with the Methylene Blue-modified 17-mer containing the *Sss*I binding site. *Sss*I was titrated into a solution of *Sss*I-binding buffer with 160 μM sinefungin, starting at 15 nM. Each increasing *Sss*I concentration was allowed to bind on the electrode for 30 min. before scanning. Calculation of % signal remaining was made from quantified SWV peak areas. Error bars represent the standard deviation across 8 electrodes measured for each point. SWV traces for an example electrode in the filled square data series are shown overlaid (inset). The circled points in the binding curve correspond to the SWV traces of the same color including background scan (red), 15 nM *Sss*I (orange), 50 nM *Sss*I (green), and 100 nM *Sss*I (purple). All SWV scans were performed in the *Sss*I-containing titration solution at 15 Hz with an Ag/AgCl reference electrode.

general loss of dynamic freedom at surfaces complicates the kinetics of protein binding on DNA-modified electrodes. However, it is clear that DNA binding in solution and on surfaces both occur on the same nanomolar concentration scale. Additionally, since these differences between solution and surface systems generally make DNA-binding at surfaces more difficult, it is reasonable that an *Sss*I concentration higher than the K_d is required to see a binding response. Thus, the *Sss*I concentration range that elicits an electrochemical response is realistic and consistent with active DNA binding by *Sss*I.

Reversibility and Cofactor Dependence of *Sss*I Binding

In order to confirm that the observed signal decrease is due to DNA-binding by *Sss*I, the dissociation of bound *Sss*I by competitor DNA was measured. Electrodes were bound with 100 nM *Sss*I with 160 μM sinefungin for 45 minutes to cause a maximum initial signal decrease (Figure 5.11). Consistent with previous concentration dependence experiments, a signal loss of 35% ± 5% (by the CV cathodic peak area) was observed for binding by 100 nM *Sss*I. Lambda DNA was then used as a competitor substrate in solution to dissociate *Sss*I. Although rinsing *Sss*I-bound electrodes with buffer alone does not restore the signal, incubation with 5 μg/mL lambda DNA for 20 minutes results in near complete signal restoration (96% ± 2% of original signal, by CV cathodic peak area). This result indicates that signal loss is due to direct binding of the protein to the DNA of the DNA-modified electrode and that this binding is fully reversible by the introduction of an alternative DNA substrate in solution.

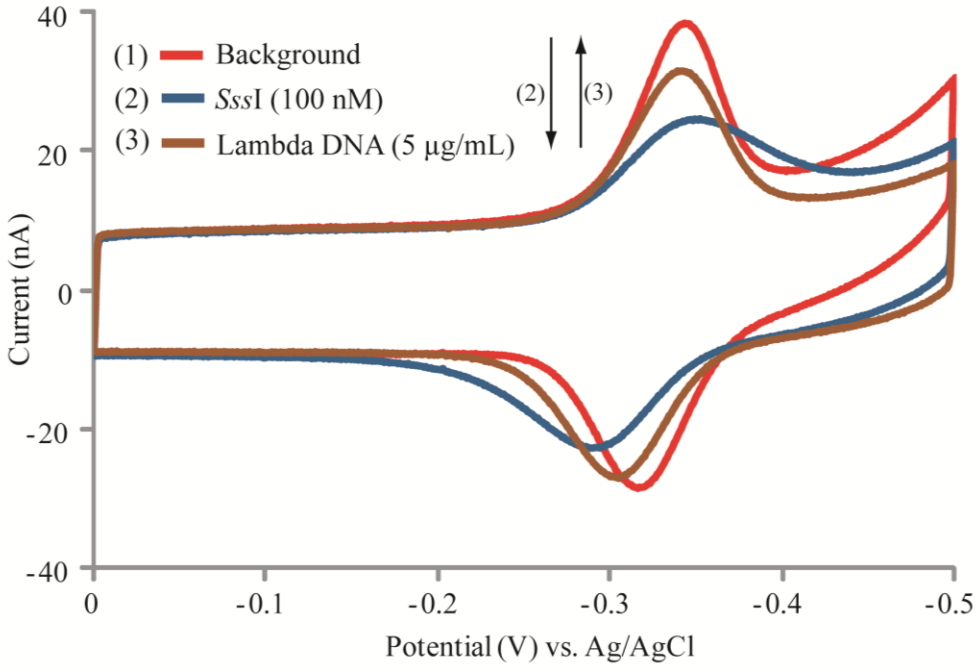

Figure 5.11 Competitor DNA restores electrochemical signal loss from *Sss*I binding. Electrodes were modified with the Methylene Blue-modified 17-mer containing the *Sss*I binding site. After a background scan (red trace), binding of 100 nM *Sss*I with 160 µM sinefungin was first allowed to go to completion for 45 min. (blue trace). Lambda DNA (5 µg/mL) was then titrated directly into the *Sss*I-containing solution and allowed to incubate on the electrodes for 20 min. (brown trace). CV scans of a representative electrode are shown overlaid. All scans were performed directly in the test solutions (*Sss*I-binding buffer alone, buffer with *Sss*I and sinefungin, buffer with *Sss*I, sinefungin, and Lambda DNA). CV scans were performed at a 100 mV/s scan rate with an Ag/AgCl reference electrode.

As another control to confirm that signal decreases are a result of the active binding of *Sss*I to DNA, the importance of the sinefungin cofactor in the observed signal loss was evaluated. Biochemical studies of C-5-cytosine DNA methyltransferases have shown that the affinity of these proteins for DNA is significantly increased by the presence of their cofactor (42, 43); *Hha*I, for example, shows a 500-fold increase in affinity for DNA binding with the addition of cofactor (42). While only a 1% ± 1% signal decrease (by CV cathodic peak area) was observed upon addition of 50 nM *Sss*I without the sinefungin cofactor, a 20% ± 3% signal decrease was observed when 50 nM *Sss*I with 160 μM sinefungin was added (Figure 5.12). This decrease is consistent with what was previously observed for 50 nM *Sss*I in concentration dependence experiments. Importantly, treatment of DNA-modified electrodes with sinefungin alone does not result in any measurable signal decrease. The dependence of the electrochemical signal loss on the presence of both *Sss*I and cofactor provides further support that this signal loss is due to the active, biologically relevant binding of *Sss*I specifically to the DNA of the DNA-modified electrode.

Effect of DNA Methylation and Sequence on *Sss*I Binding

The nature of *Sss*I binding on DNA-modified electrodes was further investigated by using substrate DNA that contains a fully methylated *Sss*I binding site. By assembling unmethylated DNA and fully methylated DNA side by side on the same chip, *Sss*I binding was examined in terms of the variables described previously (time dependence, concentration dependence, reversibility, and cofactor dependence). In order to pick out subtle differences in response, changes in signal were analyzed from SWV data.

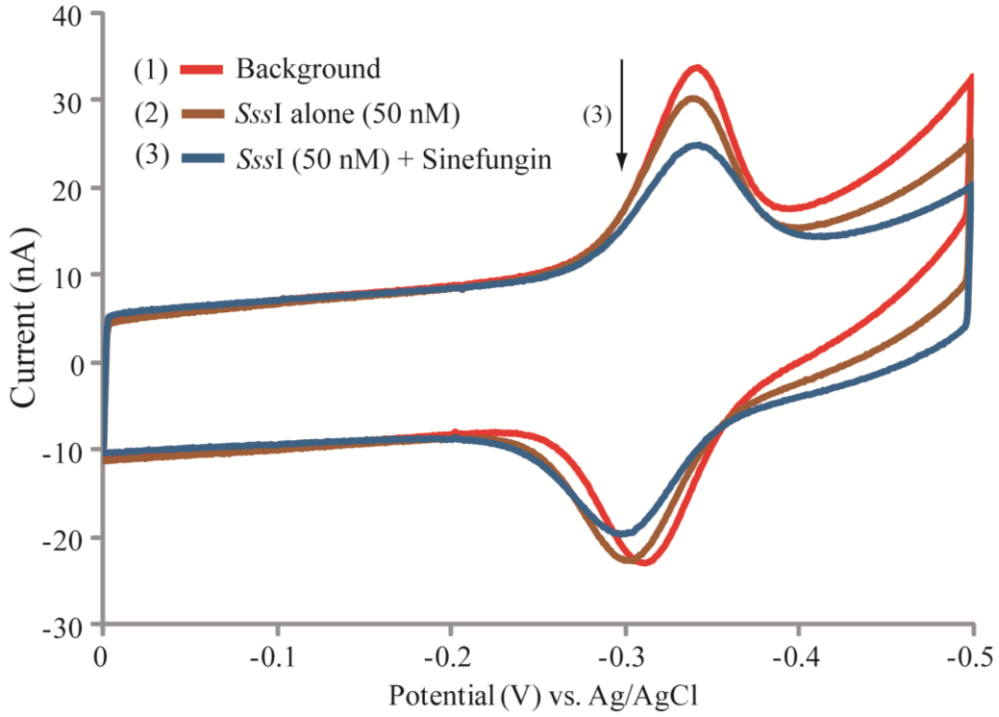

Figure 5.12 Signal loss by *Sss*I is cofactor-dependent. Electrodes were modified with the Methylene Blue-modified 17-mer containing the *Sss*I binding site. After a background scan (red trace), 50 nM *Sss*I alone was allowed to incubate on the electrodes for 45 min. (brown trace). Following this, the electrode was rinsed and 50 nM *Sss*I with 160 µM sinefungin was allowed to incubate for 45 min. (blue trace). CV scans for a representative electrode are shown overlaid. All scans were performed directly in the test solutions (*Sss*I-binding buffer alone, buffer with *Sss*I alone, and buffer with *Sss*I and sinefungin). CV scans were performed at a 100 mV/s scan rate with an Ag/AgCl reference electrode.

Importantly, the average SWV signal size was the same (within error) for DNA with an unmethylated binding site (7.9 nC ± 0.5 nC) and DNA with a fully methylated binding site (8.8 ± 0.4 nC).

For all variables tested, the binding response was identical for both DNA types; DNA with the fully methylated binding site showed the same time dependence, cofactor dependence, and reversibility as the unmethylated DNA. The percent change in SWV signal was also the same (within error) for the two DNA types across the range of *Sss*I concentrations tested (15 nM–100 nM). Responses to 50 nM and 100 nM *Sss*I are quantified in Figure 5.13 (50 nM: 45% ± 2% signal loss for unmethylated DNA and 43% ± 2% for fully methylated DNA; 100 nM: 62% ± 1% signal loss for unmethylated DNA and 60% ± 2% for fully methylated DNA). C-5-cytosine DNA methyltransferases have previously been shown to have reduced affinity (~10-fold) for DNA with a fully methylated binding site (43, 44). However, a crystal structure of *Hha*I methylase bound to fully methylated DNA shows that base flipping of the methylated cytosine still occurs with this bound complex (45). Clearly, any reduced affinity for the fully methylated substrate is not electrochemically resolved with the DNA-modified electrodes tested here. The data indicate that *Sss*I binding and base flipping occurs on both substrates at the *Sss*I concentrations that are required for detection with this platform.

Next, nonspecific binding by *Sss*I to DNA without the binding site was evaluated. A 17-mer without the *Sss*I binding site was designed by maintaining a sequence identical to the 17-mer with the 5′-CG-3′ binding site but changing the 5′-C to a T. *Sss*I binding to these substrates was examined side by side on multiplexed chips. As in the previous substrate comparison, the SWV signal size was the same (within error) for these two

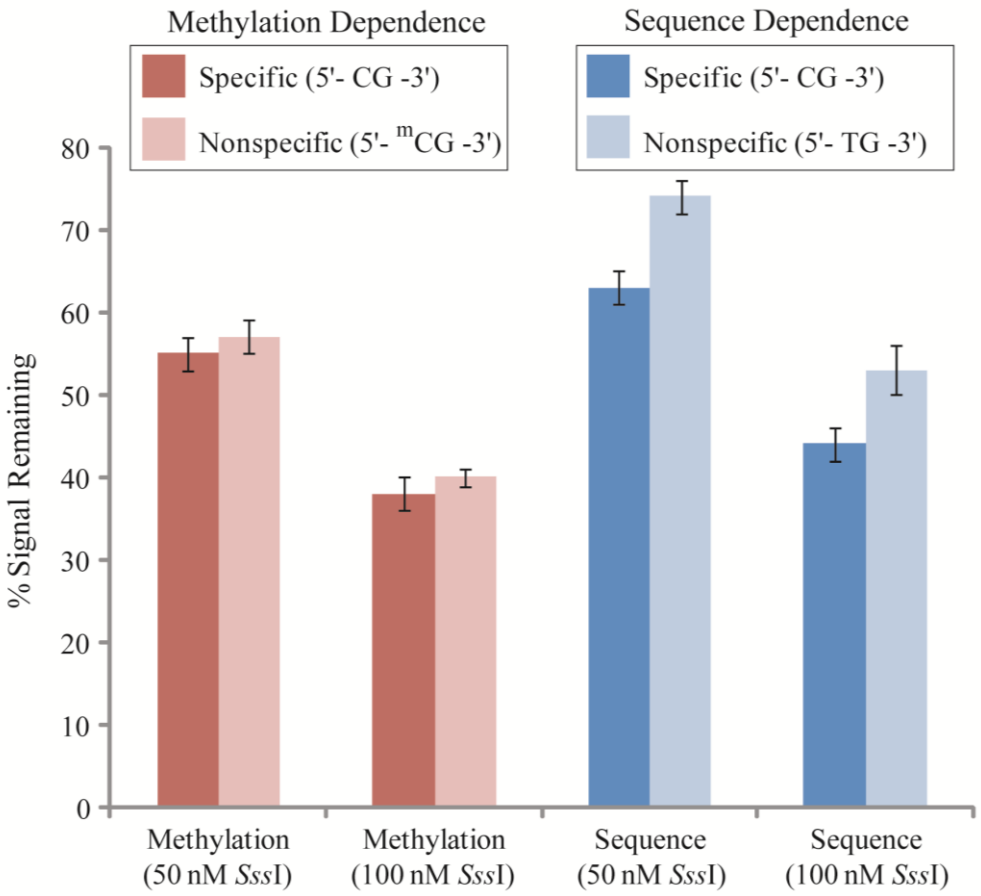

Figure 5.13 Effect of *Sss*I binding on nonspecific substrates. Comparative *Sss*I binding is shown in terms of binding site methylation (reds) and DNA sequence (blues). Binding on the nonspecific substrates—DNA with a fully methylated binding site (light red) and DNA without a binding site (light blue)—is compared to binding on the specific, unmethylated substrate that contains the *Sss*I binding site (dark red and dark blue). Binding comparisons on specific and nonspecific substrates for each variable (methylation status or sequence) were performed side by side on the same chip and at least two chips were analyzed for each variable and *Sss*I concentration. The percentage signal remaining was calculated from quantified SW data and averaged across the replicates. The error bars show the standard deviation across all electrodes tested for a given DNA substrate and *Sss*I concentration.

substrates across four chips (4.9 nC ± 0.3 nC for DNA with the binding site and 4.5 nC ± 0.4 nC for DNA without the binding site). Binding by 50 nM and 100 nM *Sss*I was measured separately on two chips for each concentration. After calculating the percentage change in signal from *Sss*I binding for both DNA types, the difference in percentage change between DNA types averaged across the replicates.

Overall, the DNA substrate with the *Sss*I binding site showed approximately 10% more signal loss than the substrate without the binding site. This result was observed for both 50 nM and 100 nM *Sss*I binding and is shown in Figure 5.13 (50 nM: 11% ± 2% greater change in the DNA substrate with the *Sss*I binding site; 100 nM: 9% ± 2% greater change in the DNA substrate with the *Sss*I binding site). Although this difference is small, it is likely significant; the identical initial signal size given by the two types of DNA provides a solid foundation for legitimate comparisons and this effect was consistently observed across multiple replicates. Additionally, the previous comparison of binding on two distinct DNA substrates that yielded no measurable difference (DNA with an unmethylated or fully methylated binding site), gives precedence for a negative result and supports the significance of a measured difference in this system.

Previous biochemical studies of C-5-cytosine DNA methyltransferases provide information for the interpretation of this result. For *Hha*I, which recognizes the site 5′-GCGC-3′, a single base change to this site causes a 60–300-fold decrease in its binding affinity (as determined by gel shift), depending on the base that is changed (46). Although a similar study has not been performed for *Sss*I, it is unlikely that the shift in K_d for nonspecific binding by *Sss*I would be as dramatic as what is observed for *Hha*I; *Sss*I already binds DNA 55-fold less tightly than *Hha*I (Kd = 11 nM vs. 0.2 nM, respectively)

and recognizes a shorter, inherently less specific sequence (39, 46). However, a clear decrease in binding is observed by gel shift upon substitution of the 5′-C for T within the binding site (47). The mode of *Sss*I action is also important to consider; while other C-5-cytosine DNA methyltransferases such as *Hha*I bind their specific DNA site and then dissociate, *Sss*I has been found to bind DNA nonspecifically and methylate DNA processively (48). Although *Sss*I catalyzes methylation completely and exclusively at 5′-CG-3′ sites (38), it binds duplex DNA regardless of the presence of this site (48).

Additionally, it should be noted that for the low density films that are necessary to accommodate protein binding in this assay, there may be some contribution to the Methylene Blue redox signal from direct contact of the probe with the electrode surface, in addition to reduction that occurs by DNA CT (31). It is unclear how specific and nonspecific binding by *Sss*I affects these two reduction modes. However, it is possible that the combination of these reduction modes decreases the capacity of the assay to distinguish sequence-specific binding because it provides more opportunities for nonspecific *Sss*I binding to interfere with probe reduction. Nonspecific binding of *Sss*I may either distort the structure of the DNA π-stack and shut off DNA CT or prevent direct reduction of the Methylene Blue probe at the surface. Both actions would decrease the sequence specificity reported by this assay.

Thus, for *Sss*I on DNA-modified electrodes, nonspecific binding likely occurs for both DNA types, whether or not they contain the 5′-CG-3′ binding site. This nonspecific binding clearly causes a significant decrease in the electrochemical signal in this system. Like binding experiments on DNA with a fully methylated binding site, any difference in the affinity of *Sss*I for the nonspecific and specific DNA substrates may not be resolved

on this platform. For DNA that does contain the 5′-CG-3′ binding site, *Sss*I can flip the 5′-C base out of the DNA π-stack, an interaction that is known to attenuate DNA CT. Since the inactive cofactor sinefungin is used for these experiments, once *Sss*I binds and flips this base it should largely stay bound in this position. This additional interaction, in combination with any resolvable difference in the affinity of *Sss*I for the two substrates, may account for the added 10% decrease in signal observed for DNA that contains the *Sss*I binding site. Because nonspecific and specific, base-flipping protein-DNA interactions may occur simultaneously, it is not possible to distinguish what mode of interaction accounts for what portion of signal loss for the two different DNA substrates. Despite this, these results indicate that *Sss*I interacts with the two DNA substrates differently and that this difference may be measured electrochemically.

Summary and Conclusions

The work described here outlines efforts toward the development of an electrochemical assay to monitor protein-DNA binding interactions. This assay utilizes DNA-modified electrodes and relies on the sensitivity of DNA CT to structural perturbations of the π-stack to report protein binding. Improvements were made upon previous work with this assay by the incorporation of covalent redox probes—Nile Blue and Methylene Blue—that are versatile and robust, and the extension of this detection scheme to a multiplexed chip format that allows for more complex experiments and side-by-side comparisons. The effect of common protein buffer components on the electrochemical signal was evaluated. Positively charged components, including spermidine and $MgCl_2$, were found to significantly enhance electrochemical signal size while retaining mismatch discrimination.

Binding by *Sss*I Methylase on multiplexed, DNA-modified electrodes was evaluated with Methylene Blue-modified DNA substrates. Signal loss and significant CV peak broadening was observed upon electrode treatment with *Sss*I and the measured time dependence, concentration dependence, cofactor dependence, and reversibility of this signal loss all indicate that it is due to direct *Sss*I-DNA binding. In general, significant substrate specificities for this binding could not be distinguished with this electrochemical assay; the same response was measured for unmethylated and fully methylated DNA substrates and only 10% more signal loss was observed for DNA with the specific *Sss*I binding site over DNA that does not contain the *Sss*I binding site. In terms of methylation status, this lack of measurable substrate specificity indicates that the decrease in affinity for the fully methylated binding site cannot be resolved with this

assay and active binding and base flipping of the already methylated target base occurs. In terms of sequence, the very subtle difference in substrate specificity is likely due to the nonspecific, processive mode of *Sss*I-DNA binding that clearly impacts the electrochemical signal in this system.

This work illustrates the challenges that still exist for the development of sensitive electrochemical assays for the detection of protein-DNA interactions. For detection schemes that rely on electrochemical decreases from protein binding, like the assay developed here, future work must focus on the optimization of redox probes and DNA-modified electrode film morphologies that more sensitively report and distinguish specific protein binding. Until improvements are made in this area, such assays may be best suited to evaluate binding in controlled, purified samples in which conditions that assure specific binding have already been identified in solution and may be translated to the surface.

Even considering this current limitation, this multiplexed assay that easily, rapidly, and inexpensively provides an electrical readout of protein-DNA interactions promises to be useful in a variety of research applications. Alongside work to improve the specificity of this assay, the current assay may be used in combination with solution experiments to improve our understanding of how protein-DNA binding in solution compares to binding at surfaces. More detailed analysis of the differences between solution and surface binding will help with the development of more effective detection schemes, devices, and data interpretation as detection strategies shift toward surface platforms and the inherent advantages that they carry. Additionally, given that the most dramatic differential in this assay is observed for the comparison of situations in which

protein is bound or unbound (such as in the case of cofactor dependence and reversibility experiments, regardless of whether that binding is a specific or nonspecific mode), this assay would be well suited for applications that require this binary report. Examples of such applications include screening for drugs that inhibit protein-DNA binding, analysis of how cofactors or changes in buffer conditions affect protein binding, and observation of complex processes that involve protein-DNA interactions in real-time. Here, by evaluating the current limitations of this assay as well as demonstrating its most positive and useful attributes, we can focus future work on improving its capacity to report substrate specificity and exploiting it in applications for which its capacity to report protein binding is best suited.

References

1. Lemon, B. and Tjian, R. (2000) *Genes Dev. 14*, 2551–2569.

2. Jeltsch, A. (2002) *ChemBioChem. 3*, 274-293.

3. Engelkamp, D. and van Heyningen, V. (1996) *Curr. Opin. Genet. Dev. 6*, 334-342.

4. Mullighan, C.G., Goorha, S., Radtke, I., Miller, C.B., Coustan-Smith, E., Dalton, J.D., Girtman, K., Mathew, S., Ma, J., Pounds, S.B., Su, X.P., Pui, C.H., Relling, M.V., Evans, W.E., Shurtleff, S.A., and Downing, J.R. (2007) *Nature 446*, 758-64.

5. Vaquerizas, J.M., Kummerfeld, S.K., Teichmann, S.A., and Luscombe, N.M. (2009) *Nature Rev. Genet. 10*, 252-263.

6. Baylin, S.B. and Herman, J.G. (2000) *Trends Genet. 16*, 168-174.

7. Linhart, H.G, Lin, H., Yamada, Y., Moran, E., Steine, E. J., Gokhale, S., Lo, G., Cantu, E., Ehrich, M., He, T., Meissner, A., and Jaenisch, R. (2007) *Gene. Dev. 21*, 3110-3122.

8. Conroy, P.J., Hearty, S., Leonard, P., and O'Kennedy, R. J. (2009) *Sem. Cell Dev. Biol. 20*, 10-26.

9. Warsinke, A. (2009) *Anal. Bioanal. Chem. 393*, 1393-1405.

10. Sikder, D. and Kodadek, T. (2005) *Curr. Opin. Biotech. 9*, 38-45.

11. Bulyk, M.L. (2006) *Curr. Opin. Biotech. 17*, 422-430.

12. Greil, F., Moorman, C., and van Steensel, B. (2006) *Meth. Enzymol. 410*, 342-359.

13. Heyduk, T. and Heyduk, E. (2002) *Nat. Biotech 20*, 171-176.

14. Tothill, I.E. (2009) *Sem. Cell Dev. Biol. 20*, 55-62.

15. Sadik, O.A., Aluoch, A.O., and Zhou, A. (2009) *Biosens. Bioelect. 24*, 2749-2765.

16. Drummond, T.G., Hill, M.G., and Barton, J.K. (2003) *Nat. Biotechnol. 21*, 1192-1199.

17. Bakker, E., and Qin, Y. (2006) *Anal. Chem. 78*, 3973-3983.

18. Gorodetsky, A.A., Buzzeo, M.C., and Barton, J.K. (2008) *Bioconj. Chem. 19*, 2285-2296.

19. Genereux, J.G. and Barton, J.K. (2010) *Chem. Rev. 110,* 1642-1662.

20. O'Neil, M.A. and Barton, J.K. (2005) *Charge Transfer in DNA: From Mechanism to Application.* Wagenknecht, H.A. Wiley-VCH, Ed., 27.

21. Kelley, S.O., Boon, E.M, Barton, J.K., Jackson, N., and Hill, M.G. (1999) *Nuc. Acids Res. 27,* 4830-4837.

22. Boon, E.M., Ceres, D.M., Drummond, T.G., Hill, M.G., and Barton, J.K. (2000) *Nature Biotechnol. 18,* 1096-1100.

23. Boal, A.K. and Barton, J.K. (2005) *Bioconjugate Chem. 16,* 312-321.

24. Boon, E.M., Salas, J.E., and Barton, J.K. (2002) *Nature Biotechnol. 20,* 282-286.

25. Gorodetsky, A.A., Ebrahim, A., and Barton, J.K. (2008) J. Am. Chem. Soc. 130, 2924-2925.

26. Bheemanaik, S., Reddy, Y.V.R., and Rao, D.N. (2006) *Biochem. J. 399,* 177-190.

27. Roberts, R.J. and Cheng, X.D. (1998) *Annu. Rev. Biochem. 67,* 181-198.

28. Vilkaitis, G., Dong, A.P., Wienhold, E., Cheng, X.D., and Klimasauskas, S. (2000) *J. Biol. Chem. 275,* 38722-38730.

29. Kim, Y.C., Geiger, J.H., Hahn, S., and Sigler, P.B. (1993) *Nature 365,* 512-520.

30. Bleichenbacher, M., Tan, S., and Richmond, T.J. (2003) *J. Mol. Biol. 332,* 783-793.

31. Pheeney, C.G. and Barton, J.K. (2012) *Langmuir 28,* 7063-7070.

32. Slinker, J.D., Muren, N.B., Gorodetsky, A.A., and Barton, J.K. (2010) *J. Am. Chem. Soc. 132,* 2769–2774.

33. Kelley, S.O. and Barton, J.K. (1997) *Bioconj. Chem. 8,* 31-37.

34. Gosule, L.C. and Schellman, J.A. (1976) *Nature 259,* 333-335.

35. Kas'yanenko, N.A. and Dribinskii, B.A. (2007) *J. Struct. Chem. 48,* 729-733

36. Slinker, J.D., Muren, N.B., Renfrew, S.E., and Barton, J.K. (2011) *Nature Chem. 3,* 230-235.

37. Pheeney, C.G., Guerra, L.F., and Barton, J.K. (2012) *Proc. Natl. Acad. Sci. 109,* 11528-11533.

38. Renbaum, P., Abrahamove, D., Fainsod, A., Wilson, G.G., Rottem, S., and Razin, A. (1990) *Nuc. Acids Res*. *18*, 1145-1152.

39. Renbaum, P. and Razin, A. (1995) *J. Mol. Biol*. *248*, 19-26.

40. Sankpal, U.T. and Rao, D.N. (2002) *Crit. Rev. Biochem. Mol. Biol*. *37*, 167-197.

41. Darii, M.V., Kirsanova, O.V., Drutsa, V.L., Kochetkov, S.N., and Gromova, E.S. (2007) *Mol. Biol. 41*, 110-117.

42. Lindstrom, W.M., Flynn, J., and Reich, N.O. (2000) *J. Biol. Chem. 275*, 4912-4919.

43. Dubey, A. and Roberts, R.J. (1992) *Nuc. Acids Res. 20*, 3167-3173.

44. Klimasauskas, S. and Roberts, R.J. (1995) *Nuc. Acids Res. 23*, 1388-1395.

45. O'Gara, M., Klimasauskas, S., Roberts, R.J., and Cheng, X.D. (1996) *J. Mol. Biol. 261*, 634-645.

46. Youngblood, B., Buller, F., and Reich, N.O. (2006) *Biochemistry 45*, 15563-15572.

47. Renbaum, P. and Razin, A. (1995) *Gene 157*, 177-179.

48. Renbaum, P. and Razin, A. (1992) *FEBS Lett. 313*, 243-247.

Chapter 6

Electrochemical Assay for the Detection of Methyltransferase Activity

Introduction

In mammals, DNA methylation is the most prominent form of epigenetic gene regulation and is a critical long-term gene silencing mechanism (1, 2). This covalent addition of a methyl group to the carbon-5 position of cytosine at predominantly 5′-CG-3′ sites is catalyzed by enzymes called DNA methyltransferases which use the cofactor S-adenosyl-L-methionine (SAM) as a methyl donor. DNA methylation is central to many normal cellular processes including development, X chromosome inactivation, control of gene expression by repression, and silencing of transposons, among others (2, 3). However, aberrant DNA methylation has been associated with multiple disease states (4) including developmental abnormalities such as IFC syndrome (5) and Rett syndrome (6), autoimmune diseases such as lupus (7), and many types of cancer (8–10).

The link between abnormal DNA methylation and cancer has recently become an area of intense, widespread research and both excessive methylation (hypermethylation) and deficient methylation (hypomethylation) have been identified in diverse tumor types (9, 11). While hypermethylation can contribute to oncogenesis by the silencing of tumor suppressor genes (10), hypomethylation may activate oncogenes or latent retrotransposons, or cause chromosome instability (9). In many cases, these harmful methylation states have been linked to the abnormal expression and activity of methyltransferases (10, 12–17).

Mammalian DNA methyltransferases include Dnmt1, Dnmt3a, and Dnmt3b and while all three catalyze the same reaction, they play different roles in establishing methylation patterns in the genome. Dnmt1 transmits methylation patterns across cell divisions by completing methylation on newly replicated strands at 5′-CG-3′ sites that

carry methylation on the template strand (3). Thus Dnmt1 is called a "maintenance" methyltransferase and displays a significant preference for hemimethylated DNA substrates (18, 19). Dnmt3a and Dnmt3b, in contrast, have been identified as "*de novo*" methyltransferases because of their activity at unmethylated 5′-CG-3′ sites, primarily during embryogenesis when the genome is largely unmethylated and methylation patterns must be set (3, 20). Studies that link these methyltransferases to a variety of cancers make it clear that their inherently different functions carry over to unique roles in these maladies. Furthermore, the interaction and cooperation between these methyltransferases (21–23) adds an additional layer of complexity to their regulation in healthy cells and their disregulation that is now being identified in a growing number of cancers.

In this multifaceted and newly developing field, much is still not understood about the role of methyltransferases in cancer initiation and progression. Gaining this understanding is an attractive goal as abnormalilties in methylation activity usually occur far before other signs of malignancy and could thus be used as indicators for early detection of cancer (9, 10). Additionally, identification of cancers with a certain methylation phenotype (hypermethylation or hypomethylation) can help specify an effective course of treatment (9, 24). Perhaps the most enticing motivation though, is that like other epigenetic modifications methylation is reversible; the correction of harmful methylation states reveals healthy, functional DNA that was there all along. This great potential for reversal makes methyltransferases an especially attractive therapeutic target (9, 10). As we move toward a more complete understanding of methylation in cancer, effective and accessible assays for methyltransferase activity will be critical at every step along the way. From fundamental studies of methyltransferase activity in cancer cells, to

the identification of anti-methylation drug therapies, to the screening of patients for early diagnosis of methylation-related cancers, our ability to quickly and accurately measure methyltransferase activity will dictate how well we can expand our understanding at the interface of epigenetics and cancer, and make practical use of this information for diagnostics and therapeutics.

Toward this purpose, a variety of methods have been developed for the measurement of DNA methylation and methyltransferase activity (25). While the most common current strategies involve radioactive labeling with [methyl-^{3}H]-SAM (26–28), other methods include PCR-based bisulfite conversion (29, 30), HPLC (31), and fluorescence and colorometric assays (32–34). Another subset of methylation assays are based on digestion of DNA by methylation-sensitive restriction enzymes from bacterial restriction/modification systems. In these assays, methylation of a specific DNA sequence confers protection from digestion by the corresponding restriction enzyme and results are typically visualized by electrophoresis and southern blot (35, 36) or fluorescence (37–42). Although the desire to avoid radioactive substrates has motivated the development of these diverse non-radioactive methods, such alternatives carry their own significant drawbacks. These include time-consuming sample preparation and analysis, costly detection equipment, expensive antibodies and fluorescently labeled substrates, an inability to expand to high throughput analysis of multiple samples, and detection schemes that are incompatible with human methyltransferases.

Electrochemical platforms overcome many of these drawbacks, providing low-cost, portable sensors that have great potential for multiplexing and use in clinical settings (43–45). Despite these advantages and the clear benefits of electrochemistry as a

non-radioactive method, relatively little work has been done to develop electrochemical platforms for the detection of methyltransferase activity. The electrochemical methods that have been reported include the direct electrocatalytic oxidation of individual DNA bases as a means to detect 5-methylcytosine (46) and several strategies that use methylation-sensitive restriction enzymes. These strategies include include restriction-based signal modulation with DNA-functionalized gold nanoparticles (47); restriction-facilitated binding of redox-active moieties, such as carbon nantubes (48), probe-modified DNA (49), and redox-active enzymes (50); and DNA monolayers with methylation-sensitive restriction sites that bear either electrochemical (51–54) or photoelectrochemical (55) reporters. Though diverse, these previous electrochemical approaches are very limited in that they are either demonstrated with synthetic 5-methylcytosine alone and not enzymatic methylation or they are only applicable for the detection of bacterial methyltransferase activity. Because human methyltransferase activity depends on the methylation state of the DNA target (hemimethylated or unmethylated), assays for the detection and study of human methyltransferases must allow for the use of both substrates.

Here we describe a new electrochemical assay for the detection of methyltransferase activity in which either a hemimethylated or unmethylated substrate may be used for the sensitive detection of both bacterial and human methyltransferase activity. In this assay, DNA-modified electrodes bearing a covalent redox probe are combined with a methylation-sensitive restriction enzyme to convert methylation into an electrical signal (Figure 6.1). By utilizing a covalent redox probe that is reduced by DNA-mediated charge transport (DNA CT), we take advantage of this robust, exquisitely

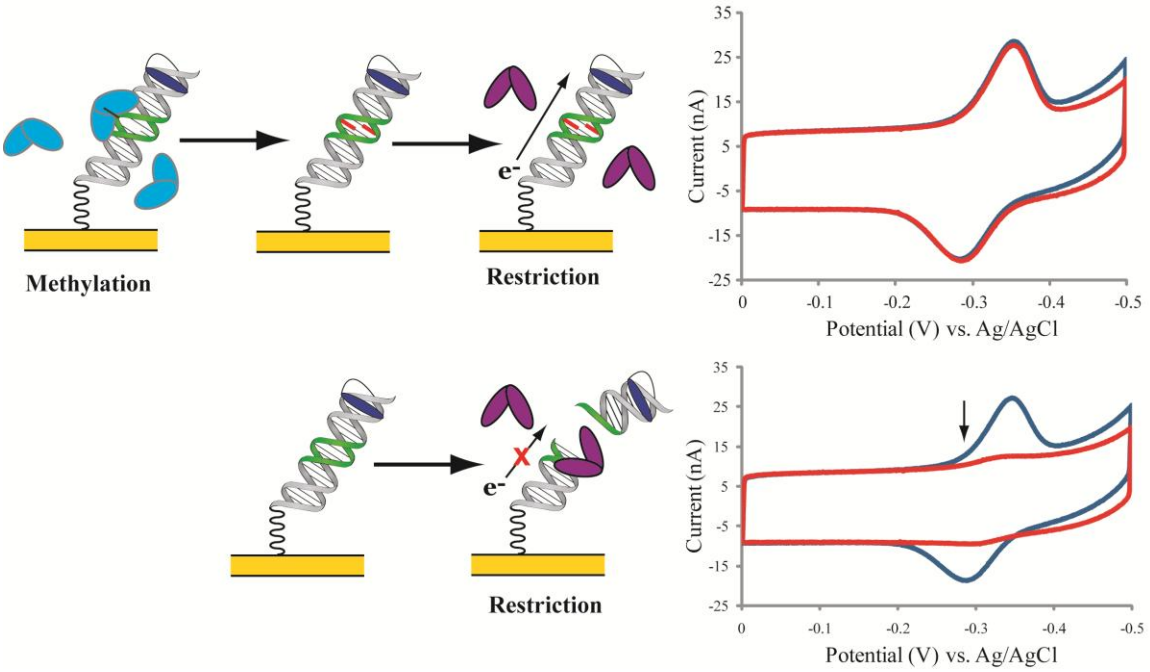

Figure 6.1 Assay for the electrochemical detection of methyltransferase activity. DNA-modified electrodes with the overlapping recognition site of a methyltransferase and restriction enzyme (green section in DNA) are prepared. In the presence of active methylases (top left), the DNA-modified electrodes become methylated and protected from cutting during subsequent treatment with a restriction enzyme. Thus by cyclic voltammetry (top right), the covalent redox probe exhibits a "signal ON" result both before (blue) and after (red) restriction enzyme treatment. In the absence of active methyltransferases (bottom left), the DNA remains unmethylated and is readily cut by the restriction enzyme. This "signal OFF" result is reported through cyclic voltammetry (bottom right) by signal attenuation upon restriction enzyme treatment.

sensitive, and well characterized chemistry (56, 57). Such DNA-modified electrodes have been used previously to detect mismatches (58-61), lesions (62), and protein binding (63, 64) or restriction activity (60, 61, 65). Here, electrodes are modified with DNA that contains the human methylation site (5′-CG-3′) within the recognition site of a methylation-sensitive restriction enzyme. Upon treatment of the electrodes with active methyltransferases, these sites become methylated, protecting the DNA from restriction during subsequent restriction enzyme treatment. With the DNA intact, the redox signal from the probe is retained ("signal ON") and indicates the presence of active methylases. If the electrode is not treated with active methyltransferases, the DNA remains unmethylated and is readily cut, causing the nearly complete disappearance of the redox signal ("signal OFF").

This assay is demonstrated with either the *BstU*I or B*ssH*II endonuclease restriction site (5′- CGCG - 3′ or 5′-GCGCGC-3′, respectively). For *BstU*I, methylation of any of the cytosines within the recognition site protects the DNA from restriction. For *BssH*II, full methylation of either of the two 5′-CG-3′ sites within its recognition sequence is required to block restriction. Importantly, this means that a hemimethylated substrate (5′-G^{m}CGCGC-3′) may be used with *BssH*II for this assay as this DNA is still readily cut if it is not further methylated This substrate versatility is critical for studies that involve the primary human methytransferase Dnmt1 which has a strong preference for hemimethylated 5′-^{m}CG-3′ sites. This work is the first reported electrochemical strategy that facilitates detection of human methyltransferase activity. We demonstrate this assay for the detection of bacterial and human samples in a multiplexed, low cost

format that may easily be applied to high throughput studies or utilized in research and clinical laboratories.

Materials and Methods

Materials

All standard and modified phosphoramidites were purchased from Glen Research. Modified Methylene Blue dye for coupling was synthesized as described previously (66). S-adenosyl-L-methionine (SAM) and Lambda DNA were purchased in solution from New England Biolabs and aliquots were stored at -20°C. Tritiated SAM (^{3}H-SAM) was purchased from Perkin Elmer and aliquots were stored at -20°C. All other chemicals for the preparation of protein buffers and DNA-modified electrodes, and for use in radioactive methyltransferase activity experiments were purchased from Sigma-Aldrich and used as recieved. Multiplexed chips were fabricated at Caltech as described previously (60). Reagents for cell culture were purchased from Invitrogen and used as received.

Protein Preparation

All proteins were purchased from commercial sources. *Sss*I methyltransferase, *BstU*I restriction endonuclease, *BssH*II restriction endonuclease, *Rsa*I restriction endonuclease, and BSA were purchased from New England Biolabs, stored at -20°C, and used as received unless otherwise indicated. Protease from *Streptomyces griseus* was purchased as a dry powder from Sigma-Aldrich and stored as a 250 μM solution in 40% glycerol in phosphate buffer without salt (5 mM phosphate, pH 7) at -20ºC. Human

Dnmt1 was purchased from BPS Bioscience and aliquots were stored at -80°C. As Dnmt1 and *BssH*II require a 37°C heated incubation to show activity, these proteins were purified by size exclusion spin column (10 kDa cutoff, Amicon) prior to electrochemistry experiments to remove dithiothreitol (DTT) which disrupts DNA-modified electrodes upon heating. This step also functioned to desalt Dnmt1 whose activity is inhibited by NaCl and Mg^{2+}. The purification was performed according to manufacturer instructions at 4°C and Dnmt1 was exchanged into the Dnmt1 reaction buffer (50 mM Tris-HCl, 1 mM EDTA, 5% Glycerol, pH 7.8), while *BssH*II was exchanged into the general methylation/restriction (M/R) activity buffer (10 mM Tris-HCl, 50 mM NaCl, 10 mM $MgCl_2$, pH 7.9) . This step was not required for the preparation of *Sss*I, *BstU*I, or *Rsa*I as DTT in unheated solution was not found to disrupt DNA-modified electrodes.

Nuclear Lysate Preparation

HCT116 cell lines, including parent and $DNMT1^{-/-}$ lines, were acquired from the Vogelstein group at Johns Hopkins and cultured as described previously (23, 27). Briefly, cells were cultured in McCoy's 5A modified medium supplemented with 10% fetal bovine serum and 1% penicillin/streptomycin. To prepare nuclear lysates, cells were harvested, counted, and aliquoted appropriately to ensure an equal number of cells for each sample (~10^7 cells per sample). Nuclear extraction was performed using the NE-PER Nuclear and Cytoplasmic Extraction Reagents Kit (Pierce), according to the manufacturer's protocol. Nuclear lysates were aliquoted and stored at -80°C.

The protein concentration of nuclear lysates was measured by BCA Protein Assay (Pierce). Expression of Dnmt1 was analyzed by western blot based on work described

previously (23, 27). Briefly, an equivalent amount of total nuclear protein (200 μg) for each lysate sample was resolved on a 4-20% Tris-HCl gel (75 minutes at 200 V) before transfer to a polyvinylidene fluoride membrane (Millipore). Membranes were blocked with 5% nonfat milk in TBST buffer. Incubation with a rabbit polyclonal primary antibody for Dnmt1 (New England Biolabs, M0231S; 1:2000 dilution) and rabbit polyclonal primary antibody for Lamin A (Santa Cruz Biotechnology, sc-20680; 1:1000 dilution) was carried out for 18 hours at 4°C with shaking. An Alexa Fluor-conjugated goat anti-rabbit secondary antibody (Invitrogen, A-21076; 1:10,000 dilution) was then used to detect the immunocomplexes by scanning at 680 nm with an Odyssey IR Imaging System (LI-COR).

DNA Sequences

All DNA sequences used in these experiments are summarized in Table 6.1. For the detection of methyltransferase activity with *BstU*I, electrodes were modified with the sequence 5′-HS- $(CH_2)_6$ - GACTGA*GTAC*TCGCGACT GA -3' with a Methylene Blue-modified complement. The unmethylated *BstU*I restriction site (5′- CGCG - 3′) is underlined. As a control, this sequence also contains the *Rsa*I restriction site (5′-*GTAC*-3') which is italicized. For control experiments with synthetically methylated DNA, the *BstU*I restriction site in the above sequence was replaced with a fully methylated restriction site (5′- $^{m}CG^{m}CG$ -3') and a Methylene Blue-modified complement that also contains the fully methylated restriction site was used.

For the detection of methyltransferase activity with *BssH*II, electrodes were modified with the sequence 5′-HS- $(CH_2)_6$ - GACTGAGTACTGCGCGCACTGA -3'

Table 6.1 DNA sequences used for electrochemical detection of methyltransferase activity. The *BstU*I or *BssH*II restriction site is indicated in red. The *Rsa*I restriction site is indicated by bold type. For all DNA, the Methylene Blue redox probe is covalently attached to the terminal 5′-T.

DNA Substrate	Sequence
*BstU*I, Unmethylated	5'-HS- $(CH_2)_6$ - GACTGA**GTAC**TCGCGACTGA-3' CTGACT**CATG**AGCGCTGACT
*BstU*I, Fully Methylated	5'-HS- $(CH_2)_6$ - GACTGA**GTAC**T^{m}CG^{m}CGACTGA-3' CTGACT**CATG**AG^{m}CG^{m}CTGACT
*BssH*II, Unmethylated	5'-HS- $(CH_2)_6$ - GACTGAGTACTGCGCGCACTGA-3' CTGACTCATGACGCGCGTGACT
*BssH*II, Hemimethylated	5'-HS- $(CH_2)_6$ - GACTGAGTACTG^{m}CGCGCACTGA-3' CTGACTCATGACGCGCGTGACT
*BssH*II, Fully Methylated	5'-HS- $(CH_2)_6$ - GACTGAGTACTG^{m}CGCGCACTGA-3' CTGACTCATGACG^{m}CGCGTGACT

with a Methylene Blue-modified complement. The unmethylated *BssH*II restriction site (5′- GCGCGC - 3′) is underlined. A hemimethylated DNA substrate was prepared by replacing the unmethylated *BssH*II restriction site with a hemimethylated restriction site (5′- G^{m}CGCGC -3') and utilizing an unmethylated Methylene Blue-modified complement. DNA with full methylation of one of the 5′- GC - 3′ pairs in this sequence was prepared using the same hemimethylated restriction site but using a methylated Methylene Blue-modified complement (5′- GCG^{m}CGC -3'). As an additional control, DNA with the unmethylated *BstU*I restriction site was used to measure *BssH*II activity on DNA without a *BssH*II restriction site.

DNA Synthesis

All DNA was synthesized on an Applied Biosystems 3400 DNA synthesizer. Thiolated strands were prepared with a C6-S-S phosphoramidite at the 5′ terminus. Strands containing methylated cytosine were synthesized with a 5-methyl dC-CE phosphoramidite. DNA for Methylene Blue coupling was prepared with regular phosphoramidites and an amino-C6-dT phosphoramidite at the 5′ terminus. All DNA was purified by reverse-phase HPLC with a polymeric PLRP-S column (Agilent) and characterized by mass spectrometry. All DNA stocks were desalted, resuspended in phosphate buffer (5 mM phosphate, 50 mM NaCl, pH 7), and quantified by UV/Vis absorption at 260 nm. Equimolar amounts (50 μM) of complementary strands were combined and thermally annealed.

For Methylene Blue-modified DNA, coupling was carried out in solution as described previously (66) and the structure of the final product is shown in figure 6.2.

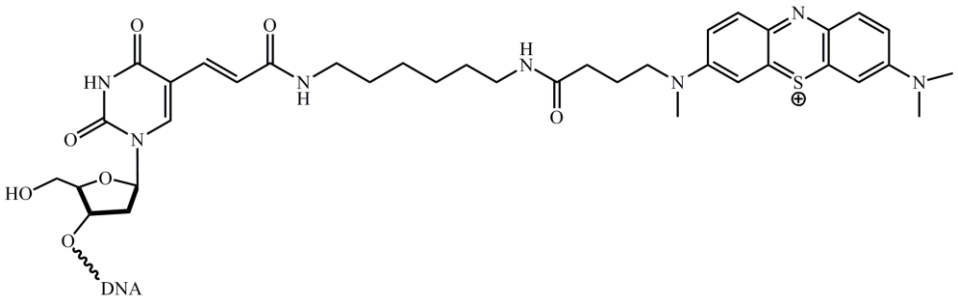

Figure 6.2 Structure of covalent Methylene Blue redox probe used for the detection of methyltransferase activity. The probe is attached to the terminal 5′-T at the end of the DNA opposite the alkanethiol linker.

Briefly, DNA that had been purified by reverse-phase HPLC with the dimethoxy trityl group removed was suspended in 0.1 M $NaHCO_3$ and combined with an equimolar amount of modified Methylene Blue dye in DMSO. The mixture was allowed to shake overnight at room temperature. The coupled DNA was then purified from the free dye using a Nap-5 size exclusion column (GE Healthcare) before further purification by HPLC. For thiolated DNA, after initial HPLC purification, the disulfide was reduced to the free thiol in 100 mM dithiothreitol in 100 mM Tris-HCl buffer pH 8.3 at room temperature for 45 minutes, purified on a Nap-5 column, and further purified by HPLC.

Multiplexed Chip Preparation and Assembly

Prior to application of DNA solutions, chips were cleaned with acetone and isopropanol, dried, and further cleaned by exposure to UV ozone for 5 minutes. The chips were then assembled with a rubber gasket and clamp, and a solution of 25 µM DNA in phosphate buffer was immediately applied to each quadrant of the chip (25 µL DNA per quadrant). The DNA was allowed to assemble on the chip overnight in a humidified environment at room temperature.

Electrochemistry

All electrochemistry was carried out with a standard potentiostat and multiplexer console (CH Instruments). A three-electrode system was employed including a Pt wire auxiliary electrode and Ag/AgCl reference electrode (Cypress Systems). Chips were first backfilled with 1 mM mercaptohexanol in phosphate buffer with 5% glycerol for 45 minutes at room temperature. For all electrochemistry, cyclic voltammetry (CV) scans

were performed at a 100 mV/s scan rate over the potential window of 0 mV to -500 mV. Scans were taken in 200 μL of the specified buffer in the common well of the chip. Signal size was measured as the CV cathodic peak area.

For the detection of *Sss*I activity, after thorough rinsing of the mercaptohexanol backfilling solution, background scans were performed in the M/R activity buffer. Individual quadrants of the chip were then treated with *Sss*I in M/R activity buffer with 160 μM SAM cofactor. A reaction volume of 10 μL was used for each quadrant. The *Sss*I solution was allowed to incubate on the chip at room temperature for 2 hours. At that time, the solution was removed, the chip was rinsed in M/R activity buffer, and a solution of 10 μg/mL Lambda DNA in M/R activity buffer was applied and allowed to incubate on the chip for 45 minutes at room temperature to force the dissociation of any protein still bound to the DNA-modified electrode. Following this, a rinse with 500 mM NaCl in M/R activity buffer was performed to ensure complete protein dissociation. The chip was rinsed with M/R activity buffer to remove residual salt and a background scan was taken. Next, 1,000 units/mL of *BstU*I in M/R activity buffer was applied to the chip and allowed to incubate at room temperature for 2 hours before a final scan. As a control, after completion of the assay, chips were treated with 1,000 units/mL *Rsa*I in M/R activity buffer at room temperature for 30 minutes and then scanned for signal loss.

A similar procedure was followed for the detection of purified Dnmt1 activity on a hemimethylated substrate. Dnmt1 activity buffer is not optimal for electrochemistry because it lacks salts (such as NaCl and $MgCl_2$, which are known to inhibit Dnmt1) (67) and spermidine (which may also interfere with Dnmt1 activity because of its positive charge), both buffer components that are known to enhance the signal size of DNA-

modified electrodes. Because of this, after the methylation reaction had been allowed to proceed in Dnmt1 activity buffer, an optimized scanning buffer (5 mM phosphate, 50 mM NaCl, 4 mM $MgCl_2$, 4 mM spermidine, 50 μM EDTA, 10% glycerol, pH 7) was used for all electrochemical scans of activity by Dnmt1. As both Dnmt1 and *BssH*II show decreased activity in this scanning buffer, chips were thoroughly rinsed in the appropriate buffer for the subsequent step before proceeding. After a background scan, chips were treated with Dnmt1 in Dnmt1 activity buffer with 100 μg/mL BSA and 160 μM SAM. A reaction volume of 10 μL was used for each quadrant. The chip was heated at 37°C in an incubator for 2 hours. During this incubation, the chip was stored in a humidified container in order to prevent evaporation. The chip was then treated with Lambda DNA at room temperature followed by a NaCl rinse, as described previously. After a background scan in the scanning buffer, 1,500 units/mL of *BssH*II was applied to the chip and allowed to incubate at 37°C for 1 hour. A final scan was then taken.

For electrochemical detection of methyltransferase activity in cell lysates, the same procedure used for purified Dnmt1 was employed; a reaction volume of 10 μL with 25 mg/mL lysate and 160 μM SAM was used to treat each quadrant at 37°C for 2 hours. Then, specifically for lysate samples, the lysate solution was removed and chips were treated with a 1 μM protease solution in phosphate buffer (5 mM phosphate, 50 mM NaCl, pH 7) for 90 min at 37ºC. Chips were then rinsed thoroughly with scanning buffer to remove any residual protease. A background scan in scanning buffer was then taken, followed by *BssH*II treatment and a final scan, as described previously.

^{3}H-SAM Methylase Activity Assay

The methyltransferase activity of purified protein samples and nuclear lysates was determined by a conventional ^{3}H-SAM methylase activity assay, with a procedure based partially on previous work (23, 27). Briefly, 20 μL reactions were prepared with 20 μM DNA, 0.5 μCi ^{3}H-SAM (~3 μM), and the sample of interest in its appropriate activity buffer (15 nM Dnmt1 or 12 mg/mL nuclear lysate). For reactions with Dnmt1, 100 μg/mL BSA was also included. For the DNA substrate, the same *BssH*II unmethylated and hemimethylated 22-mer sequence that had been used for the electrochemical assay with *BssH*II restriction was employed (Table 6.1) but without any probe or thiol modifications. For each experiment, positive (15 nM *Sss*I) and negative (no protein) controls were included as points of reference. To prepare a heat-inactivated nuclear lysate control, the mixed sample was heated at 65°C for 35 min. before processing with the other samples. Reactions were mixed thoroughly and allowed to incubate at 37°C for 2 hours. The reactions were then stopped with 30 μL of a 10 % TCA solution, spotted onto DE81 filter paper (Whatman), and allowed to air dry for 15 minutes. The filter papers were then soaked separately in 10 mL of 50 mM Na_2HPO_4 for 15 min., followed by individual rinsing with 50 mM Na_2HPO_4 and 95% cold ethanol. The filter papers were then dried at 37°C for 30 min. before measurement by liquid scintillation counting.

Results and Discussion

Detection of SAM-dependent *Sss*I Methyltransferase Activity

Initial work on this assay was performed with *Sss*I methyltransferase, which binds the site 5′-CG-3′ and methylates the C-5 position of the target cytosine (68). *Sss*I was

selected because it is considered the bacterial analog to human methyltransferases, which bind and methylate the same sequence (68). For the development of this assay, it was first important to confirm that any protection of the DNA from restriction after methyltransferase treatment is due exclusively to DNA methylation. To do this, the dependence of *Sss*I-mediated protection on the SAM cofactor was evaluated. As SAM is the methyl donor in the methylation reaction, it is required for DNA methylation. Multiplexed chips were modified in three quadrants with the unmethylated *BstU*I 20-mer and treated side-by-side with 15 nM *Sss*I with SAM, 15 nM *Sss*I alone, or SAM alone. As a control, the fourth quadrant was modified with the synthetically methylated *BstU*I 20-mer and left untreated. Chips were then treated with *BstU*I to visualize the DNA protection that had occurred (Figure 6.3).

After *Sss*I-treatment of the electrodes, large electrochemical signals are observed from the Methylene Blue-modified DNA film. Importantly, the electrodes are treated with competitor DNA and thoroughly rinsed in order to remove bound *Sss*I which can attenuate the electrochemical signal (63) and interfere with the assay. It should be noted that for the low density films that are necessary to accommodate protein binding in this assay, there is some contribution to the Methylene Blue redox signal from direct contact of the probe with the electrode surface, in addition to reduction that occurs by DNA CT (66). However, as this is a restriction-based assay in which both surface and DNA-mediated reduction are equally shut off by cutting, this combination of reduction modes does not affect the performance of the assay.

Clearly, from these data, signal protection is dependent on the combined treatment of *Sss*I and SAM. While the electrodes treated with *Sss*I and SAM show near

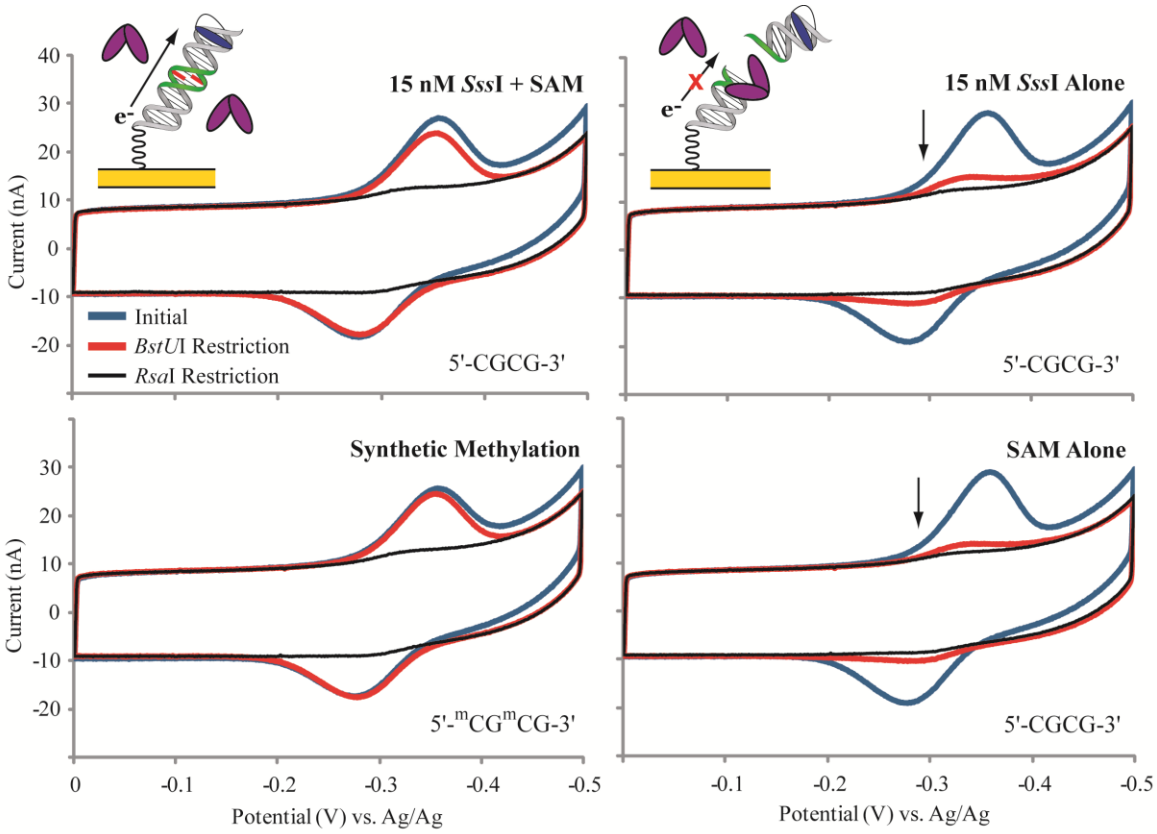

Figure 6.3 *Sss*I protection from *BstU*I restriction is dependent on the SAM cofactor. Chips were modified in three quadrants with the unmethylated *BstU*I 20-mer (top row and bottom right) and in one quadrant with the synthetically methylated *BstU*I 20-mer (bottom left). DNA protection was evaluated side by side on the same chip: the unmethylated DNA quadrants were treated with 20 nM *Sss*I + SAM (160 μM) (top left), 20 nM *Sss*I alone (top right), or SAM alone (160 μM) (bottom right), while the synthetically methylated quadrant was left untreated (blue traces). The chip was then treated in all quadrants with *BstU*I (1,000 units/mL) (red traces). Finally, the chip was treated in all quadrants with *Rsa*I (1,000 units/mL) (black trace). All scans were performed in M/R activity buffer. CV scans were performed at a 100 mV/s scan rate with an Ag/AgCl reference electrode.

complete signal protection (98% ± 2%), *Sss*I alone or SAM alone show the same, minimal signal protection (12% ± 1% and 13% ± 1%, respectively). As expected, the synthetically methylated DNA shows complete protection (no measurable signal decrease). The SAM-dependence of *Sss*I-mediated signal protection as well as the same lack of protection by either moiety alone provides strong evidence that the observed signal protection is an effective report of DNA methylation.

To further rule out other possible modes of DNA protection, such as *Sss*I-DNA binding or nonspecific protein aggregation that physically blocks the *BstU*I restriction site, chips were then treated with a second restriction enzyme, *Rsa*I. Importantly, *Sss*I does not have the capacity to methylate and protect the *Rsa*I recognition site against restriction and thus any observed protection would necessarily be due to an alternative mode. With this treatment, the remaining redox signals for all DNA types are reduced to the same, near complete level of attenuation (4% ± 1% signal remaining for all). In this DNA substrate, the *Rsa*I recognition site is located just one base away from the *Sss*I recognition site and is therefore well within the binding footprint of *Sss*I, which covers at least 7 nucleotides on each side of the binding site (69). Thus, if *Sss*I-DNA binding or nonspecific aggregation of *Sss*I were preventing the access of *BstU*I to the DNA this physical block would also prevent the access of *Rsa*I. This result indicates that all DNA on the electrode is readily accessible to cleavage by a restriction enzyme, even after treatment with *Sss*I and/or SAM. Thus the observed *Sss*I-mediated signal protection is due specifically and exclusively to DNA methylation catalyzed by this methyltransferase.

Concentration Dependence of *Sss*I Methyltransferase Activity

Next, the concentration range over which *Sss*I methyltransferase activity may be detected with this assay was evaluated. Multiplexed chips modified with the *BstU*I unmethylated 20-mer were treated with a range of *Sss*I concentrations (0–16 nM) including up to four different concentrations on the same chip surface (Figure 6.4, inset). An activity curve, based on the percent signal protected from *BstU*I restriction at each concentration of *Sss*I, was compiled from 4 chips with 4-8 electrodes measured at each concentration (Figure 6.4). Near complete signal protection is observed with *Sss*I concentrations of 8 nM and higher (96 % ± 3% at 8 nM; 99% ± 1% at 16 nM). Between the narrow *Sss*I concentration range of 4 nM and 2 nM there is a sharp loss of signal protection (91% ± 5% at 4 nM; 21% ± 5% at 2 nM). Below 2 nM *Sss*I, signal protection is not distinguished from the baseline signal that remains when electrodes are left untreated (7% ± 1%).

The sharp change from almost no protection to near complete protection that occurs between 2–4 nM *Sss*I is a detection limit that likely reflects the binding affinity of *Sss*I (11 nM) (70), the specific activity of the sample, and the morphological accessibility of the DNA film. The narrow dynamic range of this assay indicates that it may be used to distinguish very small relative differences in the concentration and/or activity of methyltransferase samples within this range. Additionally, such dramatic switching behavior suggests that this assay may be best employed in its current form for ON/OFF detection of methyltransferase activity rather than quantification: although the specific concentration of methyltransferase solutions that fall within the dynamic range may be determined, discrete concentrations above and below this range cannot be distinguished.

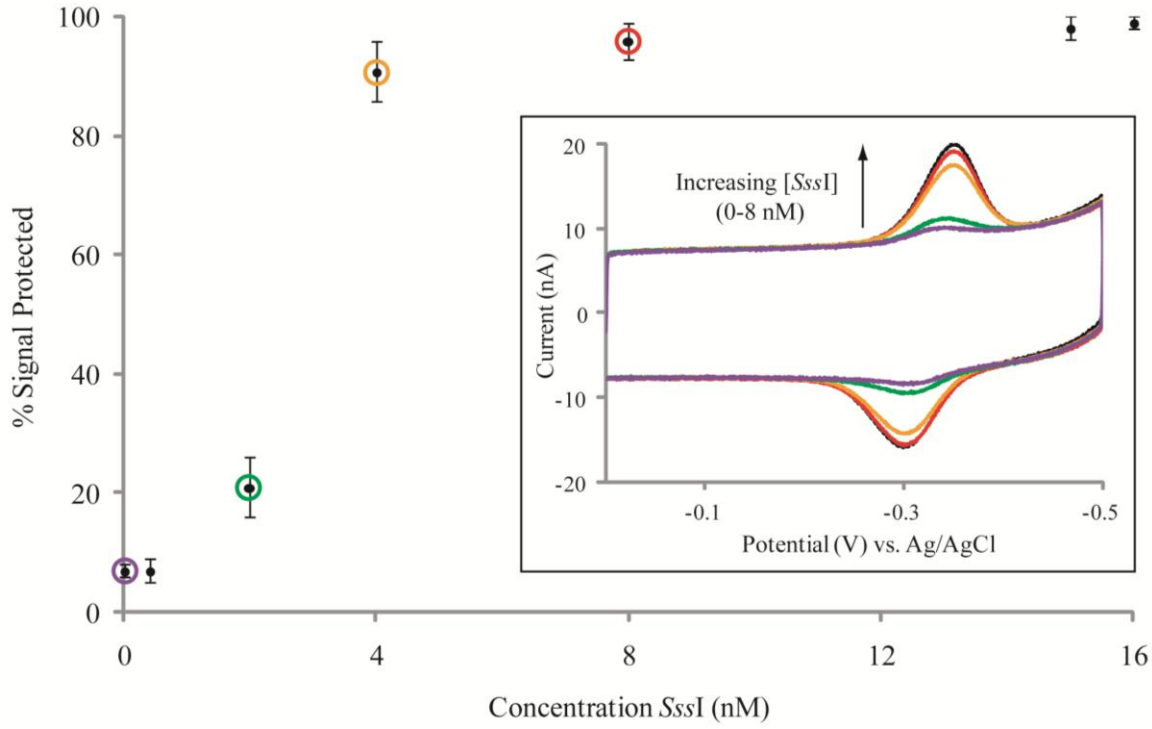

Figure 6.4 DNA protection by *Sss*I methylation is concentration-dependent. Chips were modified in all quadrants with the unmethylated *BstU*I 20-mer. DNA protection by various concentrations of *Sss*I was evaluated side by side on the same chip, and CV signals from representative electrodes of an example chip are shown (inset). Overlaid CV traces include the initial signal before *BstU*I treatment (black, dashed), 8 nM *Sss*I (red), 4 nM *Sss*I (orange), 2 nM *Sss*I (green), and untreated (purple). Quantification of the observed signal protection across 4 separate chips is displayed as an *Sss*I activity curve where the circled points correspond to the concentrations tested on the example chip. Error bars represent the standard deviation among 4–8 electrodes for each point. All scans were performed in M/R activity buffer. CV scans were performed at a 100 mV/s scan rate with an Ag/AgCl reference electrode.

Nevertheless, given the small sample volume required (10 μL), these results demonstrate that this assay may be used to readily detect *Sss*I methyltransferase activity down to 20 fmoles of protein.

The sensitivity and dynamic range of this assay for the measurement of *Sss*I activity may be compared to other strategies for the detection of methyltransferase activity. Although specific assay characterization data for *Sss*I are not available for fluorescence and colorimetric methods in solution, the assay described here is superior in terms of the sample volume required; only 10 μL of methyltransferase sample is required for this assay while at least 75–115 μL is typically required for these solution methods (32, 38). Additionally, these more conventional solution methods require costly antibodies, reagents, and scanning equipment that are not necessary for the electrochemical approach described here.

Several electrochemical assays, employing a variety of redox reporters, have been described for the detection of *Sss*I activity based on *Sss*I-catalyzed methylation protection of DNA films from cutting by the *Hpa*II restriction enzyme (51–54). Because different batches of *Sss*I can show different levels of enzymatic activity, *Sss*I concentrations in these reports are given in terms of units of activity, where one unit is defined as the amount of *Sss*I required to protect 1 μg of Lambda DNA in a total reaction volume of 20 μl in 1 hour at 37°C against cleavage by a restriction enzyme (71). Based on measurements of the specific batch of protein used for these experiments, the dynamic range of 2-8 nM for the assay presented here converts to a range of 30-60 units/mL. In general, other assays in the literature report wider dynamic ranges (0.5-355 units/mL (51), 0.1-450 units/mL (52), 0.1-40 units/mL (53), and 0.5-50 units/mL (54)) and lower

detection limits (0.1 units/mL (51), 0.05 units/mL (52), 0.04 units/mL (53), and 0.1 units/mL (54)). However, these experiments were all conducted with a single electrode format and the sample volumes required for analysis are not reported, so the total protein required for detection may not be compared. Notably, the amount of *Sss*I required for full protection of the DNA-modified electrode and the largest "signal ON" response in the assay described here is the same or lower than these other assays. This characteristic is advantageous for applications that require a simple ON/OFF report. Additionally, the previously described assays do not present a format that allows for the detection of human methyltransferase activity. As development of such a format was a central goal of work described here, effort has not yet been directed at pushing toward lower detection limits or expanding the dynamic range of this assay, and thus substantial improvements are still possible in these areas.

Not surprisingly, points within the dynamic range (2–8 nM) show the greatest variability in signal protection. This variability can be considered in terms of two separate sources. First, a small degree of variability in signal protection is observed between electrodes in the same quadrant, on the same chip. For example, at 4 nM *Sss*I, the standard deviation for percent protection among electrodes in the same quandrant is ~ ± 3% while for 0 nM or 16 nM it is ~ ± 1%. This variability likely reflects subtle morphological differences or defects in DNA film formation that either facilitate or inhibit DNA methylation. The impact of these slight physical differences between DNA-modified electrodes is amplified and only apparent within this narrow concentration range in which *Sss*I activity may be measured.

A second source of variability in this dynamic region arises from measurements between different chips for which different *Sss*I serial dilutions were prepared. For example, at 4 nM *Sss*I, the standard deviation for percent protection between electrodes on different chips treated with separately prepared *Sss*I solutions increases from ± 3% to ± 5% while for 0 nM or 16 nM it remains at ± 1%. It is possible that some of this increased variability may come from greater morphological differences between DNA-modified electrodes on different chips, but this is not expected to be a significant contribution; batch processing of multiplexed chips ensures uniform gold electrode surfaces (60) and the consistent signal size measured across chips modified with this target DNA (5.7 nC ± 0.4 nC across 5 chips, 76 electrodes) confirms this electrode uniformity. Instead, the increased variability between separately performed experiments in this region is likely due to the inherent lack of accuracy associated with manually preparing consistent protein solutions at discrete concentrations between 2–8 nM. The fact that this assay reflects this variability is further support for its use in distinguishing subtle concentration and activity differences between samples. Importantly, this source of variability is eliminated when a consistent set of serial dilutions is analyzed side by side on the same chip. Thus, the most meaningful comparisons with this assay are those made on the same chip surface with samples that share as much of the same preparation as possible.

A Hemimethylated Substrate for the Detection of Dnmt1 Methyltransferase Activity

For this assay to be relevant for the detection of human disease states that involve aberrant methyltransferase activity, it must have the capability to detect the activity of

human methyltransferases. Specifically, to detect the most abundant human methyltransferase, Dnmt1, this assay must accommodate the strong preference of Dnmt1 for activity at hemimethylated 5′-^{m}CG-3′ sites. Although use of the *BstU*I restriction endonuclease in this assay, shown here, is clearly effective for the detection of methyltransferase activity on unmethylated substrates, this particular methylation-protection system cannot be used to detect activity on hemimethylated substrates; hemimethylation alone protects DNA from *BstU*I restriction, making any further methylation indistinguishable with this assay. Because of this, a new restriction endonuclease, B*ssH*II, which recognizes the site 5′-GCGCGC-3′, was incorporated into the assay. Importantly, *BssH*II requires full methylation of either 5′-CG-3′ site within its recognition sequence to prevent DNA restriction. Thus, both hemimethylated and unmethylated DNA substrates may be used with *BssH*II in this assay for the detection of human methyltransferase activity.

In order to make accurate comparisons of Dnmt1 activity on hemimethylated and unmethylated substrates, it was first important to establish that *BssH*II recognizes and cuts the two substrates equally. Multiplexed chips were modified in separate quadrants with the *BssH*II unmethylated and hemimethylated 22-mers. As controls, the *BssH*II fully methylated 22-mer and DNA that does not contain the *BssH*II restriction site (*BstU*I unmethylated 20-mer) were also included in separate quadrants. The results are shown in Figure 6.5. Importantly, the initial signal size is the same (within error) for the *BssH*II unmethylated (6.4 nC ± 0.3 nC) and hemimethylated (5.7 nC ± 0.4 nC) 22-mers. Upon treatment with *BssH*II, the same, near complete signal loss was observed for both DNA substrates (unmethylated: 88% ± 0.4% ; hemimethylated: 89% ± 0.8%). In contrast, only

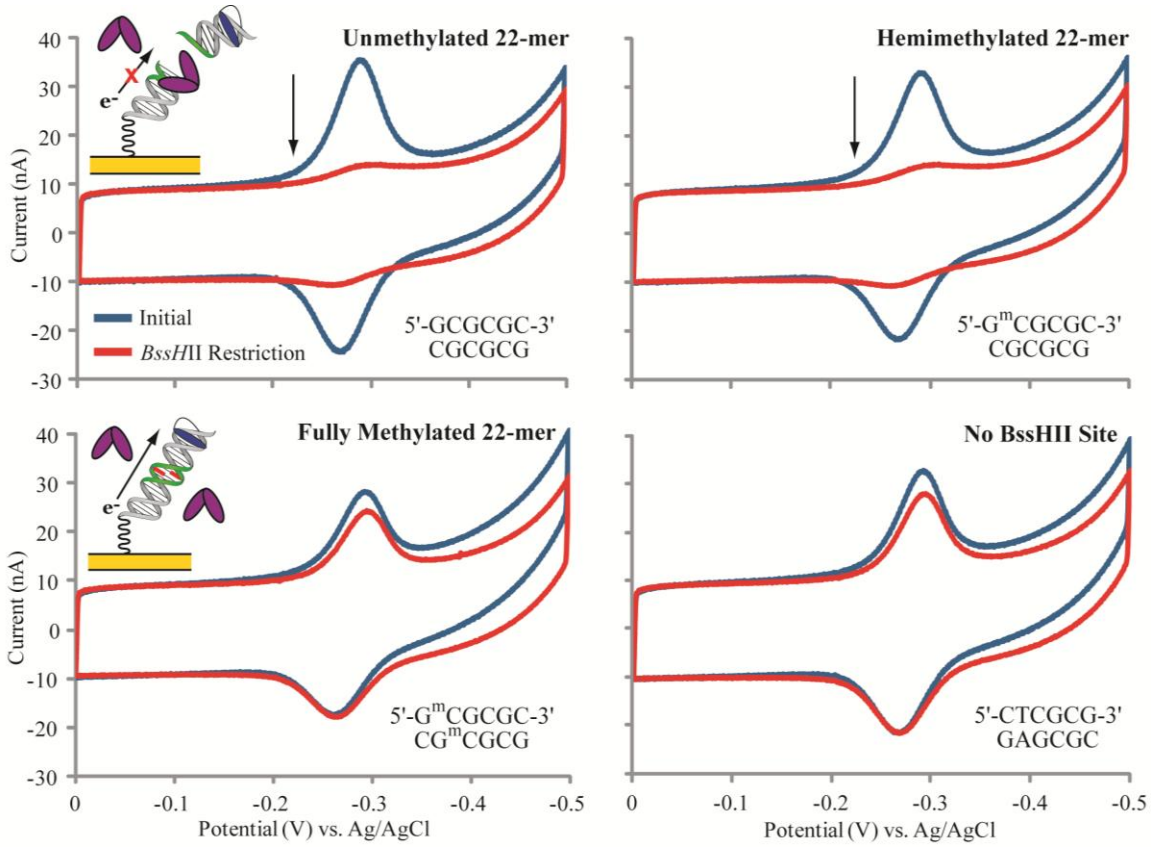

Figure 6.5. Unmethylated and hemimethylated DNA substrates are cleaved equally by *BssH*II. The chip was modified in each of four quadrants with the *BssH*II unmethylated 22-mer (top left), the *BssH*II hemimethylated 22-mer (top right), the *BssH*II fully methylated 22-mer (bottom left), and the *BstU*I unmethylated 20-mer (bottom right). Initial scans (blue traces) and scans after treatment with 1,500 units/mL *BssH*II (red traces) are shown overlaid for each DNA type. All electrochemistry was measured in the optimized scanning buffer. CV scans were performed at a 100 mV/s scan rate with an Ag/AgCl reference electrode.

small signal decreases were observed for the fully methylated DNA substrate (14% ± 2%) and DNA substrate without the *BssH*II recognition site (17% ± 2%). This degree of nonspecific signal loss, which is not due to *BssH*II restriction, was consistently observed for chips that are subjected to heating at 37°C. These results confirm that unmethylated and hemimethylated substrates may be used for the measurement and comparison of methyltransferase activity in this assay.

Detection of Dnmt1 Methyltransferase Activity

With the demonstrated capacity to utilize a hemimethylated substrate, this assay was next applied to the detection of purified Dnmt1. As a first step, the activity and hemimethylated substrate preference of the purchased Dnmt1 stock was validated by a conventional ^{3}H-SAM activity assay. In order to establish the best comparison between these results and the electrochemical assay, the same sequences used for electrochemistry (*BssH*II unmethylated and hemimethylated 22-mers) were employed without redox probe or thiol modifications. As anticipated, *Sss*I shows the same activity on both the unmethylated and hemimethylated 22-mers, while Dnmt1 shows substantially more activity on the hemimethylated 22-mer than on the unmethylated 22-mer (more than 12-fold greater activity) (Figure 6.6). The magnitude of this preference for the hemimethylated 22-mer over the unmethylated 22-mer is in agreement with previous reports for Dnmt1 (18). The lack of substrate specificity by *Sss*I also contributes to its significantly greater overall activity as compared to Dnmt1.

Upon verification of the Dnmt1 stock, the activity of this methyltransferase was next measured with the electrochemical assay. Multiplexed chips were modified in

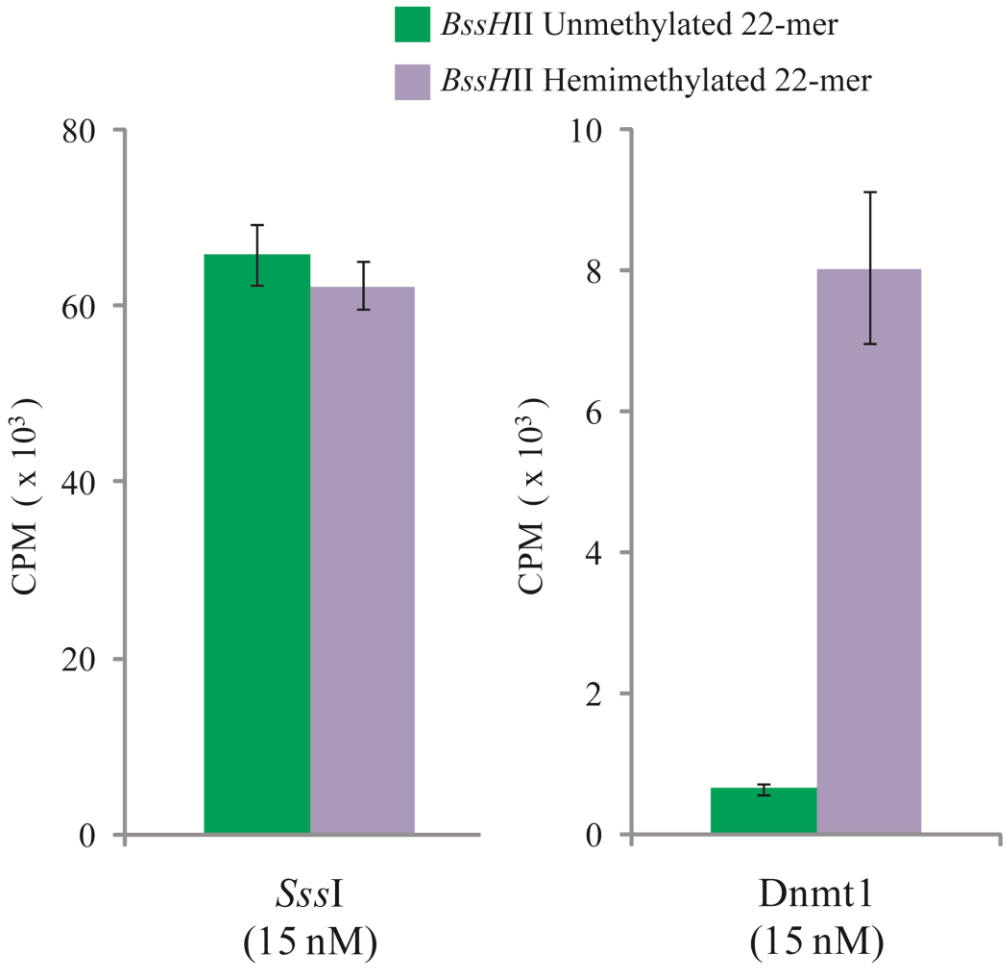

Figure 6.6 Substrate specificity of *Sss*I and Dnmt1 by ^{3}H-SAM activity assay. The methylation activity of *Sss*I (left) and Dnmt1 (right) on the *BssH*II unmethylated (green) and hemimethylated (lavender) 22-mer was evaluated with the ^{3}H-SAM activity assay. The counts per minute (CPM) by liquid scintillation counting are shown. This data for *Sss*I and Dnmt1 was collected within the same experiment, using the same ^{3}H-SAM stock and thus CPM values may be directly compared. Error bars are the standard deviation derived from three replicates within the same experiment. Although it is not pictured in the graph, the negative control in this experiment (not treated with any methyltransferase) was measured as 0.2 x 10^{3} CPM.

separate quadrants with the *BssH*II unmethylated and hemimethylated 22-mers, and DNA protection by 90 nM Dnmt1 (1 pmol total Dnmt1) was evaluated for each substrate side by side on the same chip (Figure 6.7). Just as in the ^{3}H-SAM activity assay, Dnmt1 catalyzes significantly more methylation, and thus DNA protection, on electrodes modified with the hemimethylated 22-mer (53% ± 3% signal protected) than on electrodes modified with the unmethylated 22-mer (14% ± 3% signal protected). On another set of chips, this Dnmt1 activity was also found to be dependent on the SAM cofactor (Figure 6.8). While signal protection was observed for the hemimethylated 22-mer treated with 90 nM Dnmt1 and SAM (39% ± 8% signal protected), significantly less signal protection was observed when this substrate was treated with Dnmt1 alone (17% ± 4% signal protected). In fact, this low level of signal protection was similar to what was observed on the same chip for the unmethylated 22-mer with or without SAM (18% ± 3% and 16% ± 1% signal protected, respectively).

Although full characterization of the dynamic range and detection limit of this assay for Dnmt1 has not yet been completed, these initial results may be used to make general comparisons with other methods to detect Dnmt1. No electrochemical assays for Dnmt1 have been reported, but several fluorescence-based solution methods have been described (34, 38). In these assays a 50–75 μL sample volume of Dnmt1 is required and approximately 1 pmol of Dnmt1 represents a lower limit of what may be consistently detected. Here, a 10 μL sample of Dnmt1 is required and 1 pmol of Dnmt1 is strongly detected. Future work will aim to determine an actual detection limit for Dnmt1 in this assay, as well as push this limit lower, but even this initial work suggests a favorable comparison between this assay and current methods for the detection of Dnmt1.

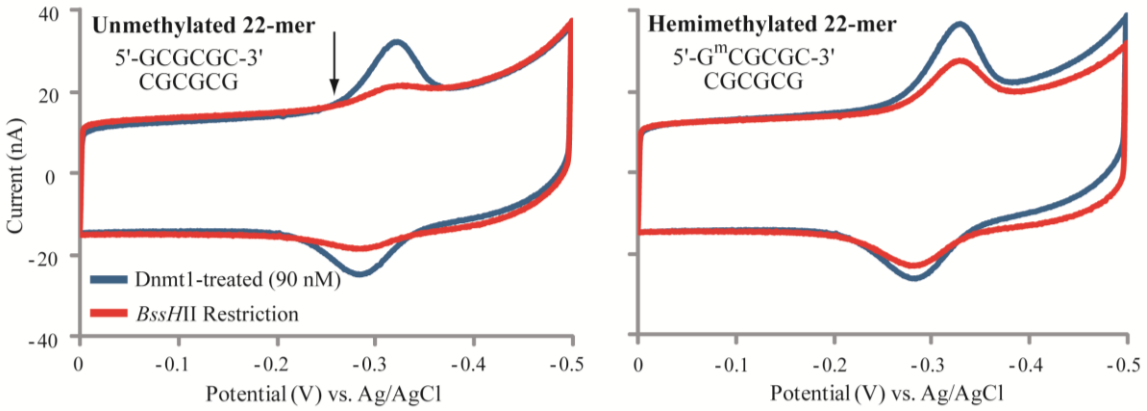

Figure 6.7. Dnmt1 preferentially protects hemimethylated DNA over unmethylated DNA. The chip was modified with the *BssH*II unmethylated 22-mer (left) and the *BssH*II hemimethylated 22-mer (right). DNA protection by 90 nM Dnmt1 was evaluated for each substrate side-by-side on the same chip. Scans after Dnmt1 treatment (blue traces) and scans after treatment with 1,500 units/mL *BssH*II (red traces) are shown overlaid for representative electrodes of each DNA type. All electrochemistry was measured in the optimized scanning buffer. CV scans were performed at a 100 mV/s scan rate with an Ag/AgCl reference electrode.

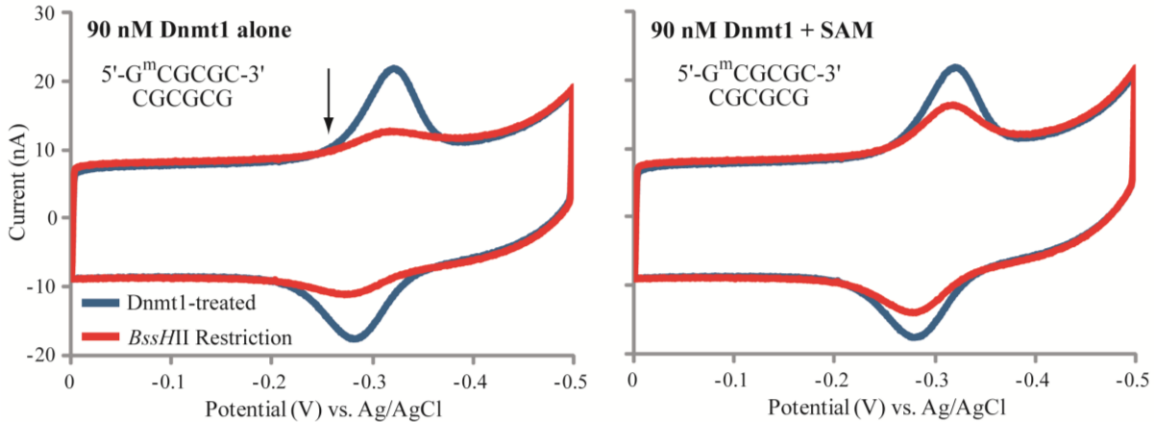

Figure 6.8 DNA protection is SAM-dependent. The illustrated quadrants of the chip were modified with the *BssH*II hemimethylated 22-mer. DNA protection was evaluated side-by-side on the same chip for quadrants treated with 90 nM Dnmt1 alone (left) or 90 nM Dnmt1 + SAM (160 μM) (right). Scans after Dnmt1 treatment (blue traces) and scans after treatment with 1,500 units/mL *BssH*II (red traces) are shown overlaid for representative electrodes of each treatment. All electrochemistry was measured in the optimized scanning buffer. CV scans were performed at a 100 mV/s scan rate with an Ag/AgCl reference electrode.

Taken together, the substrate specificity and clear SAM dependence of Dnmt1-facilitated DNA protection in this assay provide strong confirmation that this protection is the result of Dnmt1-catalyzed DNA methylation. Further, these results demonstrate that this assay is highly effective for the sensitive electrochemical detection of human methyltransferase activity; the assay is not restricted by the substrate preferences of these proteins, which are so crucial in guiding their diverse regulatory roles in living organisms. In fact, because of its substrate flexibility, this assay may be particularly suited for studies on the substrate-specific activities and cooperative interactions of the different human methyltransferases. Additionally, the amount of Dnmt1 that is required for detection by this assay is competitive with fluorescence-based solution assays that are currently used for detection of Dnmt1 activity.

Toward Detection of Methyltransferase Activity from Human Cancer Cell Lysates

One application of this assay is for the detection of human methyltransferase activity directly from the complex mixture of a cellular sample. This capability is attractive for the rapid analysis of clinical diagnostic and laboratory research samples with minimal sample preparation. Toward this goal, the human colorectal carcinoma cell line, HCT116, was used as a model sample source. Importantly, HCT116 cells are known to show gene silencing through promoter hypermethylation (72, 73) and the activity of Dnmts has been studied extensively in this cell line (23, 27, 74, 75). HCT116 variants described previously (23, 27), including the parent cell line and a Dnmt1 knockout ($Dnmt1^{-/-}$), were selected to ensure samples with inherently different levels of methyltransferase activity.

Nuclear lysates were first characterized by western blotting for the expression of Dnmt1 (Figure 6.9, inset). The presence of strong Dnmt1 expression in the parent cell line and complete absence of this methyltransferase in the Dnmt1$^{-/-}$ cell line confirms the genetic identities of the cells that should translate into differential methyltransferase activity. Following this confirmation, a conventional ^{3}H-SAM activity assay was used to measure the methyltransferase activity of these nuclear lysates. Again, to enable the most direct comparison to the electrochemical assay, the *BssH*II unmethylated and hemimethylated 22-mers were used as the DNA substrates. Importantly, nuclear lysate activity data (Figure 6.9) was collected within the same ^{3}H-SAM experiment as *Sss*I and Dnmt1 activity data (Figure 6.6) and thus CPM values may be compared directly.

Results from these experiments help to confirm the expected activity of the nuclear lysate samples in several ways. First, both parent and Dnmt1$^{-/-}$ lystates show clear methyltransferase activity (1900 ± 90 and 1100 ± 70 CPM, respectively, on the unmethylated 22-mer; 3400 ± 200 CPM and 1200 ± 200 CPM, respectively, on the hemimethylated 22-mer) that is significantly greater than an untreated control or sample treated with a heat-inactivated lysate (both ~200 CPM). Second, the lysate from the parent cell line shows greater activity on both DNA substrates than the lysate from the Dnmt1$^{-/-}$ cell line (nearly two-fold greater activity on the unmethylated 22-mer and nearly three-fold greater activity on the hemimethylated 22-mer). This result is anticipated because of the lack of Dnmt1 activity in the knockout cell line; the presence of some remaining methyltransferase activity is likely due to Dnmt3a and Dnmt3b which are still active in this cell line. Finally, the nuclear lysate from the parent cell line shows a nearly two-fold preference for the hemimethylated 22-mer while the Dnmt1$^{-/-}$ exhibits no

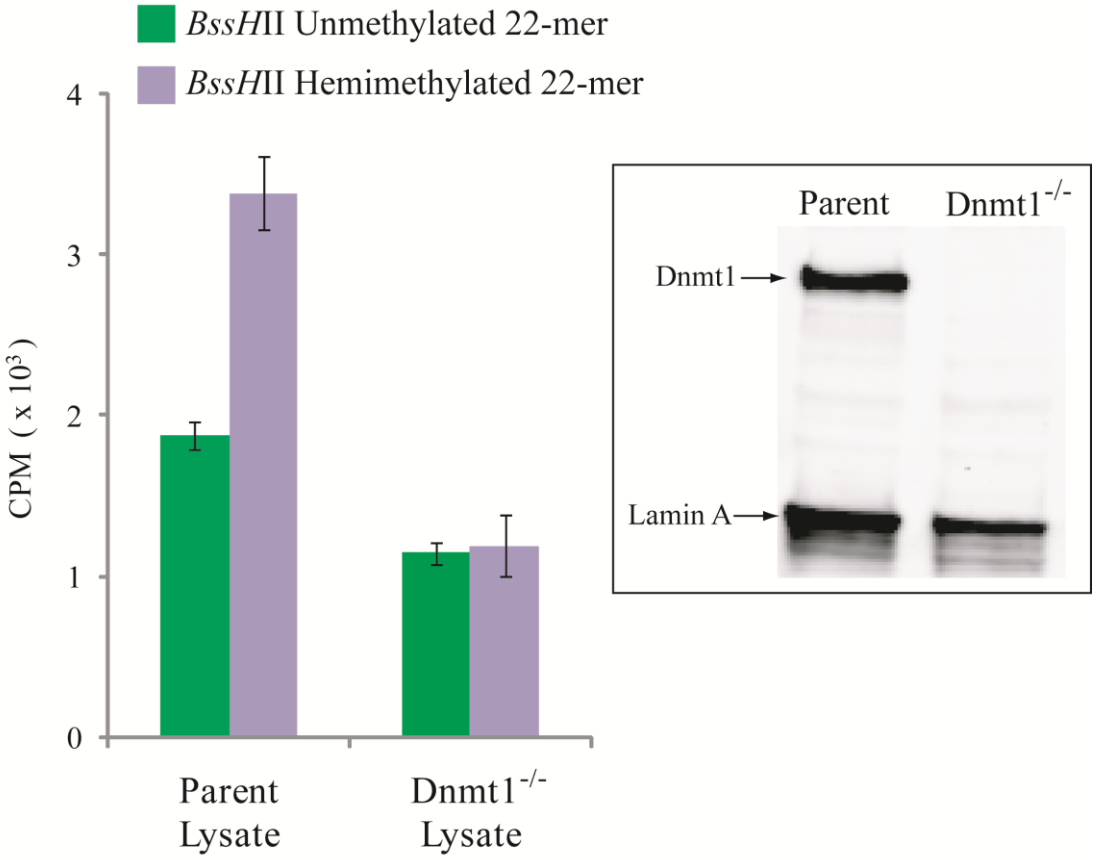

Figure 6.9 Characterization of HCT116 nuclear lysates by ^{3}H-SAM activity assay and western blot. The methylation activity of the parent and Dnmt1$^{-/-}$ nuclear lysates on the *BssH*II unmethylated (green) and hemimethylated (lavender) 22-mer was evaluated with the ^{3}H-SAM activity assay. The counts per minute (CPM) from liquid scintillation counting are shown. This data was collected within the same experiment, using the same ^{3}H-SAM stock as that for *Sss*I and Dnmt1 (Figure 6.6) and thus CPM values may be directly compared. Error bars are the standard deviation derived from three replicates within the same experiment. Although it is not pictured, a negative control (not treated with any methyltransferase) and a heat-inactivated nuclear lysate (parent) were both measured as 0.2 x 10^{3} CPM. Inset: western blot of the parent and Dnmt1$^{-/-}$ nuclear lysates for Dnmt1 and Lamin A (loading control).

significant preference. Again, the methyltransferase composition of these two cell lines may be used to explain this result; while the most prominent methyltransferase in the parent cell line, Dnmt1, is most active on hemimethylated DNA, the methyltransferases present in the Dnmt1$^{-/-}$ cell line, Dnmt3a and Dnmt3b, both have no substrate preference.

After confirming the specific activities of the nuclear lysates, these samples were next analyzed by the electrochemical assay. In contrast to purified protein samples, cellular lysates are composed of a complex mixture of proteins, DNA, metabolites, and other cellular debris, and carry significant challenges for specific detection on surface platforms. In particular for this assay, it is necessary to manage the DNA-binding proteins that are present in the sample which can nonspecifically bind the DNA on the electrode and block restriction activity and/or cause unwanted signal decreases. Upon the addition of nuclear lysates to electrodes modified with the *BssH*II 22-mers, a substantial signal decrease and peak broadening is observed (Figure 6.10). Along with this decreased signal, electrodes can no longer be cut by restriction enzymes. Several observations made it clear that this decrease is due to the active binding of various proteins to the DNA of the electrode and not digestion of the DNA by nucleases or nonspecific adsorption of biomolecules to the electrode surface: (i) the decrease occurs rapidly (within 15 minutes) and does not continue past this time and (ii) heat inactivation of the nuclear lysate completely prevents this signal decrease.

As treatment with competitor DNA was found to be ineffective at reversing this signal loss, a protease treatment step was developed. For the *BssH*II hemimethylated 22-mer treated with the parent nuclear lysate, substantial recovery of the signal is achieved after protease treatment (Figure 6.10). This result confirms that the signal decrease is due

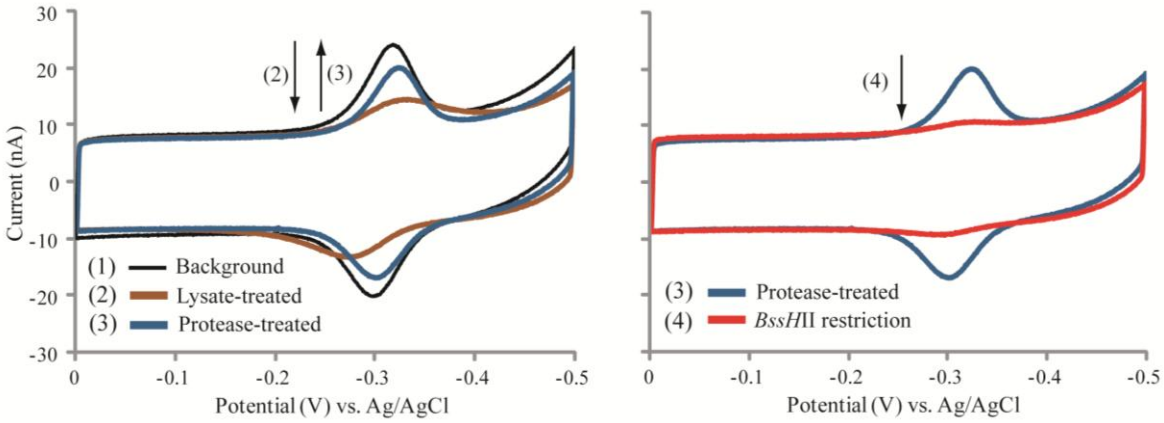

Figure 6.10 Progress toward the electrochemical detection of methyltransferase activity from HCT116 nuclear lysates. Left: protease treatment reverses signal loss caused by the nuclear lysate. The chip was modified with the *BssH*II hemimethylated 22-mer and treated with 25 mg/mL parent nuclear lysate with 160 μM SAM. The chip was then treated with 1 μM protease solution. Shown overlaid are the initial scan before lysate treatment (black trace), the scan after lysate treatment (brown trace), and the scan after protease treatment (blue trace), for a representative electrode. Right: *BssH*II is active after protease treatment. The chip was rinsed thoroughly and then treated with 1,500 units/mL *BssH*II. Shown overlaid are the initial scan after protease treatment (blue trace) and the scan after *BssH*II treatment (red trace). All electrochemistry was measured in the optimized scanning buffer. CV scans were performed at a 100 mV/s scan rate with an Ag/AgCl reference electrode.

to the extensive binding of multiple proteins in solution to the DNA of the electrode. Importantly, after protease treatment, the DNA is readily cut by *BssH*II. This indicates that, after digestion of the bound proteins, the DNA is now accessible for restriction. Although no protective activity by the nuclear lysate is observed, this protease treatment overcomes a significant obstacle that has hindered progress with cellular lysates and may be an important step toward the successful detection of methyltransferase activity in these complex samples.

Summary and Conclusions

Described here is a new assay for the electrochemical detection of methyltransferase activity that allows for the use of unmethylated and hemimethylated DNA substrates to detect activity from both bacterial and human samples. This assay utilizes DNA-modified electrodes with a methylation-sensitive restriction site that overlaps with the active site of a DNA methyltransferase. Upon treatment with active methyltransferases, methylation of this site protects the DNA-modified electrodes from subsequent cutting by a restriction enzyme, resulting in "signal ON" detection. This response was shown to depend on the presence of the methyl donor, SAM, confirming that DNA protection in this assay is indeed conferred by methylation. Additionally, it was demonstrated that methyltransferase-treated electrodes are still readily cut by a restriction enzyme that is not inhibited by methylation, indicating that DNA protection is not due to physical blocking of the DNA by bound proteins.

Characterization of the concentration dependence of this methylation-based signal protection for bacterial *Sss*I methyltransferase revealed sharp switching behavior for this assay with a narrow dynamic range of 2–8 nM *Sss*I. Thus for *Sss*I, the assay in its current form is best suited for applications that require an ON/OFF report of methyltransferase activity, rather than an accurate quantification of unknown samples. Notably, because of the small sample volumes that are required for this assay (10 μL) and the sensitive "signal ON" detection scheme, *Sss*I activity can be observed for samples as small as just 20 fmoles of protein. Although several other electrochemical assays report lower detection limits and wider dynamic ranges for *Sss*I (51–54), the lower concentration of SssI required in this assay to produce the full "signal ON" response, is actually an advantage

for ON/OFF applications. The small required sample volume, multiplexed format, and substrate flexibility that allows for the study of human methyltransferases are additional benefits of this assay over those reported previously. Also, efforts have not yet been focused on lowering the detection limit or modulating the dynamic range of this assay and these aims represent a promising area of future work.

The narrow 2–8 nM dynamic range, which falls just below the binding constant of *Sss*I, is likely a strong reflection of this binding limit; once a concentration is reached for which DNA binding is favorable, all DNA on the electrode is rapidly methylated and protected. Additional factors that likely influence this dynamic range include the activity (turnover) of the methyltransferase sample and the film morphology of the DNA on the surface. Of these contributions, the morphological accessibility of the DNA film is the factor that may be modulated in future work to possibly expand this dynamic range. Different film morphologies (e.g. fully accessible duplexes spaced evenly across the surface or dense island patches of DNA for which only outer duplexes are accessible to protein activity), may present more or less challenging landscapes for a given methyltransferase to fully protect from restriction. By creating DNA film morphologies that are more difficult to fully protect, it may be possible to accurately quantify samples of unknown methyltransferase concentration over a wider range. It is also important to consider that, due to vast differences in binding constant, size, turnover rate, optimal reaction temperature, and substrate preference of different methyltransferases, the concentration-dependent response, including the size of the dynamic range, for this assay will likely be highly methyltransferase-specific. It will be necessary to evaluate this for

each methyltransferase of interest in order to determine how this assay may be applied to work with a particular methyltransferase.

Detection of activity by Dnmt1, the most prominent human methyltransferase, was also demonstrated here with this assay. Importantly, the use of a restriction enzyme (*BssH*II) that requires full methylation of a 5′-CG-3′ site within its recognition site allowed for the incorporation of a hemimethylated DNA substrate. The strong preference of Dnmt1 to methylate hemimethylated DNA was first confirmed by a conventional ^{3}H-SAM activity assay on the same DNA substrates used for electrochemistry. This preference was then reflected electrochemically by substantially more protection of electrodes modified with hemimethylated DNA as compared to those modified with unmethylated DNA. Dnmt1 activity was also shown electrochemically to be dependent on the methyl donor, SAM, confirming methylation as the mode of protection. Though a lower detection limit has not yet been determined for this assay, strong detection of 1 pmol of Dnmt1 indicates that this assay is already competitive with current fluorescence-based solution methods for Dnmt1 detection (34, 38). Although differential methyltransferase expression and activity was confirmed for a human colorectal carcinoma cell line (HCT116) model system by western blot and ^{3}H-SAM activity assay, activity directly from nuclear lysates has not yet been measured electrochemically. However, progress with the development of a protease treatment to reverse the detrimental effects of nonspecific binding by the nuclear lysate makes continued work toward this goal promising.

These results represent the first reported detection of human methyltransferase activity by an electrochemical method. Not only does the ability to use both an

unmethylated and hemimethylated substrate in this assay enable, for the first time, the electrochemical measurement of activity by human Dnmt1, this flexibility will be valuable for studies on how substrate specificities influence methylation activities. Importantly, the electrochemical format of this assay requires minimal equipment, is low cost, and allows for multiplexing and extension to high throughput studies. Side-by-side activity experiments on unmethylated vs. hemimethylated substrates would allow for the rapid analysis of the substrate-specific methylation activity of a given sample. This type of experiment could be applied to a range of basic research, diagnostic, and therapeutic work with human methyltransferases including the study of cooperative activities between methyltransferases, the investigation into how "maintenance" and "*de novo*" activities contribute to cancer initiation, the characterization of cancer methylation phenotype, and the development and screening of methyltransferase-specific drug therapies.

References

1. Daniel, F.I., Cherubini, K., Yurgel, L., de Figueiredo, M.A., and Salum, F.G. (2011) *Cancer 117*, 677-687.

2. Jones, P.A. and Miranda, T.B. (2007) *J. Cell. Phys. 213*, 384-390.

3. Jeltsch, A. (2002) *ChemBioChem. 3*, 274-293.

4. Attwood, J.T., Yung, R.L., and Richardson, B.C. (2002) *Cell. Mol. Life Sci. 59*, 241-257.

5. Hansen, R.S., Wijmenga, C., Luo, P., Stanek, A.M., Canfield T.K., Weemaes, C.M., and Gartler, S.M. (1999) *Proc. Natl. Acad. Sci. USA. 96*, 14412-14417.

6. Chen, R., Akbarian, S., Tudor, M., and Jaenisch, R. (2001) *Nat. Genet. 27*, 327-331.

7. Richardson, B., Scheinbart, L., Strahler, J., Gross, L., Hanash, S., and Johnson, M. (1990) *Arthritis Rheum*. *33*, 1665-1673.

8. Esteller, M. (2002) *Oncogene 21*, 5427-5440.

9. Das, P.M. and Singal, R. (2004) *J. Clin. Oncol*. *22*, 4632-4642.

10. Baylin, S.B. and Herman, J.G. (2000) *Trends Genet*. *16*, 168-174.

11. Baylin, S.B., Herman J.G., Graff, J.R., Vertino, P.M., and Issa, J.P. (1998) *Adv. Cancer. Res*. *72*, 141-196.

12. Robertson, K.D., Uzvolgyi, E. Liang, G., Talmadge, C., Sumegi, J., Gonzales, F.A., and Jones, P.A. (1999) *Nuc. Acid. Res. 27*, 2291-2298.

13. Rajendran, G., Shanmuganandam, K., Bendre, A., Mujumdar, D., Goel, A., and Shiras, A. (2011) *J. Neurooncol. 104*, 483-494.

14. Shukla, V., Coumoul, X., Lahusen, T., Wang, R., Xu, X., Vassilopoulos, A., Xiao, C., Lee, M., Man, Y., Ouchi, M., Ouchi, T., and Deng, C. (2010) *Cell Res*. *20*, 1201-1215.

15. Roll, J.D., Rivenbark, A.G., Jones, W.D., and Coleman, W.B. (2008) *Mol. Cancer 7*, 15-29.

16. Nosho, K., Shima, K., Irahara, N., Kure, S., Baba, Y., Kirkner, G.J., Chen, L., Gokhale, S., Hazra, A., Spiegelman, D., Giovannucci, E.L., Jaenisch, R., Fuchs, C.S., and Ogino, S. (2009) *Clin. Cancer Res. 15*, 3663-3671.

17. Linhart, H.G, Lin, H., Yamada, Y., Moran, E., Steine, E.J., Gokhale, S., Lo, G., Cantu, E., Ehrich, M., He, T., Meissner, A., and Jaenisch, R. (2007) *Genes Dev. 21*, 3110-3122.

18. Pradhan, S., Bacolla, A., Wells, R.D., and Roberts, R. J. (1995) *J. Biol. Chem*. *274*, 33002-33010.

19. Flynn, J., Glickman, J.F., and Reich, N.O. (1996) *Biochemistry 35*, 7308-7315.

20. Okano, M. Bell, D.W., Haber, D.A., and Li, E. (1999) *Cell 99*, 247-257.

21. Kim, G.D., Mi, J., Kelesoglu, N., Roberts, R.J., and Pradhan, S. (2002) *EMBO J. 21*, 4183-4195.

22. Fatemi, M., Hermann, A., Gowher, H., and Jeltsch, A. (2002) *Eur. J. Biochem*. *269*, 4981-4984.

23. Rhee, I., Bachman, K.E., Park, B.H., Jair, K., Yen, R.C., Schuebel, K.E., Cui, H. Feinberg, A.P., Lengauer, C., Kinzler, K.W., Baylin, S.B., and Vogelstein, B. (2002) *Nature 416*, 552-556.

24. Issa, J. (2004) *Nat. Rev*. *4*, 988-993.

25. Jurkowska, R.Z., Ceccaldi, A., Zhang, Y., Ariimondo, P.B., and Jeltsch, A. (2011) *Methods Mol. Biol*. *791*, 157-177.

26. Pradhan, S., Bacolla, A., Wells, R.D., and Roberts, R.J. (1999) *J. Biol. Chem. 274*, 33002-33010.

27. Rhee, I., Jair, K., Yen, R.C., Lengauer, C., Herman, J.G., Kinzler, K.W., Vogelstein, B., Baylin, S.B., Schuebel, K.E. (2000) *Nature 404*, 1003-1007.

28. Roth, M. and Jeltsch, A. (2000) *Biol. Chem. 381*, 269-272.

29. Frommer, M., McDonald, L.E., Millar, D.S., Collis, C.M., Watt, F., Grigg, G.W., Molloy, P.L., Paul, C.L. (1992) *Proc. Natl. Acad. Sci. USA. 89*, 1827-1831.

30. Zhang, Y., Rohde, C., Tierling, S., Stamerjohanns, H., Reinhardt, R., Walter, J., and Jeltsch, A. (2009) *Methods Mol. Biol. 507*, 177-187.

31. Friso, S., Choi, S., Dolnikowski, G.G., and Selhub, J. (2002) *Anal. Chem*. *74*, 4526-4531.

32. Dorgan, K.M., Wooderchak, W.L., Wynn, D.P., Karschner, E.L., Alfaro, J.F., Cui, Y., Zhou, Z.S., and Hevel, J.M. (2006) *Anal. Biochem*. *15*, 249-255.

33. Graves, T.L., Zhang, Y., and Scott, J.E. (2008) *Anal. Biochem*. *373*, 296-306.

34. DNMT Universal Assay Kit, reported results. (2012) BPS Bioscience Inc., San Diego, CA. http://www.bpsbioscience.com/methyltransferase/assay-kit/dnmt-universal-assay-kit-52035

35. Singer, J., Roberts-Ems, J., and Riggs, A.D. (1979) *Science 203*, 1019-1021.

36. Feinberg, A.P. and Vogelstein, B. (1983) *Nature 301*, 89-92.

37. Woo, Y., Rajagopalan, R., and Benkovic, S.J. (2005) *Anal. Biochem. 340*, 336-340.

38. Strivers, J.T. and Ye, Y. (2010) *Anal. Biochem*. *401*, 168-172.

39. Li, J., Yan, H., Wang, K., Tan, W., and Zhou, X. (2007) *Anal. Chem. 79*, 1050-1056.

40. Wood, R.J., McKelvie, J.C., Maynard-Smith, M.D., and Roach, P.L. (2010) *Nuc. Acids. Res. 38*, 1-11.

41. Lee, J., Kim, Y.K., and Min, D.H. (2011) *Anal. Chem*. *83*, 8906-8912.

42. Zhao, X., Chen, F., Wu, Y., Dong, Y., and Fan, C. (2013) *Biosens. Bioelect. 42*, 56-61.

43. Sadik, O.A., Aluoch, A.O., and Zhou, A. (2009) *Biosens. Bioelect. 24*, 2749-2765.

44. Drummond, T.G., Hill, M.G., and Barton, J.K. (2003) *Nat. Biotechnol. 21*, 1192-1199.

45. Bakker, E., and Qin, Y. (2006) *Anal. Chem. 78*, 3973-3983.

46. Wang, P., Mai, Z., Dai, Z., and Zou, X. (2010) *Chem. Commun. 46*, 7781-7783.

47. He, X., Su, J., Wang, Y., Wang, K., Ni, X., and Chen, Z. (2011) *Biosens. Bioelectron*. *28*, 298-303.

48. Wang, Y., He, X., Wang, K., Su, J., Chen, Z., Yan, G., and Du, Y. (2012) *Biosens. Bioelectron.* http://dx.doi.org/10.1016/j.bios.2012.08.034

49. Su, J., He, X., Wang, Y., Wang, K., Zhifeng, C., and Yan, G. (2012) *Biosens. Bioelectron. 36*, 123-128.

50. Wu, H., Liu, S., Jiang, J., Shen, G., and Yu, R. (2012) *Chem. Commun. 48*, 6280-6282.

51. Liu, S., Wu, P., Li, W., Zhang, H., and Cai, C. (2011) *Chem. Commun*. *47*, 2844-2846.

52. Li, W., Wu, P., Zhang, H., and Cai, C. (2012) *Anal. Chem*. 84, 7583-7590.

53. Yin, H., Zhou, Y., Xu, Z., Chen, L., Zhang, D., and Ai, S. (2012) *Biosens. Bioelectron.* http://dx.doi.org/10.1016/j.bios.2012.09.010

54. Wang, M., Xu, Z., Chen, L., Yin, H., and Ai, S. (2012) *Anal. Chem*. 84, 9072-9078.

55. Yamada, H., Tanabe, K., and Nishimoto, S. (2008) *Org. Biomol. Chem. 6*, 272-277.

56. Genereux, J.C. and Barton, J.K. (2010) *Chem. Rev. 110*, 1642-1662.

57. Gorodetsky, A.A., Buzzeo, M.C., and Barton, J.K. (2008) *Bioconj. Chem. 19*, 2285-2296.

58. Kelley, S.O., Boon, E.M., Barton, J.K., Jackson, N.M., and Hill, M.G. (1999) *Nuc. Acids Res. 27*, 4830-4837.

59. Boon, E.M., Ceres, D.M., Drummond, T.G., Hill, M.G. and Barton, J.K. (2000) *Nat. Biotechnol*. *18*, 1096-1100.

60. Slinker, J.D., Muren, N.B., Gorodetsky, A.A. and Barton, J.K. (2010) *J. Am. Chem. Soc. 132*, 2769–2774.

61. Slinker, J.D., Muren, N.B., Renfrew, S.E., and Barton, J.K. (2011) *Nat. Chem*. *3*, 230-235.

62. Boal, A.K. and Barton, J.K. (2005) *Bioconjugate Chem. 16*, 312-321.

63. Boon, E.M., Salas, J.E., and Barton, J.K. (2002) *Nat. Biotechnol*. *20*, 282-286.

64. Gorodetsky, A.A., Ebrahim, A., and Barton, J.K. (2008) *J. Am. Chem. Soc. 130*, 2924-2925.

65. Pheeney, C.G., Guerra, L.F., and Barton, J.K. (2012) *Proc. Natl. Acad. Sci. USA 109*, 11528-11533.

66. Pheeney, C.G. and Barton, J.K. (2012) *Langmuir 28*, 7063-7070.

67. Adams, R.L.P., McKay, E.L., Craig, L.M., and Burdon, R.H. (1979) *Biochim. Biophys. Acta* 561, 345-357.

68. Renbaum, P., Abrahamove, D., Fainsod, A., Wilson, G.G., Rottem, S., and Razin, A. (1990) *Nuc. Acids Res. 18,* 1145-1152.

69. Renbaum, P. and Razin, A. (1995) *J. Mol. Biol. 248,* 19-26.

70. Darii, M.V., Kirsanova, O.V., Drutsa, V.L., Kochetkov, S.N., and Gromova, E.S. (2007) *Mol. Biol. 41*, 110-117.

71. As defined by the manufacturer. (2012) New England Biolabs Inc., Ipswich, MA. http://www.neb.com

72. Lengauer, C., Kinzler, K.W. and Vogelstein, B. (1997) *Proc. Natl. Acad. Sci. USA 94*, 2545-2550.

73. Myohanen, S.K., Baylin, S.B., and Herman, J.G. (1998) *Cancer Res. 58,* 591-593.

74. Robert, M., Morin, S., Beaulieu, N., Gauthier, F., Chute, I.C., Barsalou, A., and MacLeod, A.R. (2002) *Nat. Genet. 33*, 61-65.

75. Chen, T., Hevi, S., Gay, F., Tsujimoto, N., He, T., Zhang, B., Ueda, Y., and Li, E. (2007) *Nat. Genet. 39,* 391-396.

Chapter 7

Summary and Perspective

DNA-mediated charge transport (DNA CT) is a unique chemical phenomenon that arises from the physical structure and dynamics of DNA. Extensive work, from diverse experimental vantage points, in solution, on surfaces, and with single molecule techniques has established a solid foundation to understand this chemistry (1). Like graphite and other materials with extensive π-orbital networks, the π-stacked array of heterocyclic aromatic base pairs that forms the core of the linear DNA molecule creates a conductive path that can transmit charge over long distances (2, 3). In contrast to other π-stacked solids, though, the structure of DNA in solution is dynamic, with constant fluctuations in the physical alignment, and resulting π-orbital overlap, of neighboring base pairs. These dynamical changes in orientation determine the timescale of DNA CT (picoseconds to millisecond) and influence the mechanism; the transient formation of electronically aligned, multi-base domains over which charge can delocalize is what makes DNA CT an energetically favorable process and actually gates the flow of charge through this molecule (1, 4). Given the critical role of structure in this chemistry, it is not surprising that DNA CT is exquisitely sensitive to physical disruptions of the base pair π-stack. Mismatched or damaged bases (5, 6) as well as protein binding and restriction activity (7) have all been shown to attenuate DNA CT.

In this thesis work, we have built up and out from this foundation in several new directions including work to address the following questions: *"How does DNA CT vary over regimes of increasing distance?"* and *"How may we exploit this sensitive chemistry for the multiplexed, electrochemical detection of proteins?"* In order to investigate these questions with our DNA-modified electrodes, which allow for ground state, electrochemical measurements, it was first necessary to expand this platform to a

multiplexed chip format (8). We designed and fabricated silicon chips with sixteen individually addressable gold electrodes that may be modified with up to four different types of DNA, and verified that this platform supports DNA-mediated electrochemistry. This improved electrochemical format allows for side-by-side controls and provides greater consistency and reproducibility than single electrodes. As such, this multiplexed platform opens the door for the complex experiments that are necessary to measure the distance dependence of DNA CT and apply this chemistry to biosensing.

Although previous work in solution suggested that the distance dependence of DNA CT is very shallow (9), DNA CT over long distances in the ground state had not yet been measured. An understanding of this fundamental property is critical as we consider how we might use DNA as a molecular wire in nanoelectronics as well as how nature may already use DNA CT for long distance signaling and the coordination of cellular processes (10). Using DNA-modified electrodes on multiplexed chips, we measured DNA CT over 34 nm (100 bp), the longest distance over which this chemistry has been measured to date (3). Remarkably, the signal size and attenuation from the incorporation of a single base mismatch is the same for the 100-mer as for much shorter, 17-mer DNA. Also like the 17-mer, the rate of DNA CT through the 100-mer is limited by the C6 alkanethiol linker that anchors the DNA to the electrode. Thus, over 34 nm of DNA, the distance dependence of DNA CT is too shallow to be resolved above the limits of the platform used to make the measurement. Though a β value for DNA could not be directly calculated, we made a conservative estimate of β as 0.05 $Å^{-1}$ for DNA. This shallow distance dependence agrees with previous excited state solution measurements, and indicates that DNA is competitive with the longest and most conductive molecular

wires reported. Ongoing work to measure the distance dependence of DNA CT in single DNA molecules with the carbon nanotube-DNA (CNT-DNA) platform suggests that the actual distance dependence of DNA CT may be even shallower: a preliminary β value of 0.01 $Å^{-1}$ was extrapolated from conductivity measurements across three DNA lengths.

DNA CT was also used for the detection of DNA methyltransferases by both single molecule and multiplexed, electrochemical platforms. These proteins are attractive targets as their aberrant expression and activity has been identified as an early indicator of multiple types of cancer (11). The DNA-binding action of methyltransferases, which includes flipping a base out of the π-stack in order to add a methyl group, was previously shown by electrochemistry to disrupt DNA CT (7). With CNT-DNA devices, we used this property for the single molecule detection of binding by *Sss*I methyltransferase, the bacterial analog to human methyltransferases (12). In addition to binding, we showed that these devices can also be used to detect methylation, as this chemical modification alters the subsequent protein binding affinity of the device.

Multiplexed, electrochemical detection of methyltransferase binding and activity was explored by two different strategies. First, we worked to detect *Sss*I by the same approach used with the CNT-DNA devices; binding and base flipping by *Sss*I on the DNA-modified electrode causes a disruption of DNA CT that may be measured electrochemically. In this way we monitored binding by *Sss*I that is concentration- and cofactor-dependent as well as reversible with competitor DNA. Importantly, this assay is general and may be easily extended to the detection of other proteins that distort the DNA π-stack upon binding. However, we determined that this "signal OFF" approach is susceptible to signal attenuation caused by nonspecific protein binding, a problematic

issue that would be amplified in more complex samples, such as cell lysates, that contain a host of interfering proteins. Thus, this strategy may be best used in its current form to detect protein binding from controlled samples (such as for anti-methylation drug screening) as well as characterize protein-DNA interactions and improve our understanding of how protein-DNA binding at surfaces may be compared to binding in solution.

In a second line of work, we developed a new electrochemical assay for the detection of methyltransferase activity. In this assay, methylation of the DNA-modified electrode confers protection from cutting during subsequent treatment with a restriction enzyme. With the methylated DNA intact, the redox signal from the probe is retained, and thus indicates the presence of active methyltransferases in the sample. We showed that this assay is effective for the sensitive, rapid detection of both bacterial and human methyltransferase activity in small sample volumes (10 μL). Uniquely, the design of this assay allows for the use of both hemimethylated and unmethylated DNA, a feature that is important for work with human methyltransferases which show differing preferences for these substrates. This capacity to use a hemimethylated substrate allowed, for the first time, the electrochemical detection of Dnmt1, the most prominent human methyltransferase. We used this assay to demonstrate the cofactor dependence and substrate specificity of Dnmt1 activity. The "signal ON" nature of this assay makes it more resistant to the problems associated with nonspecific binding from complex samples and thus ongoing work to detect methyltransferase activity directly from human cancer cell lysates is promising. Importantly, the electrochemical format of this assay requires minimal equipment, is low cost, and could be easily applied to high throughput

studies, making it an accessible option for a variety of research and clinical settings. The capacity to accommodate human samples and the substrate flexibility of this assay will allow it to be used for diverse applications. A notable example is its use to assess the substrate-specific methylation activity of a sample, a key factor in cancer pathogenesis, which is important for work on both diagnostic and therapeutic approaches to methylation-related cancers.

Highlighted by this thesis work are two of the most fascinating, defining characteristics of DNA CT: the capacity to proceed over very long distances and the exquisite sensitivity to subtle structural perturbations. When considered generally, removed from the traditional context for DNA, these characteristics describe a process that may be used for long-distance sensing and signaling, a mechanism for transmitting information between spatially separated locations. When considered back in the context that has been established for DNA, this process is facilitated by a material that may be easily synthesized and manipulated in the laboratory, and that, at this moment, is being replicated by the mile inside every living organism on the planet. Consideration of both contexts in combination results in a flowering of possibilities that are at once challenging and exciting to imagine. We have systematically built a solid foundation for understanding how these defining characteristics of DNA CT arise from the structure of DNA itself. With this, we are well equipped to explore how this mechanism for long-distance sensing and signaling plays out in living organisms and envision how we might also utilize it to sensitively transmit information on the nanoscale. This work represents several fresh steps toward illuminating the wide reach of this chemistry, but clearly there is still much left to understand and to create.

References

1. Muren, N. B, Olmon, E. O., and Barton, J. K. (2012) *Phys. Chem. Chem. Phys. 14*, 1375-13771.

2. Guo, X., Gorodetsky, A.A., Hone, J., and Barton, J.K. (2008) *Nature Nanotech*. *3*, 163-167.

3. Slinker, J.D., Muren, N.B., Renfrew, S.E., and Barton, J.K. (2011) *Nature Chem*. *3*, 230-235.

4. Genereux, J.G. and Barton, J.K. (2010) *Chem. Rev. 110*, 1642-1662.

5. Boon, E.M., Ceres, D.M., Drummond, T.G., Hill, M.G., and Barton, J.K. (2000) *Nature Biotechnol*. *18*, 1096-1100

6. Boal, A.K. and Barton, J.K. (2005) *Bioconjugate Chem. 16*, 312-321.

7. Boon, E.M., Salas, J.E., and Barton, J.K. (2002) *Nature Biotechnol*. *20*, 282-286.

8. Slinker, J.D., Muren, N.B., Gorodetsky, A.A., and Barton, J.K. (2010) *J. Am. Chem. Soc. 132*, 2769–2774.

9. Núñez, M.E., Hall, D.B., and Barton, J.K. (1999) *Chem. Biol. 6*, 85-97.

10. Genereux, J.C., Boal, A.K., and Barton, J.K. (2010) *J. Am. Chem. Soc. 132*, 891-905.

11. Das, P.M. and Singal, R. (2004) *J. Clin. Oncol*. *22*, 4632-4642.

12. Wang, H., Muren, N. B., Ordinario, D., Gorodetsky, A.A., Barton, J.K., and Nuckolls, C. (2012) *Chem. Sci*. *3*, 62-65.